Fluorescence Resonance Energy Transfer (FRET) Systems for Biomedical Sensor Applications

By

Aoibhéann Bird B.Sc. (Hons)

A Thesis presented

to

Dublin City University

For The Degree Of Doctor Of Philosophy

Research Supervisor:

Prof. Colette McDonagh

School of Physical Sciences,

Dublin City University.

July 2010

Declaration

I hereby certify that this material, which I now submit for assessment on the programme of study leading to the award of Doctor of Philosophy is entirely my own work, that I have exercised reasonable care to ensure that the work is original, and does not to the best of my knowledge breach any law of copyright, and has not been taken from the work of others save and to the extent that such work has been cited and acknowledged within the text of my work.

Signed: _____ (Candidate) ID No.: _____

Date: _____

Acknowledgements

First and foremost, I would like to thank my supervisor Prof. Colette McDonagh for her constant encouragement and guidance throughout my Ph.D. I am truly grateful for your support through the ups and downs. I would also like to thank Prof. Brian MacCraith for his invaluable input and assistance to the project.

For creating a wonderful place to come in to every day, I would like to thank all the members of the Optical Sensors Laboratory and the Biomedical Diagnostics Institute, both past and present. You are a fantastic group of people and it has been my pleasure to drink the many hundreds of cups of tea with you, in particular Rob, Christy, Ondra, John, Rob, Scott, Helen, Conor and Colm.

I especially want to thank Ondra, who was a fantastic source of information on all things related to nanoparticles. Your theoretical models, and patience at trying to explain them to me, were truly appreciated. I learnt an incredible amount from you. Thanks for your time and patience.

To Rob Nooney and Scott, thanks for putting up with my constant chemistry questions in the lab every day, you made it a wonderful place to work. Huge appreciation also to Vlado for unraveling the complexities of biochemistry and the world of DNA to me. Thanks for sharing your bench and your wealth of knowledge so patiently.

I would also like to thank Helen McEvoy for all her help on how to write and present my work over the past few years. Your fabulous ability to make it all sound so professional and interesting, boosted my spirits and re-energised me.

I also wish to thank the members of the NCSR and the School of Physical Sciences who have helped make my time at DCU so productive and pleasurable.

A big thank you to the DCU SubAqua Club for braving the cold waters with me. Your friendship and the adventures we've had, made the past few years hugely enjoyable. To all my friends outside of DCU, especially the Lauras, Áine, Deane, Barry, and Eoin. Thank you for your friendship, patience and support, it meant the world to me. I promise to have more time now.

Finally, to my parents and Niúl (& Lynsey) and Derdriú (& Cameron and Ciara!), thank you for looking after, supporting and encouraging me, even from afar. I could never have done it without you.

Abstract

This thesis investigates the use of Fluorescence Resonance Energy Transfer (FRET) for biomedical sensor applications. FRET is a process by which energy is transferred, via long range dipole-dipole interactions, from a donor molecule (D) in an excited electronic state to an acceptor molecule (A). The emission band of D must overlap the absorption band of A in order for FRET to occur. FRET is employed in a variety of biomedical applications, including the study of cell biology and protein folding/unfolding and is also used for enhanced optical bioassays. The distance dependence of the FRET interaction enables the technique to be used as a molecular ruler to report, for example, on conformational changes in biomolecules. The first phase of this work involved the design and implementation of a model 2-D FRET platform that is compatible with optical biochips. The donor-acceptor pair used was a Ruthenium-complex/Cy5 system where the donor-acceptor separation was controlled using highly reproducible polyelectrolyte spacer layers, which were deposited using a layer-by-layer technique. The FRET process was demonstrated in both fluorescence intensity and lifetime mode. The interaction between FRET and the plasmonic enhancement of fluorescence in the presence of adjacent metal nanoparticles was also investigated. Dipole-dipole interactions limit the FRET effect to donor-acceptor distances of typically less than 10nm. The use of the plasmonic effect to increase this distance, which would facilitate the use of FRET in a wider variety of applications, was explored. The size, shape and composition of metal nanoparticles were tailored to give a resonance absorption which optimises the enhancement of the dye fluorescence. As well developing a 2-D solid planar platform, the FRET-plasmonic interaction was also investigated in solution phase, by designing a model that incorporated donor and acceptor-labeled oligonucleotides as controlled spacers and spherical gold and silver nanoparticles for plasmonic enhancement. Throughout the work, theoretical calculations were carried out, and, where relevant, theoretical predictions were compared with experimental measurements. Apart from designing two FRET-plasmonic investigation models, a key result to emerge from this work is that while individual plasmonic enhancement of the donor and acceptor is occurring in the presence of metal nanoparticles, no plasmonic enhancement of the FRET

interaction is observed for the experimental systems. Theoretical modeling confirmed the reduction of the FRET efficiency.

Contents

List of Figures

Glossary

A - Acceptor

D - Donor

DMF - (dimethylformamide)

DNA - Deoxyribonucleic acid

EDC - (1-(3-Dimethylaminopropyl)-3-ethylcarbodiimide hydrochloride

FRET - Fluorescence Resonance Energy Transfer

FLIM - Fluorescence Lifetime Imaging Microscopy

LbL - Layer by Layer

LSPR - Localised Surface Plasmon Resonance

MEF - Metal Enhanced Fluorescence

MHA - Mercapto-hexadecanoic-acid

NP - Nanoparticle

PAC - poly(acrylic acid)

PAH - Poly(allyamine hydrochloride)

PDAC - poly(diallyldimethylammonium chloride)

PDMS - poly(dimethylsiloxane)

PEL - Polyelectrolyte

PSS - poly(styrene sulphonate)

Ru-complex - (Bis(2,2'-bipyridine)-5-isothiocyanato-phenanthroline)ruthenium

Ru-PEL - Ru-complex conjugated to PAH

SPR - Surface Plasmon Resonance

Chapter 1

Introduction

1.1 Introduction and Context

There is increasing interest in point-of-care (POC) biosensors and biodiagnostics, which would enable diagnosis and treatment to take place in doctors' surgeries or in the home rather than in the hospital environment. This has obvious benefits to patients and society in general, for example fast and more cost effective diagnosis and treatment. The work presented here explores the enhanced performance of POC devices through the employment of novel nano-materials and miniaturisable optical platforms. In particular, the thesis explores the use of Fluorescence Resonance Energy Transfer (FRET) and FRET in combination with metal nanoparticles (NPs), in order to enhance the performance of optical biosensors. This chapter gives a brief introduction to the main elements of the work: (i) the FRET mechanism, (ii) examples of FRET-based systems, and (iii) the interaction between metal nanoparticles (NPs) and fluorescent dyes. An introduction to biosensors is also provided. The chapter will conclude with a description of the thesis structure and objectives.

1.2 Principles of Nanobiophotonics

Nanobiophotonics is the amalgamation of photonics, nanotechnology, lasers and biomedical science and is a field that is receiving considerable attention world wide. The increased life expectancy of the world population presents many prob-

lems in the area of health management, and the outputs of nanobiophotonics can provide tools for earlier detection of diseases and improved management of these conditions. It is a multidisciplinary area involving the combination of biological sensing, optical diagnostics, signal processing and communications. This work attempts to apply nanobiophotonic principles to the investigation of a FRET-based biosensor platform. Elements of nanobiophotonics used include metal nanoparticles, polymer nano-layers, fluorescence dyes and fluorescently labeled DNA.

1.3 Biosensors

A biosensor is a device which can detect disease related molecules using biological recognition elements [1]. These disease related molecules may be antibodies, antigens, nucleic acids or other biologically relevant small molecules, which are markers for a particular disease or condition [2–8]. The biological recognition elements contain biomolecules such as antibodies, DNA probes or enzymes, which recognise a particular disease marker or analyte. The reaction between the biomolecule and the analyte results in physical or chemical changes that can result in the production of heat, mass, light, electrons or ions [1]. The analyte can also be labeled with a biomarker or tag, such as an enzyme, radioisotope or dye. If the dye is fluorescent, the device is then known as a fluorescence-based biosensor. This is the type of biosensor is considered here.

There are many biosensors commercially available on the market, such as the ELISA (Enzyme-Linked ImmunoSorbent Assay), Biacore and PicoQuant systems. An ELISA system is a protein diagnostic tool which can detect the presence of an antigen or antibody in a sample, through a colour change which is optically detected. Some newer techniques that use the general principles of the ELISA protocol can result in higher sensitivities and allow for multiplexing, where multiple antigens or antibodies can be detected from a single sample. They can incorporate electrochemiluminescent and fluorogenic markers [9, 10].

The BIAcore^{TM} system from Biacore is an example of a surface plasmon based biosensor, specialising in measuring protein-protein interactions and binding affinity. The technology is based on surface plasmon resonance (SPR), an

optical phenomenon using thin metal films and the principle of plasmon resonance that enables the detection of unlabeled interactants in real time. The limitations of this biosensor are the non-specific adsorption of molecules onto the surface and its high sensitivity to temperature [11–13].

The PicoQuant GmbH system is an example of a very sensitive fluorescence-based biosensor. It utilises fluorescence decay lifetimes (see Section 4.2.4) and it is possible to detect a single fluorescent molecule and its orientation with this system [14, 15]. This can lower the limit of detection dramatically to a point where the sensitivity of the sensor is only limited by the diffusion rate of the reagent and the affinity of the biomolecule to the detection zone. However the high quality optics and sensitive detectors used in this system result in it being a very expensive, large bench-top device used only in laboratories with skilled personnel and cannot be implemented in low-cost portable biosensors.

There is a demand for simple, compact, low-cost devices that can detect a low concentration of antigens. There are a few strategies being employed to enhance the sensitivity of fluorescence-based biosensors to achieve this goal. One of these strategies is TIRF (Total Internal Reflection Fluorescence), which suppresses the signal from unbound labeled molecules in a solution [16]. This is achieved by coupling the excitation beam into the substrate at an angle greater than the critical angle, so that the beam is internally reflected along it. The beam does not propagate into the sensing area, instead the evanescent field of the beam excites the area but this extends only a few nanometres into the solution. As a result the bulk solution does not fluoresce and the system detects only interactions at the surface. A similar effect to this is Supercritial Angle Fluorescence (SAF) [17–19], which both excites and collects the emission of surface bound fluorophores above the critical angle, this enables a distinction between surface interactions and the unbound bulk fluorescence. Surface Plasmon Coupled Emission (SPCE) exploits the heightened anisotropic emission of a fluorophore above a thin metallic layer and again uses this to distinguish surface interactions from the bulk fluorescence [20–22]. Though these techniques are susceptible to surface roughness they have the potential to lower the limit of detection of optical biosensors and allow for higher sensitivity to disease markers in samples. Highly

sensitive, portable, low-cost biosensors would facilitate the earlier detection and management of diseases.

1.4 Fluorescence Resonance Energy Transfer

Föster Resonance Energy Transfer (FRET) is a process by which the extra energy of a fluorescent molecule in an excited electronic state (donor) is transferred to a chromophore molecule (acceptor) [23]. Although not necessary, in most cases the acceptor is also a fluorescent molecule. In this case, FRET also stands for Fluorescence Resonance Energy Transfer.

FRET is a process by which energy is transferred non-radiatively, via long range dipole-dipole interactions, from a donor molecule (D) in an excited electronic state to an acceptor molecule (A). The emission band of D must overlap sufficiently with the absorption band of A in order for FRET to occur and the rate of transfer of energy is dependent on the separation of the two molecules. FRET can be an accurate measurement of molecular proximity at angstrom distances (10-100Å). The physics and chemistry of fluorescence resonance energy transfer have been well studied theoretically for years [23–25] but only with recent technical advances has it become feasible to apply FRET to biomedical research [26–33]. The efficiency of FRET is dependent on the inverse sixth power of intermolecular separation (see Section 2.3.1), making it a sensitive technique for investigating a variety of biological phenomena that gives rise to distance changes of this order. Therefore one of the main applications of FRET is as a spectroscopic ruler, which can probe distances on the nanometre scale through fluorescence measurements, based on Försters basic rate equation for a donor and acceptor pair at a distance r from each other.

As with all biosensors, sensitivity is vitally important and there are many ways of increasing the FRET efficiency to achieve this. The FRET efficiency is the quantum yield of the energy transfer transition. It can be increased with an increase in the percentage of donor and acceptor overlap spectrum, by using different dye pairs, however this also causes an increase in the bleedthrough signal in the FRET channel [26]. The efficiency of FRET could also be improved by

optimising the concentration of the fluorophore used, but if the concentration is too high energy transfer can occur between donor-donor or acceptor-acceptor molecules (known as homo-FRET), preventing energy transfer between the donor and the acceptor. This is discussed further in Section 2.3. While highly efficient traditional FRET systems are beneficial, it would be desirable to have a FRET system that was not limited to the 10nm interaction distance. This would enable molecular interactions to be investigated that occur beyond this distance. Some work has been done to achieve this goal [33–35], but so far nothing greater than a 75% increase in the Förster Radius, has been reported.

1.5 Current Applications of FRET

There are several FRET measurement techniques available, and the efficiency of energy transfer can be measured using fluorescence intensities or fluorescence lifetimes. Intensity-based imaging techniques applying the method of FRET spectroscopy and microscopy (wide field, confocal, and multiphoton) have facilitated the study of cellular events, such as signal transduction and gene transcription inside intact living cells [36]. If FRET occurs, the acceptor signal increases and the donor signal decreases. After removing the background and autofluorescence signal the transfer efficiency can be calculated. Intensity-based FRET techniques still suffer from some drawbacks, including photobleaching, detector noise, autofluorescence and light source instability. In addition these techniques do not have high speed time resolution to fully characterise the dynamics of complex cellular structures.

Fluorescence Lifetime Imaging Microscopy (FLIM) is another technique that allows the measurement of dynamic events at a very high temporal resolution. Lifetime measurements are independent of excitation intensity and fluorophore concentration, which removes some of the problems experienced with intensity-based microscopy such as spectral bleedthrough. The distance between the donor and acceptor labels can accurately be calculated by measuring the donor lifetime in the presence and the absence of the acceptor. The use of fluorescence lifetimes can determine the spatial distribution of labeled molecules, enabling certain struc-

tures, such as cells, to be mapped [37]. It can also be used to distinguish two dyes of similar spectral characteristics but differing lifetimes.

Fluorescence sensor molecules for imaging cellular molecules have been increasingly researched in the last two decades [38–41]. FRET imaging is used in many different ways in biodiagnostics. Ratiometric fluorescence sensors have been developed using distance changes [30, 42–45]. FRET sensors have also been used to determine cell structure and the surface distribution of membrane proteins [46] and protein folding interactions [47–49]. Proteins are complex organic compounds composed of amino acids, which are molecules which contain carboxyl (COOH) and amine (NH_2) functional groups [50]. The arrangement of the amino acids determine both the function and 3-D folded structure of the protein. To design these types of FRET sensors it is necessary to have the donor and acceptor located on opposite sides of a protein so that when the protein is in its unfolded, relaxed state there is little or no energy transfer.

When the protein folds, the donor and acceptor are within the FRET limit, energy transfer occurs, and the emission of the acceptor increases. The distance between the two dyes can be measured using the ratio of their emissions, and therefore the state of the protein can be determined. Fig. 1.1 illustrates the processes of protein folding and unfolding detection using FRET. This process has also been used in the detection of sugars such as maltose, using maltose binding protein (MBP). Upon binding maltose, the MBP undergoes a conformation change that brings the donor and acceptor into close proximity and increases the FRET [51]. Applications of these sensors are in the food and beverage industry for direct use of their maltose sensing capabilities, specifically in beer and bread production which utilize maltose as the primary sugar source. Adaptations of these sensors can be use in the detection of other sugars such a glucose, for the monitoring of levels in diabetic patients [52, 53].

Antigen - antibody interactions can also be measured using FRET immunoassays [54–56]. Antibodies are a sub-group of proteins which due to high availability and specificity are one of the major types of biomolecules employed in biosensors. Antibodies are part of the immune system. When a foreign molecule, known as an antigen, enters the body, it stimulates a class of white cells known

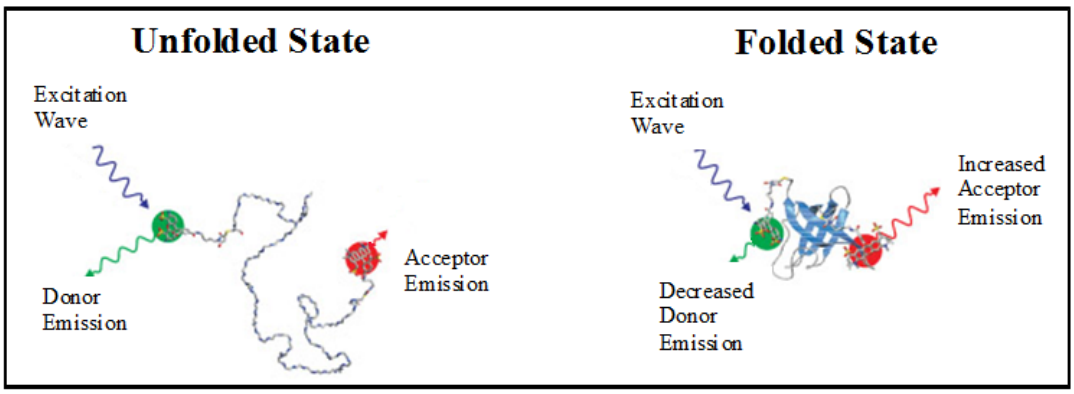

Figure 1.1: Illustration of FRET with protein folding/unfolding.

as B-lymphocytes to mature into antibody producing plasma cells, which produce antibodies with binding sites specific to that antigen [57]. The antibody binds to the antigen and marks it for destruction by the body. The basis of an immunoassay is the detection of antigens through the use of antibodies. FRET-based immunoassays are designed with the donor attached to an antibody and the acceptor attached to an antigen or to another antibody, as shown in Fig. 1.2. FRET occurs when the components are sequentially bound together and the donor is excited. Reduction of the concentration of the antigen will result in a lower FRET signal [58]. This FRET system is more favourable compared to a single dye-labeled detection antibody due to the specificity of emission being detected only from bound antibodies and not that of the bulk fluorescence. Compared to TIRF and SAF systems, a FRET-based immunoassay allows this discrimination without the need to couple light into the system at specific angles or the need for highly uniform surfaces that will internally reflect the light. FRET pairs can also have a large Stokes shift (see Section 2.2.2) which reduces the need for sophisticated filters separating the excitation beam from the emission profile. Fluorescence immunoassays can be divided into two categories, heterogeneous and homogeneous. Heterogeneous immunoassays involve the physical separation of the assay mixture before detection. FRET immunoassays are homogeneous, which means that they can be conducted entirely in the original sample mixture and require few manipulations.

FRET-based DNA sensors have been developed and can be used in the detection of mutations or areas of mismatch in DNA sequences [59–61]. Genetic

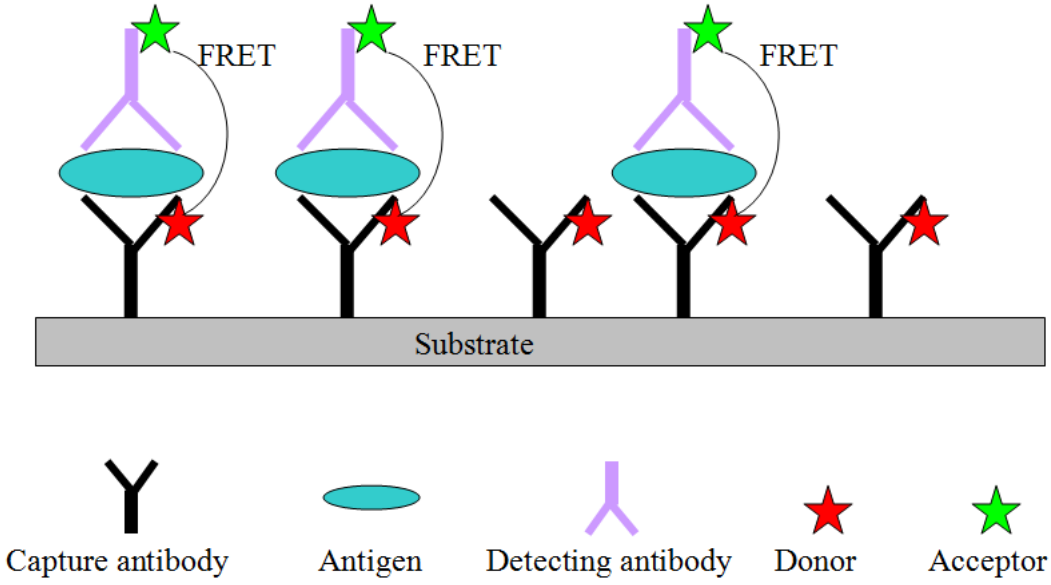

Figure 1.2: Illustration of a FRET immunoassay.

testing is a growing area of interest for diagnostics and forensics. This involves determining the presence or absence of known DNA polymorphisms or mutations in a sample. Large scale studies can be performed using homogeneous assays, which provide flexibility and ease of use [62]. A known DNA sequence is labeled with a donor molecule, if a sample DNA sequence labeled with an acceptor molecule matches the known one, they hybridise and energy transfer between the FRET pair occurs, as shown in Fig. 1.3. Hybridisation is the process whereby two complementary sequences of single stranded DNA form a hybrid double-stranded DNA. This is described in more detail in Chapter 2.

Clearly, there are many different types of FRET-based biosensors, but they are all limited by the 10nm dipole-dipole interaction distance. This reduces their applicability to systems that span further distances. As part of this work the interaction between FRET and the plasmonic enhancement of fluorescence in the presence of adjacent metal nanoparticles is investigated. The use of the plasmonic effect to increase the limit over which FRET occurs, would facilitate the use of FRET in a wider variety of applications, by extending the length of the molecular ruler. For instance, measuring large-scale conformational changes in nucleo-protein assemblies, large biological molecules, protein complexes and moderate lengths of DNA.

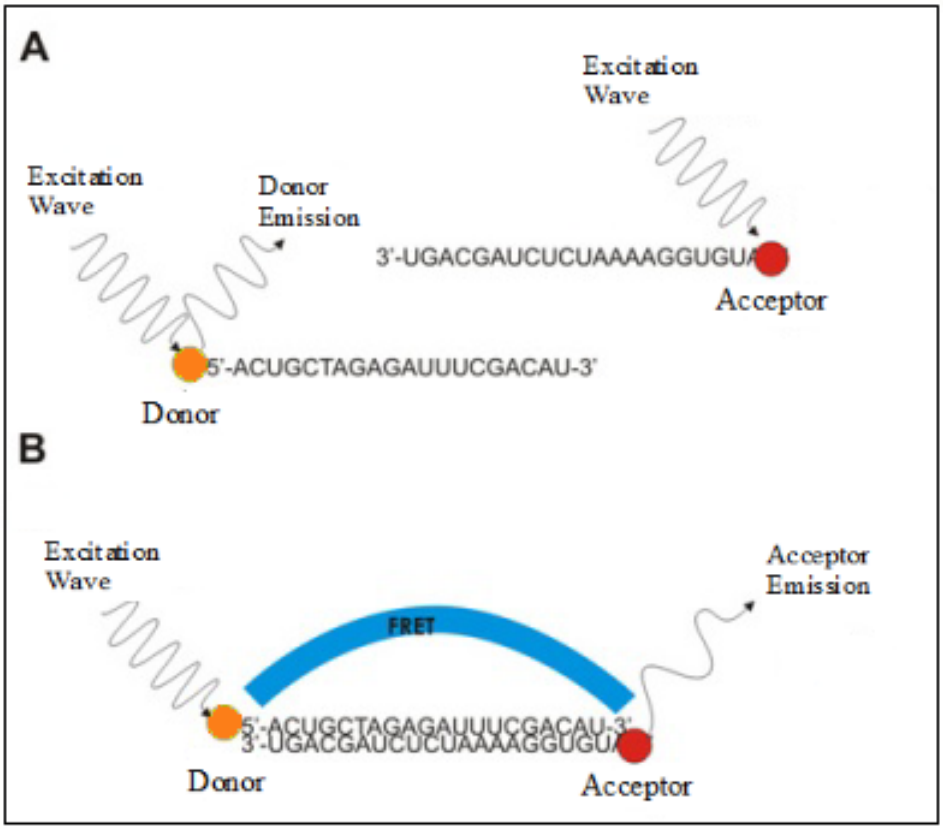

Figure 1.3: Illustration of a FRET DNA sensor.

1.6 Plasmonic Enhancement using Metal Nanoparticles

The incorporation of metal nanoparticles (NPs) into a FRET system is explored in this work, with a view to enhancing the distance over which FRET occurs by exploiting the plasmonic enhancement of fluorescence. A nanoparticle is defined as a particle where at least one dimension is less than 100nm [63]. NPs have special physical and chemical properties, due to their small dimensions and these are exploited in many different applications. Metal NPs have a strong absorption in the visible spectrum which gives them a specific colour depending on their composition and shape [64]. Gold NPs are responsible for the brilliant reds seen in stained glass windows and silver NPs are typically yellow in colour. For centuries these properties have been of interest and scientific research on metal NPs dates back to at least 1857 with Michael Faraday [65]. In 1908 Mie presented a solution to Maxwell's equations [66–68], which describes the extinction spectra

of spherical particles. To this day Mie's solution remains of great interest [69] especially in the area of nanooptics [70] and medical diagnostics [71]. When NPs are irradiated with visible light they exhibit a strong local electromagnetic field around the particle, which can interact with adjacent NPs. This means that they can be used to guide light below the diffraction limit [72, 73] in optical set ups such as optical waveguides, mirrors, beam splitters or even logical switches of sizes smaller than the wavelength of the light used [74].

Optical detection and spectroscopy of single molecules and single NPs has been achieved with the use of surface-enhanced Raman scattering [75]. Individual silver colloidal NPs can be used to amplify the spectroscopic signatures of adsorbed molecules through intense, stable vibrational Raman signals. These are just a few examples of the applications that NPs have within industry today. There is much work going on globally into the research and development of these particles and how to harness their potential in many new areas.

Metal NPs can be used in fluorescence-based biosensors to improve their performance. It was theoretically formulated [76–78] and experimentally discovered [79, 80] that metal NPs enhance the fluorescence signal from molecules near the NPs. The enhancement is caused by the increased electromagnetic field around the NPs, which makes them act like an antenna and amplifies the received and emitted signal. Several authors have investigated the various parameters that affect the metal NPs enhancement of the fluorescence and have tried to optimise them [81–87]. Measurements of the effect on a single fluorescent dye and a NP were also investigated [88, 89]. However, understanding the complex behaviour of electromagnetic field interacting with the metal structures is needed to find the optimal nanostructure for enhancement of fluorescence [90, 91]. It has been reported that this enhancement has increased the sensitivity and decreased the limit of detection in some fluorescently-labeled biosensors [92–95]. Positioning the metal NPs close to the biorecognition elements increases the fluorescence from the dye-labeled analyte and therefore increases the performance of the biosensor. In this work, the focus is on the novel concept of enhancing the FRET interaction via plasmonics through the use of metal NPs.

1.7 Thesis Structure

Chapter 1 provides an introduction to the work and describes the applications of FRET in biosensors and introduces the role of metal NPs in fluorescence enhancement.

Chapter 2 introduces the principles of fluorescence and Fluorescence Resonance Energy Transfer (FRET). It also describes the optical properties of metal NPs, especially the effect of localised surface plasmon resonance. The plasmonic enhancement of fluorescence is also explored.

Chapter 3 deals primarily with the common materials, instrumentation and methods used throughout the work. Experimental methods specific to particular experiments are described in the relevant chapters.

Chapter 4 investigates FRET in a two dimensional configuration on a planar surface. The main motivation is the potential to use FRET on optical biochips for Point Of Care (POC) applications. The planar configuration along with polyelectrolytes for controllable layer spacing are compatible with 2-D biochip arrays. This study also focuses on combining FRET with the plasmonic interaction in order to extend the Förster radius. The plasmonic interaction results in significant enhancements in fluorescence when a fluorophore is in the vicinity of a metal NP. Metal NPs, whose size, shape and composition are tailored to the spectroscopic properties of the donor and acceptor molecules, were deposited at varying distances from the donor/acceptor system and the resulting FRET behaviour was characterised using spectral analysis. Results were then correlated to theoretical calculations.

Chapter 5 describes an alternative approach to that described in Chapter 4. FRET was investigated in solution using two complementary donor and acceptor labeled oligonucleotides (DNA strands). The labeled oligonucleotides were then attached to gold and silver NPs and the plasmonic interaction was investigated. The resulting FRET behaviour was measured using spectral analysis and the results were then compared to a theoretical model.

Finally, Chapter 6 summarises the results achieved during the research and revisits the objectives of the work and discusses future perspectives.

1.8 Thesis Objectives

The main objectives of this work were to:

(a) Design a model system to demonstrate planar FRET with Ruthenium-complex (D) and Cy5 (A).

(b) Develop a strategy for accurate control of D-A separation: Polyelectrolyte layers (PELs).

(c) Measure transfer efficiency (E_T) - compare with theory.

(d) Investigate the plasmonic effect of metal NPs on the transfer efficiency of 2-D FRET.

(e) Investigate the plasmonic effect of metal NPs on the transfer efficiency in solution FRET.

References

[1] S. Y. Rabbany, B. L. Donner, and F. S. Ligler. Optical immunosensors. *Critical reviews in Biomedical Engineering*, 22(5/6):307–346, 1994.

[2] N. L. Rosi and C. A. Mirkin. Nanostructures in biodiagnostics. *Chemical Reviews*, 105:1547–1562, 2005.

[3] E. Katz and I. Willner. Integrated nanoparticle-biomolecule hybrid systems: Synthesis, properties, and applications. *Angew. Chem. Int. Ed.*, 43:6042–6108, 2004.

[4] S. G. Penn, L. He, and M. J. Natan. Nanoparticles for bioanalysis. *Current Opinion in Chemical Biology*, 7(5):609–615, 2003.

[5] N. Nath and A. Chilkoti. Label free colorimetric biosensing using nanoparticles. *Journal of Fluorescence*, 14(4):377–389, 2004.

[6] F. Frederix, J. M. Friedt, K. H. Choi, W. Laureyn, A. Campitelli, D. Mondelaers, G. Maes, and G. Borghs. Biosensing based on light absorption of nanoscaled gold and silver particles. *Anal. Chem.*, 75:6894–6900, 2003.

[7] D. A. Stuart, A. J. Haes, C. R. Yonzon, E. M. Hicks, and R. P. Van Duyne. Biological applications of localised surface plasmonic phenomenae. *IEE Proc.-Nanobiotechnology*, 152(1):13–32, 2005.

[8] M. Seydack. Nanoparticle labels in immunosensing using optical detection methods. *Biosensors and Bioelectronics*, 20:2454–2469, 2005.

[9] S. Leng, J. McElhaney, J. Walston, D. Xie, N. Fedarko, and G. Kuchel. Elisa and multiplex technologies for cytokine measurement in inflammation and aging research. *A Biol Sci Med Sci*, 63:879–884, 2008.

[10] M. Adler, S. Schulz, and M. Spengler. Cytokine quantification in drug development: A comparison of sensitive immunoassay platforms. *Chimera Biotech*, 2009.

[11] H. Raether. *Surface plasmons on smooth and rough surfaces and on gratings.* Springer tracts in modern physics, 111. Springer-Verlag, Berlin; New York, 1988.

[12] J. Homola, S. S. Yee, and G. Gauglitz. Surface plasmon resonance sensor: review. *Sensor and Actuators B*, 54:3–15, 1999.

[13] D. K. Kambhampati and W. Knoll. Surface-plasmon optical techniques. *Current Opinion in Colloid & Interface Sci.*, 4:273–280, 1999.

[14] A. P. Bartko and R. M. Dickson. Imaging three-dimensional single molecule orientations. *Journal of Physical Chemistry B*, 103:11237–11241, 1999.

[15] H. Gersen, M. F. Garcia-Parajo, L. Novotny, J. A. Veerman, L. Kuipers, and N. F. Van Hulst. Near-field effects in single molecule emission. *Journal of Microscopy*, 202(Pt 2, May):374–378, 2001.

[16] K. E. Sapsford, Y. S. Shubin, J. B. Delehanty, J. P. Golden, C. R. Taitt, L. C. Shriver-Lake, and F. S. Ligler. Fluorescence-based array biosensors for detection of biohazards. *Journal of Applied Microbiology*, 96:47–58, 2004.

[17] T. Ruckstuhl, M. Rank, and S. Seeger. Highly sensitive biosensing using a supercritical angle fluorescence (SAF) instrument. *Biosensors and Bioelectronics*, 18:1193–1199, 2003.

[18] T. Ruckstuhl and D. Verdes. Supercritical angle fluorescence microscopy. *Optics express*, 12(18):4246–4254, 2004.

[19] D. Kurzbuch, J. Bakker, J. Melin, C. Jonsson, T. Ruckstuhl, and B. D. MacCraith. A biochip reader using super critical angle fluorescence. *Sensors and Actuators B-Chemical*, 137(1):1–6, 2009.

[20] J. R. Lakowicz, C. D. Geddes, I. Gryczynski, J. Malicka, Z. Gryczynski, K. Aslan, J. Lukomska, E. Matveeva, J. A. Zhang, R. Badugu, and

J. Huang. Advances in surface-enhanced fluorescence. *Journal of Fluorescence*, 14(4):425–441, 2004.

[21] M. Trnavsky, J. Enderlein, T. Ruckstuhl, C. McDonagh, and B. D. MacCraith. Experimental and theoretical evaluation of surface plasmon-coupled emission for sensitive fluorescence detection. *JOURNAL OF BIOMEDICAL OPTICS*, 13(5), 2008.

[22] J. S. Yuk, M. Trnavsky, C. McDonagh, and B. D. MacCraith. Surface plasmon-coupled emission (SPCE)-based immunoassay using a novel paraboloid array biochip. *Biosensors and Bioelectronics*, 25(6):1344–1349, 2010.

[23] T. Förster. Intermolecular energy transfer and fluorescence. *Ann. Physics*, 2:55–75, 1948. [Translated by R. S. Knox].

[24] L. Stryer. Fluorescence energy transfer as a spectroscopic ruler. *Annu. Rev. Biochem.*, 47:819–846, 1978.

[25] J. R. Lakowicz. *Principles of fluorescence spectroscopy.* Kluwer Academic/Plenum Publishers, New York, 1999.

[26] G. W. Gordon, G. Berry, X. H. Liang, B. Levine, and B. Herman. Quantitative fluorescence resonance energy transfer measurements using fluorescence microscopy. *Biophysical Journal*, 74(5):2702–2713, 1998.

[27] C. Berney and G. Danuser. FRET or no FRET: A quantitative comparison. *Biophysical Journal*, 84(6):3992–4010, 2003.

[28] A. R. Clapp, I. L. Medintz, H. T. Uyeda, B. R. Fisher, E. R. Goldman, M. G. Bawendi, and H. Mattoussi. Quantum dot-based multiplexed fluorescence resonance energy transfer. *Journal of the American Chemical Society*, 127(51):18212–18221, 2005.

[29] G. Crivat, S. M. Da Silva, D. R. Reyes, L. E. Locascio, M. Gaitan, N. Rosenzweig, and Z. Rosenzweig. Quantum dot FRET-based probes in thin films grown in microfluidic channels. *Journal of the American Chemical Society*, 132(5):1460–1461, 2010.

[30] J.E. Gonzalez and R.Y. Tsien. Voltage sensing by fluorescence resonance energy transfer in single cells. *Biophysical Journal*, 69(4):1272–1280, 1995.

[31] I. L. Medintz, A. R. Clapp, H. Mattoussi, E. R. Goldman, B. Fisher, and J. M. Mauro. Self-assembled nanoscale biosensors based on quantum dot FRET donors. *Nature Materials*, 2(9):630–638, 2003.

[32] K. Kikuchi, H. Takakusa, and T. Nagano. Recent advances in the design of small molecule-based FRET sensors for cell biology. *Trends in Analytical Chemistry*, 23(6):407–415, 2004.

[33] J. R. Lakowicz, J. Zhang, and Y. Fu. Enhanced frster resonance energy transfer (FRET) on single metal particle. *J Phys Chem C Nanomater Interfaces*, 111(1):50–56, 2007.

[34] J. R. Lakowicz, J. Zhang, Y. Fu, and M. H. Chowdhury. Enhanced forster resonance energy transfer on single metal particle. 2. dependence on donor and acceptor separation distance, particle size, and distance from metal surface. *The Journal of Physical Chemistry C*, 111(32):11784–11792, 2007.

[35] M. Lessard-Viger, M. Rioux, L. Rainville, and D. Boudreau. FRET enhancement in multilayer core-shell nanoparticles. *Nano Letters*, 2009.

[36] A. Periasamy. *Methods in cellular imaging*. Published for the American Physiological Society by Oxford University Press, Oxford; New York, 2001.

[37] M. Peter, S. M. Ameer-Beg, M. K. Y. Hughes, M. D. Keppler, S. Prag, M. Marsh, B. Vojnovic, and T. Ng. Multiphoton-FLIM quantification of the EGFP-mRFP1 FRET pair for localization of membrane receptor-kinase interactions. *Biophysical Journal*, 88:1224–1237, 2005.

[38] J. Szllosi, S. Damjanovich, and L. Mtyus. Application of fluorescence resonance energy transfer in the clinical laboratory: Routine and research. *Cytometry*, 34(4):159–179, 1998.

[39] R.Y. Tsien. Fluorescence imaging creates a window on the cell. *Chemical and Engineering News*, 72(29):34–44, 1994.

[40] A. W. Czarnik. Desperately seeking sensors. *Chemistry and Biology*, 2(7):423–428, 1995.

[41] K. Rurack and U. Resch-Genge. Rigidization, preorientation and electronic decouplingthe magic triangle for the design of highly efficient fluorescent sensors and switches. *Chem. Soc. Rev.*, 31:116–127, 2002.

[42] X. D. Ge, L. Tolosa, and G. Rao. Dual-labeled glucose binding protein for ratiometric measurements of glucose. *Analytical Chemistry*, 76(5):1403–1410, 2004.

[43] Y. Kawanishi, K. Kikuchi, H. Takakusa, S. Mizukami, Y. Urano, T. Higuchi, and T. Nagano. Design and synthesis of intramolecular resonance-energy transfer probes for use in ratiometric measurements in aqueous solution. *Angewandte Chemie*, 39(19):3438–3440, 2000.

[44] H. Takakusa, K. Kikuchi, Y. Urano, T. Higuchi, and T. Nagano. Intramolecular fluorescence resonance energy transfer system with coumarin donor included in -cyclodextrin. *Analytical Chemistry*, 73(5):939–942, 2001.

[45] H. Takakusa, K. Kikuchi, Y. Urano, S. Sakamoto, K. Yamaguchi, and T. Nagano. Design and synthesis of an enzyme-cleavable sensor molecule for phosphodiesterase activity based on fluorescence resonance energy transfer. *Journal of the American Chemical Society*, 124(8):1653–1657, 2002.

[46] H.R Petty, H. Poo, and B. Fox. Ligation of CD3 triggers transmembrane proximity between LFA-1 and cortical microfilaments in a cytotoxic T cell clone derived from tumor infiltrating lymphocytes:a quantitative resonance energy transfer study. *J Cell Biol.*, 159:176–180, 1994.

[47] E. A. Lipman, B. Schuler, O. Bakajin, and W. A. Eaton. Single-molecule measurement of protein folding kinetics. *Science*, 301(5637):1233–1235, 2003.

[48] I. L. Medintz, J. H. Konnert, A. R. Clapp, I. Stanish, M. E. Twigg, H. Mattoussi, J. M. Mauro, and J. R. Deschamps. A fluorescence resonance energy transfer-derived structure of a quantum dot-protein bioconjugate nanoassem-

bly. *Proceedings of the National Academy of Sciences of the United States of America*, 101(26):9612–9617, 2004.

[49] K. E. Sapsford, L. Berti, and I. L. Medintz. Materials for fluorescence resonance energy transfer analysis: Beyond traditional donor-acceptor combinations. *Angewandte Chemie International Edition*, 45(28):4562–4589, 2006.

[50] C. A. Villee. *Biology*. Saunders College Pub., Philadelphia, 1989.

[51] I. L. Medintz, E. R. Goldman, M. E. Lassman, and J. M. Mauro. A fluorescence resonance energy transfer sensor based on maltose binding protein. *Bioconjugate Chemistry*, 14(5):909–918, 2003.

[52] L. Tolosa, H. Szmacinski, G. Rao, and J. R. Lakowicz. Lifetime-based sensing of glucose using energy transfer with a long lifetime donor. *Analytical Biochemistry*, 250(1):102–108, 1997.

[53] S. Chinnayelka and M. J. McShane. Glucose sensors based on microcapsules containing an orange/red competitive binding resonance energy transfer assay. *Diabetes Technology and Therapeutics*, 8(3):269–278, 2006.

[54] Y. Ohiro, H. Ueda, N. Shibata, and T. Nagamune. Enhanced fluorescence resonance energy transfer immunoassay with improved sensitivity based on the fab'-based immunoconjugates. *Analytical Biochemistry*, 360(2):266–272, 2007.

[55] U. Schobel, I. Coille, A. Brecht, M. Steinwand, and G. Gauglitz. Miniaturization of a homogeneous fluorescence immunoassay based on energy transfer using nanotiter plates as high-density sample carriers. *Analytical Chemistry*, 73(21):5172–5179, 2001.

[56] U. Schobel, H. J. Egelhaaf, A. Brecht, D. Oelkrug, and G. Gauglitz. New-donor-acceptor pair for fluorescent immunoassays by energy transfer. *Bioconjugate Chemistry*, 10(6):1107–1114, 1999.

[57] H. M. McEvoy. *Development and Optimisation of Patterned Optical Immunosensors*. PhD thesis, 2005.

[58] E.F Ullman, M. Schwarzberg, and K.E Rubenstein. Fluorescent excitation transfer immunoassay. a general method for determination of antigens. *J Biol Chem*, 251:4172–4178, 1976.

[59] M. Massey, W. R. Algar, and U. J. Krull. Fluorescence resonance energy transfer (FRET) for DNA biosensors: FRET pairs and Förster distances for various dye-DNA conjugates. *Analytica Chimica Acta*, 568(1-2):181–189, 2006.

[60] C.W. Liu, Y.W. Lin, C.C. Huang, and H.T. Chang. Fluorescence detection of single-nucleotide polymorphisms using a thymidine-based molecular beacon. *Biosensors and Bioelectronics*, 24:2541–2546, 2009.

[61] B. S. Gaylord, A. J. Heeger, and G. C. Bazan. Dna detection using water-soluble conjugated polymers and peptide nucleic acid probes. *Proceedings of the National Academy of Sciences of the United States of America*, 99(17):10954–10957, 2002.

[62] X. Chen and P. Y. Kwok. Template-directed dye-terminator incorporation (TDI) assay: a homogeneous DNA diagnostic method based on fluorescence resonance energy transfer. *Nucl. Acids Res.*, 25(2):347–353, 1997.

[63] P. Christian, F. Von der Kammer, M. Baalousha, and Th. Hofmann. Nanoparticles: structure, properties, preparation and behaviour in environmental media. *Ecotoxicology*, 17(5):326–343, 2008.

[64] K. L. Kelly, E. Coronado, L. L. Zhao, and G. C. Schatz. The optical properties of metal nanoparticles: The influence of size, shape, and dielectric environment. *J. Phys. Chem B*, 107:668–677, 2003.

[65] M. Faraday. Experimental relations of gold (and other metals) to light. *Philos. Trans*, 147(145), 1857.

[66] G. Mie. Beitrage zur optik trueber medien speziell kolloidaler metalloesungen. *Ann. Phys.*, 25:377–445, 1908.

[67] M. Kerker. *The Scattering of Light and Other Electromagnetic Radiation.* Academic: New York. 1969.

[68] C. F. Bohren and D. R. Huffman. *Absorption and scattering of light by small particles*. Wiley, New York, 1983.

[69] U. Kreibig and M. Vollmer. *Optical properties of Metal Clusters*. Springer Series in Materials Science. Springer-Verlag Berlin Heidelberg, 1995.

[70] M. Quinten, A. Leitner, J. R. Krenn, and F. R. Aussenegg. Electromagnetic energy transport via linear chains of silver nanoparticles. *Opt. Lett.*, 23:1331, 1998.

[71] C. A. Mirkin, R. L. Letsinger, R. C. Mucic, and J. J. Storhoff. A DNA-based method for rationally assembling nanoparticles into macroscopic materials. *Journal of the American Chemical Society*, 382:607, 1996.

[72] S. A. Maier and H. A. Atwater. Plasmonics: Localization and guiding of electromagnetic energy in metal/dielectric structure. *Journal of applied physics*, 95:011101, 2005.

[73] S. A. Maier, M. L. Brongersma, P. G. Kik, S. Melzer, A. A. G. Requicha, and H. A. Atwater. Plasmonics - a route to nanoscale optical devices. *Advanced Materials*, 13(19, October 2):1501–1505, 2001.

[74] O. Stranik. *Plasmonic enhancement of fluorescence for biomedical diagnostics*. PhD thesis, 2007.

[75] S. Shuming Nie and S. Emory. Probing single molecules and single nanoparticles by surface-enhanced raman scattering. *Science*, 275(5303):1102, 1997.

[76] D. S. Wang and M. Kerker. Absorption and luminescence of dye-coated silver and gold particles. *Physical Review B*, 25(4):2433–2449, 1982.

[77] J. Gersten and A. Nitzan. Spectroscopic properties of molecules interacting with small dielectric particles. *Journal of Chemical Physics*, 75(3):1139–1152, 1981.

[78] H. Chew, P. J. McNulty, and M. Kerker. Model for raman and fluoresecent scattering by molecules embedded in small particles. *Physical review A*, 13(1):396–404, 1976.

[79] A. M. Glass, P. F. Liao, J. G. Bergman, and D. H. Olson. Interaction of metal particles with adsorbed dye molecules: Absorption and luminescence. *Optics Letters*, 5:368–370, 1980.

[80] A. Wokaun, H. P. Lutz, A. P. King, U. P. Wild, and R. R. Ernst. Energy-transfer in surface enhanced luminescence. *Journal of Chemical Physics*, 79(1):509–514, 1983.

[81] K. Sokolov, G. Chumanov, and T. M. Cotton. Enhancement of molecular fluorescence near the surface of colloidal metal films. *Analytical Chemistry*, 70(18):3898–3905, 1998.

[82] H. Ditlbacher, N. Felidj, J. R. Krenn, and F. R. Aussenegg. Electromagnetic interaction of fluorephores with designed two-dimentional silver nanoparticle arrays. *Appl. Phys. B Laser and Optics*, 73(4):373–377, 2001.

[83] G. Chumanov, K. Sokolov, B. W. Gregory, and T. M. Cotton. Colloidal metal-films as a substrate for surface-enhanced spectroscopy. *Journal of Physical Chemistry*, 99(23):9466–9471, 1995.

[84] R. F. Aroca, G. J. Kovacs, C. A. Jennigs, R. O. Loutfy, and P. S. Vincett. Fluorescence enhancement from langmuir-blodgett monolayers on silver island films. *Langmuir*, 4:518–521, 1988.

[85] J. Kummerlen, A. Leitner, H. Brunner, F. R. Aussenegg, and A. Wokaun. Enhanced dye fluorescence over silver island films - analysis of the distance dependence. *Molecular Physics*, 80(5):1031–1046, 1993.

[86] C. Louis, S. Roux, G. Ledoux, L. Lemelle, P. Gillet, O. Tillement, and P. Perriat. Gold nano-antennas for increasing luminiscence. *Advanced Materials*, 16(23-24):2163–2166, 2004.

[87] D. A. Weitz, S. Garoff, J. I. Gersten, and A. Nitzan. The enhancement of raman-scattering, resonance raman-scattering, and fluorescence from molecules adsorbed on a rough silver surface. *Journal of Chemical Physics*, 78(9):5324–5338, 1983.

[88] P. Anger, P. Bharadwaj, and L. Novotny. Enhancement and quenching of single-molecule fluorescence. *Physical Review Letters*, 96:113002, 2006.

[89] S. Kuhn, U. Hakanson, L. Rogobete, and V. Sandoghdar. Enhancement of single-molecule fluorescence using a gold nanoparticle as an optical nanoantenna. *Physical review letters*, 97(7 July):017402, 2006.

[90] C. McDonagh, O. Stranik, R. Nooney, and B. D MacCraith. Nanoparticle strategies for enhancing the sensitivity of fluorescence-based biochips. *Nanomedicine*, 4(6):645–656, 2009.

[91] J. R. Lakowicz, J. Malicka, I. Gryczynski, Z. Gryczynski, and C. D. Geddes. Radiative decay engineering: the role of photonic mode density in biotechnology. *Journal of physics D: Applied Physics*, 36:R240–R249, 2003.

[92] J. R. Lakowicz, B. Shen, and I. Gryczynski. Intrinsic fluorescence from DNA can be enhanced by metallic particles. *Biochem. Biophis. Res. Commun.*, 286:875–879, 2001.

[93] C. D. Geddes, H. Cao, I. Gryczynski, Z. Gryczynski, J. Fang, and J. R. Lakowicz. Metal-enhanced fluorescence (MEF) due to silver colloids on a planar surface: Potential application of indocyanine green to in vivo imaging. *Journal of Physical Chemistry A*, pages 3443–3449, 2003.

[94] C. D. Geddes and J. R. Lakowicz. Metal-enhanced fluorescence. *Journal of Fluorescence*, 12:121–129, 2002.

[95] C. R. Sabanaygam and J. R. Lakowicz. Increasing the sensitivity of DNA microarrays by metal-enhanced fluorescence using surface-bound silver nanoparticles. *Nucleic Acids Research*, pages 1–9, 2006.

Chapter 2

Theoretical Background

2.1 Introduction

In this chapter the principles of fluorescence and Fluorescence Resonance Energy Transfer are presented. Firstly, photoluminescence is explained and the concept of electron energy levels in a molecule is introduced. The absorption and emission processes of a molecule are also described. The next section defines fluorescence resonance energy transfer and the factors that influence this effect. In the last section of this chapter the interaction between fluorescent dyes and the localised surface plasmon resonance of a metal nanoparticle is introduced and explained.

2.2 Absorption and Emission Processes

Photoluminescence is the process in which a substance absorbs electromagnetic radiation of a certain energy and subsequently emits radiation of a lower energy. Two types of photoluminescence are distinguished - fluorescence and phosphorescence. In both of these cases an electron is excited to a higher energy state and then returns to a lower energy state accompanied by the emission of a photon. However, the processes by which the molecule emits the photon differ. The period of time between absorption and emission is extremely short, on the order of 10^{-8}s for fluorescence processes. In phosphorescent materials, molecules can be excited by photon absorption to energy levels, said to be metastable, which are states that last much longer, from 10^{-3}s up to even a few seconds or as long as

minutes. In a collection of such molecules, many will de-excite to the lower state quickly, but many will remain in the excited state for much longer. Hence light will be emitted even after long periods [1]. These substances are known more commonly as 'glow in the dark' materials.

In order to understand the complex processes of photoluminescence, the energy levels in a molecule must be defined. Molecules have discrete energy levels that depend on the structure of the molecule in accordance with quantum theory. A molecule can absorb electromagnetic radiation by promoting an electron to a higher energy level or in other words into an excited state. The energy levels can be classified in energy terms in the following order rotational $<$ vibrational $<$ electronic. Each of these transitions differ typically by an order of magnitude. Rotational transitions occur at lower energies in the microwave region, with energies typically of 10^{-3}eV. Vibrational transitions occur in the near infra-red, requiring energies of $> 10^{-1}$eV. Finally, electronic transitions occur in the ultraviolet and visible region of the electromagnetic spectrum, and these require higher energies of 1eV. Fig. 2.1 shows the different energy levels in a molecule and how an electron can be promoted to different levels via absorption of energy. 'A' represents pure rotational changes labeled R_1, R_2, R_3 (far infrared); 'B' represents vibrational transitions labeled V_0, V_1; 'C' represents electronic transitions (visible and ultraviolet) where E_0 is electronic ground state and E_1 is the electronic excited state.

2.2.1 Absorption Process

In order for fluorescence to occur, a molecule must first absorb a photon. If this photon has energy equal to, or greater than, the energy difference between the ground state and the excited state, it can be absorbed, otherwise the photon will be transmitted. When a photon is absorbed, its energy is transferred to the valence electron and this electron is promoted to a higher electronic orbit, thus putting the molecule into the excited state. This transition period between states is very fast, of the order of 10^{-15}s.

The molar absorptivity (ε) of a substance is a measure of how strongly it absorbs light of a given wavelength and is usually measured in $M^{-1}cm^{-1}$. Transi-

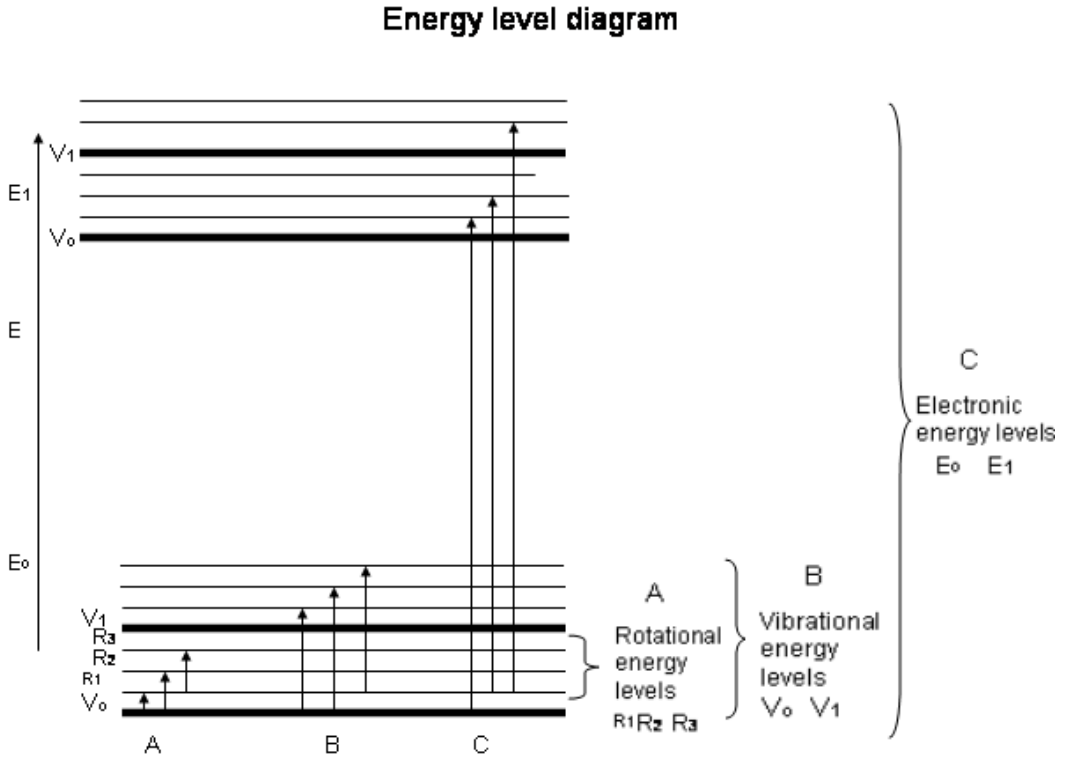

Figure 2.1: Energy level diagram describing A - the rotational changes, B - the vibrational changes and C - the electronic changes of the molecules energy.

tions which have a high probability to occur have molar absorptivities of $10^5 M^{-1}cm^{-1}$, whereas for transitions that are theoretically forbidden, the molar absorptivity is less than $10^{-4}M^{-1}cm^{-1}$ [2, 3]. Using a UV-Vis spectrophotometer (see Section 3.5.) it is possible to determine the molar absorptivity of a substance. The spectrophotometer gives an experimental value of the absorbance using transmittance values. Transmittance is the ratio of the intensity of light transmitted through a substance I_1, to the intensity of light that initially fell on the surface, I_0,

$$T = \frac{I_1}{I_0} \tag{2.1}$$

and absorbance (A) is defined as the negative logarithm of the transmittance,

$$A = -log(T) \tag{2.2}$$

The Beer Lambert Law states that there is also a logarithmic dependence between transmittance and the product of both the absorption coefficient α of the substance and the distance the light travels through the material, l; this

is illustrated in Fig. 2.2. The absorption coefficient is a product of the molar absorptivity, ε, and the concentration of absorbing species in the material, c, [4]. This gives the relationship below,

$$T = 10^{-\alpha.l} = 10^{-\varepsilon.c.l} \tag{2.3}$$

And combining Eqn.(2.2) and Eqn.(2.3) gives

$$A = \varepsilon.c.l \tag{2.4}$$

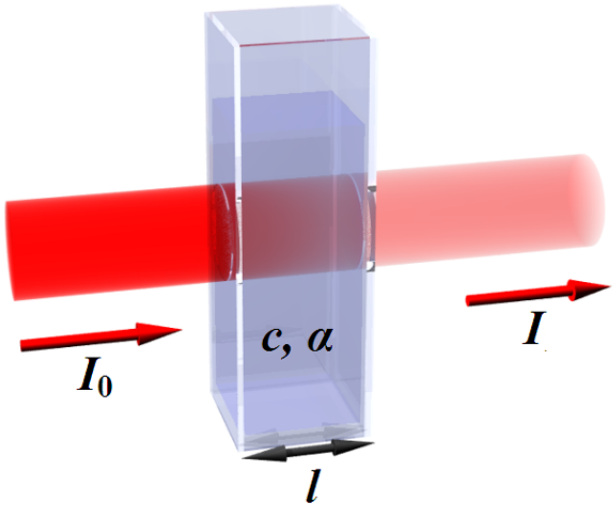

Figure 2.2: Diagram of Beer-Lambert absorption of a beam of light as it travels through a cuvette of width l.

2.2.2 Emission Process

A Jablonski diagram illustrates the electronic states of a molecule and the transitions between them. The states are arranged vertically by energy. Energetic levels with the same spin as the ground state are called singlet states and are indicated by the letter S [2]. Energetic levels with different spin to the ground state are called triplet states and are indicated by the letter T. Photoemission processes are typically dominated by transitions between singlet and triplet states. Non-radiative transitions are indicated by sinusoidal arrows and radiative transitions

by straight arrows. The vibrational ground states of each electronic state are indicated with thick lines, the higher vibrational states with thinner lines. The absorption and de-excitation processes of the molecule, as described above, are shown in the Jablonski diagram in Fig. 2.3.

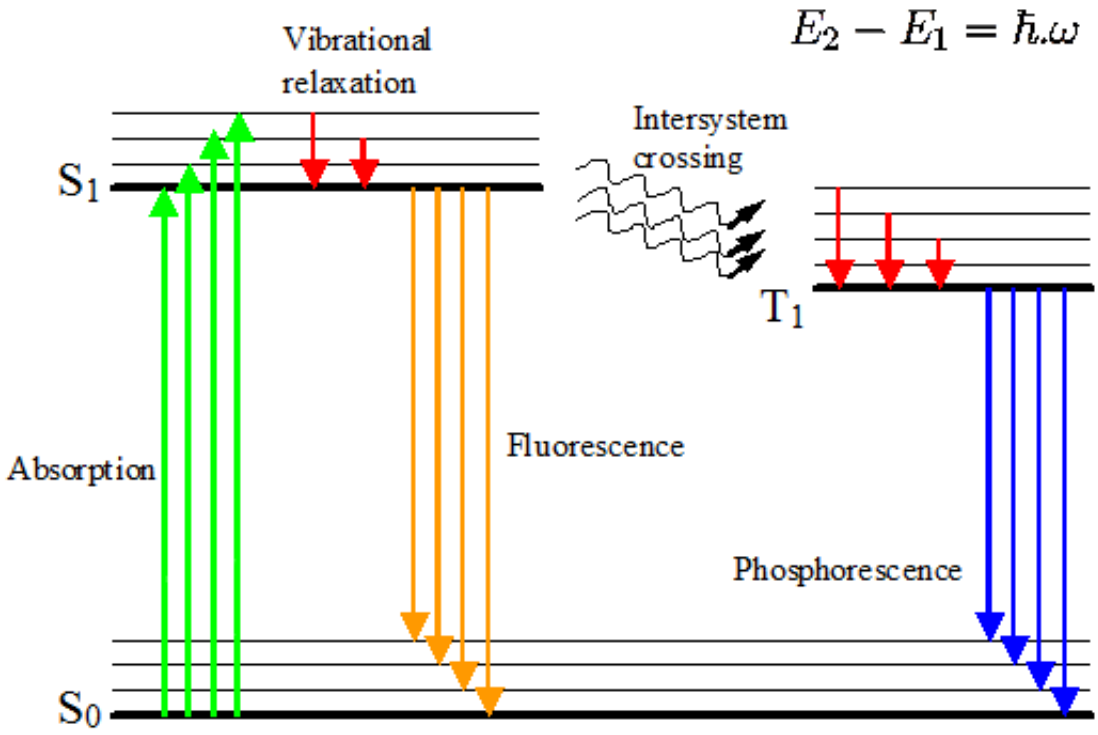

Figure 2.3: Jablonski diagram showing the de-excitation pathways of a molecule.

When an electron in a molecule has been energetically promoted to the excited state through the absorption of EM radiation, it returns to the ground state through radiative and non-radiative pathways. The radiative pathways involve photon emission and non-radiative pathways include energy transfer through collisions, resonance energy transfer through near field dipole-dipole interactions, photochemical decomposition etc. A change in the vibrational and rotational states of the molecule can also cause a loss of energy via a non-radiative route. As discussed previously, in the case of fluorescence the electron stays in the S_1 excited state typically for 10^{-8}s and returns to the ground state S_0 very quickly, on the order of 10^{-15}s. In phosphorescence, the molecule undergoes intersystem crossing where the electron in the S_1 state changes its spin and therefore its energy and relaxes into a triplet state T_1. De-excitation from this triplet state to the ground state results in the emission of a photon. The photon emitted will have

an angular frequency ω and energy $\hbar\omega$, where $\hbar$ is the reduced Planck constant. $\hbar\omega$ is related to the energy of each of the states as described by the equation in Fig. 2.3, where E_2 is the energy of the excited state and E_1 is the energy of the ground state. The emitted photon will generally have less energy than the photon that was absorbed due to rotational and vibrational changes.

The absorption and emission of energy are unique characteristics of a particular molecular structure. The difference in energy (or wavelength) between the absorbed photon and the emitted photon is known as the Stokes shift, as shown in Fig. 2.4. A large Stokes shift is often highly desirable as it reduces the need for optical filters, which are used to separate exciting light and fluorescence emission.

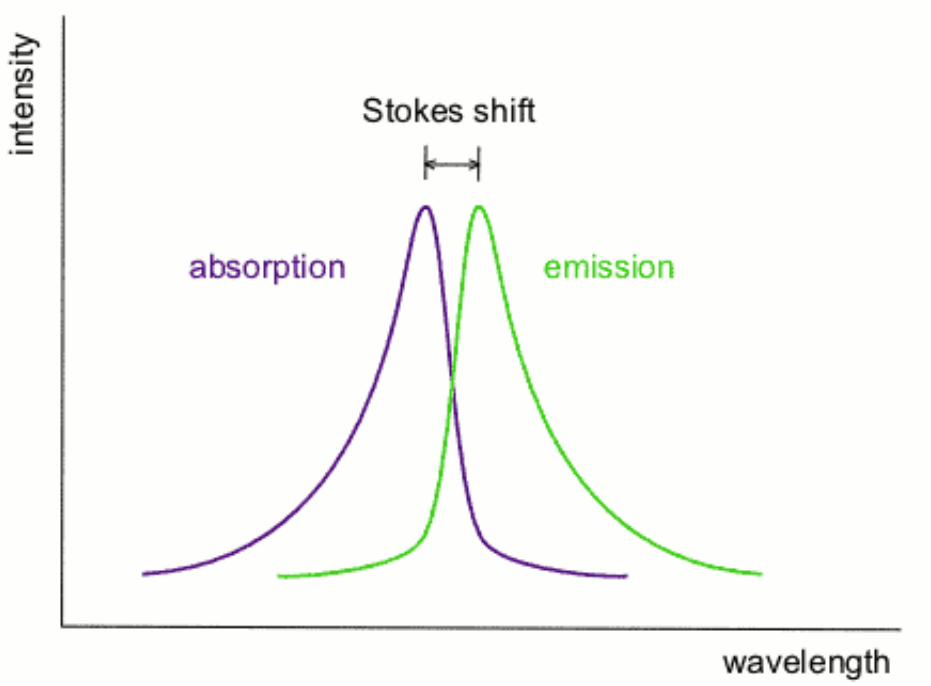

Figure 2.4: The absorption and emission bands of a molecule. The differences in wavelength between the peaks is known as the Stokes shift.

The efficiency of the fluorescence process is defined by its quantum yield, that is the ratio of the number of photons emitted to the number of photons absorbed

$$\Phi = \frac{\text{Number of photons emitted}}{\text{Number of photons absorbed}} \tag{2.5}$$

It can also be described using the rates of radiative, k_r and non-radiative, k_{nr} de-excitation of the electron.

$$\Phi = \frac{k_r}{k_r + k_{nr}} \tag{2.6}$$

The quantum yield can vary between 0 and 1, where 0 corresponds to non-fluorescing materials and 1 corresponds to highly fluorescent materials, where every photon absorbed results in a photon emitted.

The average time a molecule stays in its excited state before emitting a photon is known as the lifetime. Fluorescence intensity begins to decrease when the excitation ceases. This decrease depends on the rate of electron de-excitation and can be described by

$$I_t = I_0 e^{-\frac{t}{\tau}} \tag{2.7}$$

where

$$\frac{1}{\tau} = k_r + k_{nr} \tag{2.8}$$

τ is the fluorescence lifetime and is in the range of 10^{-8}s (0.5 - 20ns for most commonly used fluorescence transitions) [5]. For phosphorescence, the de-excitation rates are much lower than in the case of fluorescence and thus it follows that the phosphorescence lifetime is longer than that of fluorescence, typically of the order of 10^{-3}s. Lifetime is an important parameter for applications involving fluorescence resonant energy transfer. Fig. 2.5 shows the fluorescence intensity decay behaviour according to Eqn.(2.8) and how the lifetime is calculated, this will be discussed in more detail in Chapter 4. After initial excitation by a short pulse of electromagnetic radiation, the fluorescence intensity is at a maximum, I_{max}. This intensity decreases rapidly to zero, and the time taken for the intensity to reach $\frac{I_{max}}{e}$ is defined as the lifetime, τ.

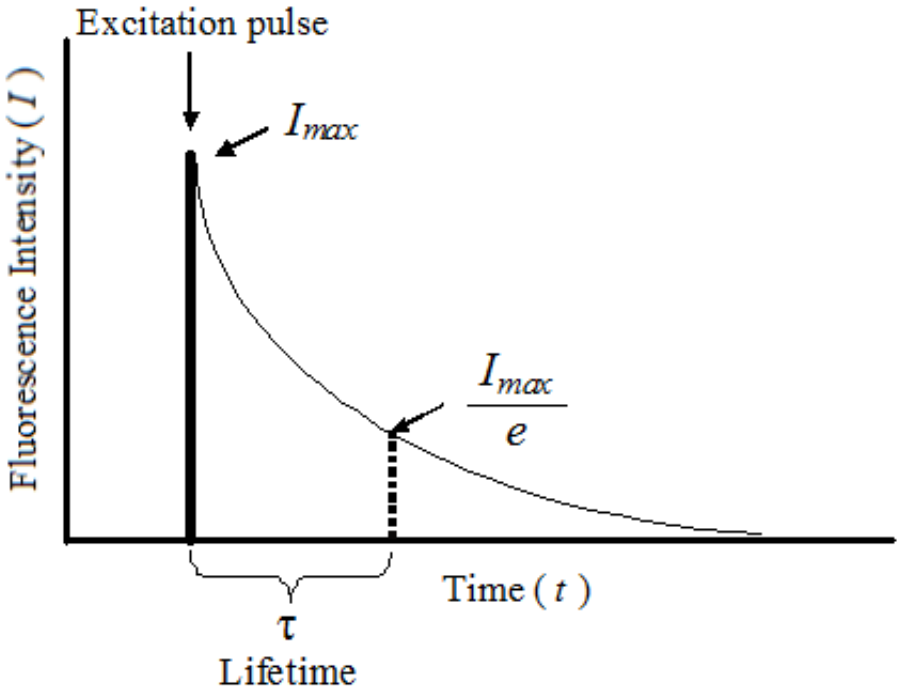

Figure 2.5: Fluorescence intensity exponential decay after excitation with a short excitation pulse.

2.3 Fluorescence Resonance Energy Transfer

As noted earlier, Föster resonance energy transfer (FRET) is a mechanism describing energy transfer between a donor molecule in an excited electronic state to an acceptor molecule [6]. The donor molecules typically emit at shorter wavelengths which overlap with the absorption spectrum of the acceptor. The energy is not emitted by the donor (D) as a photon, or absorbed as a photon by the acceptor (A), but is transferred by non-radiative pathways [5]. The perturbation of the excited D molecule on the A molecule takes place electrodynamically through space, as a dipole-dipole interaction. This interaction only takes place over a 0.5-10 nm range, limiting the distance over which FRET can occur. The rate of transfer of energy is a strong function of separation distance, and is proportional to $1/(distance)^6$. The distance at which the FRET efficiency is 50% is known as the Förster Radius (R_0) [6] and is typically in the range of 2-6nm. Suitable donor/acceptor pairs require:

- Sufficient spectral overlap of the emission and absorption spectra

- High quantum yield of donor

- High absorption coefficient of acceptor

- Matching orientations of the donor and acceptor dipoles

In order for FRET to occur the acceptor does not have to be fluorescent, but if it is, it emits a photon following transfer, which is characteristic of the acceptor fluorescence spectrum, although only D has been initially excited. Fig. 2.6 shows this process for the ideal case of two molecules with a large Stokes shift. 'A' illustrates that if the distance between the donor and acceptor molecule is beyond the FRET limit and the system is excited, donor emission can be observed but no energy transfer occurs and there is no emission of the acceptor. However when the donor and acceptor are within the FRET limit energy transfer can occur and both donor and acceptor emission can now be seen, with the donor emission reduced. 'B' shows how the emission spectra of the donor and acceptor change for non-FRET and FRET. 'C' shows how the lifetime of the donor changes for non-FRET and FRET, where a reduction in lifetime occurs. The fluorescence lifetime of a fluorophore depends on both radiative and non-radiative processes. Energy transfer from the donor molecule to the acceptor molecule causes an increase in the non-radiative rate and a decrease in the radiative rate of the donor, this results in a decreased lifetime of the donor.

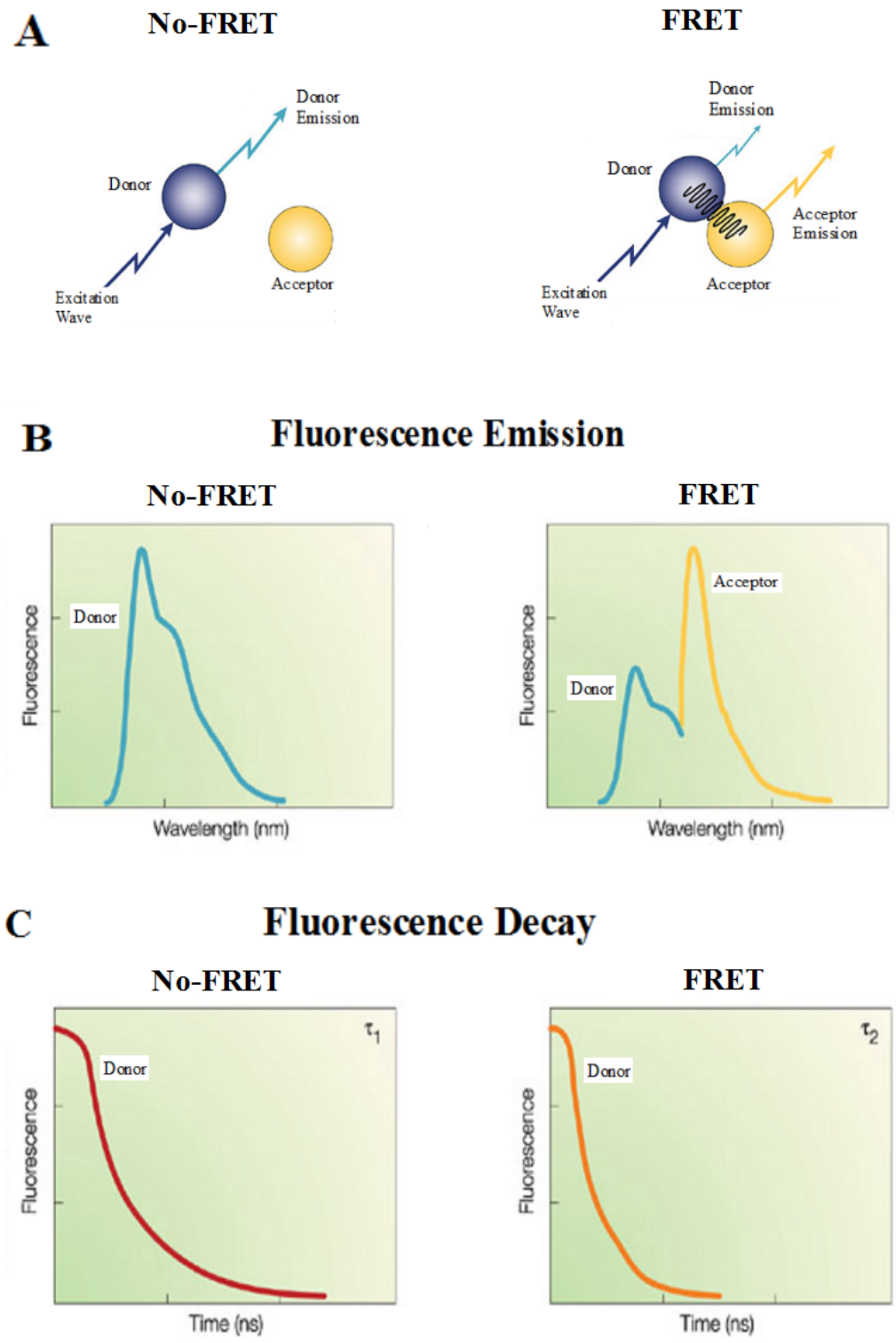

Figure 2.6: Fluorescence emission and fluorescence decay spectra of non-FRET and FRET systems. A - Donor and acceptor molecule interaction, B - Fluorescence emission for non-FRET and FRET, C - Fluorescence decay for non-FRET and FRET. Adapted from [7].

2.3.1 Mathematical Modeling of FRET

The following is a list of the various quantities involved in the equations that govern FRET. While a comprehensive treatment of the theory is outside the scope of this thesis, the principal relevant equations are developed below [5].

Rate of energy transfer	k_T
Lifetime of the Donor	τ_D
Lifetime of the D in the presence of A	τ_{DA}
Förster Radius	R_0
Molar absorptivity	ε_A
Dipole orientation factor	κ
Quantum yield of the Donor	Φ_D
Overlap integral	$J(\lambda)$
Fluorescence spectrum of the Donor	$F_D(\lambda)$
Refractive index of the medium	n
D-A separation distance	r
Fluorescence of D in the presence of A	F_{DA}
Fluorescence of D in the absence of A	F_D

The rate of energy transfer from a donor to an acceptor is given by:

$$k_T = \frac{1}{\tau_D}\left(\frac{R_0}{r}\right)^6 \tag{2.9}$$

The overlap integral ($J(\lambda)$) expresses the degree of spectral overlap between the donor emission and the acceptor absorption:

$$J(\lambda) = \frac{\int_0^\infty \varepsilon_A(\lambda).F_D(\lambda).\lambda^4 d\lambda}{\int_0^\infty F_D(\lambda)d\lambda}[M^{-1}cm^3] \tag{2.10}$$

The distance at which the FRET efficiency is 50% is known as the Förster Radius (R_0):

$$R_0 = 0.211\left[\kappa^2.n^{-4}.\Phi_D.J(\lambda)\right]^{\frac{1}{6}}[\mathring{A}] \tag{2.11}$$

where κ is the dipole orientation factor and n is the refractive index of the medium.

The efficiency of energy transfer is the fraction of photons absorbed by the donor that are transferred to the acceptor non-radiatively and is given by:

$$E_T = \frac{k_T}{\tau_D^{-1} + k_T} \tag{2.12}$$

Equations (2.9) and (2.12) can be rearranged to yield:

$$E_T = \frac{R_0^6}{R_0^6 + r^6} \tag{2.13}$$

However the transfer efficiency is typically measured using the fluorescence intensity of the donor, in the absence (F_D) and the presence (F_{DA}) of the acceptor. The transfer efficiency can also be calculated from the lifetimes under these respective conditions (τ_D and τ_{DA}):

$$E_T = 1 - \frac{\tau_{DA}}{\tau_D} \tag{2.14}$$

$$E_T = 1 - \frac{F_{DA}}{F_D} \tag{2.15}$$

These equations are derived from assumptions involving a single donor and a single acceptor separated by a fixed distance. This situation is frequently encountered for labeled proteins. A single fixed donor-acceptor distance is not found for a mixture of donors and acceptors in solution, nor for donors and acceptors dispersed randomly in membranes. This situation requires more complex expressions and such expressions are generally derived by averaging the transfer rate over the assumed spatial distribution of donor-acceptor pairs [8]. This will be discussed further in Chapter Four.

2.4 Interaction of Electromagnetic Radiation with Metal Nanoparticles

The interaction between light, fluorescent dyes and metal nanoparticles is very complex and has only been solved for specific structures [9]. There are three stages to the electromagnetic (EM) theory that describes it: (i) the interaction between the incident light and the metal nanoparticle, (ii) the interaction of the EM field around the metal nanoparticle and the fluorescent dye, and (iii) the interaction of the fluorescent dye with the metal nanoparticle. The first interaction, that of the incident light and the metal nanoparticle is predicted by Mie's theory of light scattering [10–14]. The theory predicts how plane wave illumination affects the distribution of the EM wave inside and outside the particle. A metal nanoparticle can be described as a dielectric with a positively charged core surrounded by negatively charged free electrons. When the EM wave interacts with the metal nanoparticle it acts like an oscillator, due to the movement of negative charges in the electric field, which causes polarisation on the surface. This phenomenon is demonstrated in Fig. 2.7.

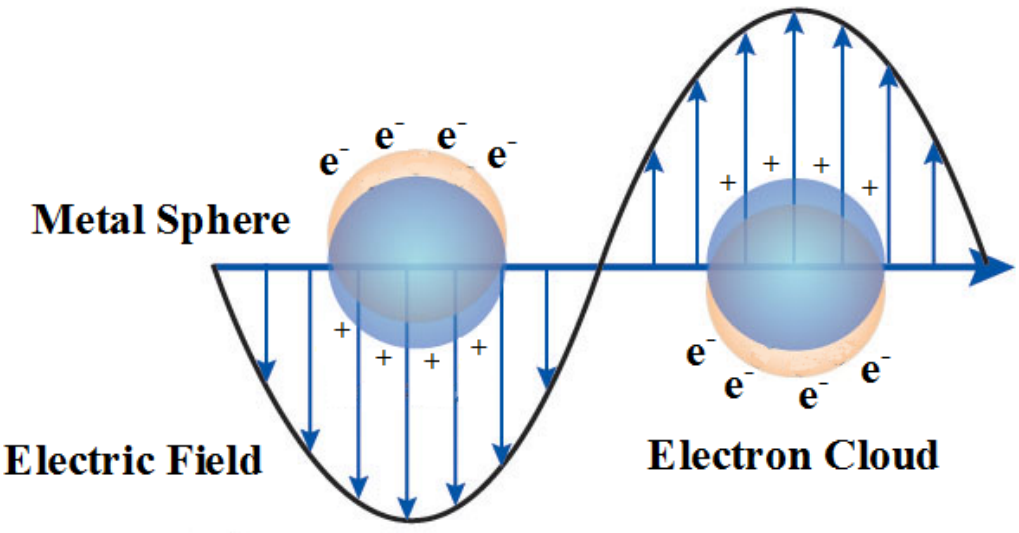

Figure 2.7: Induced polarisation of a metal nanoparticle due to interaction with electromagnetic radiation.

Localised Surface Plasmon Resonance (LSPR) occurs when the oscillating charged particle is in resonance with the incident EM wave. It is possible to observe this resonance by measuring the absorption spectrum of the metal nanoparticle. Since the wave is on the boundary of the metal and the external medium (air or water for example), these oscillations are very sensitive to any change in this boundary, such as the adsorption of molecules on to a metal surface. The Biacore surface plasmon resonance system exploits this with planar metal films for sensitive analyte detection, as mentioned in Chapter One [15]. LSPR causes an increase in the intensity of the EM field in the vicinity of the metal nanoparticle, but this increased intensity decreases rapidly with distance, and becomes insignificant within a few diameters of the nanoparticle [16]. The intensity on the surface can be two orders of magnitude greater than the initial intensity, depending on the shape of the particle. Fig. 2.8 shows a theoretical model of this localised enhancement of the electric field around an 80nm gold NP, calculated using the software package MaX-1. MaX-1 is a graphical electromagnetics platform which allows the user to compute, visualise and animate electromagnetic fields using numerical and analytical Maxwell techniques. This will be discussed further in Chapter 5.

The altered EM field around the metal nanoparticle changes the properties of a fluorescent dye that is placed in the vicinity. It can cause two enhancement effects: the first is an increase in the quantum efficiency of the dye and the second is an increase in the excitation rate of the dye. Eqn.(2.6) showed how the quantum efficiency is related to the radiative k_r, and non-radiative k_{nr}, decay rates. However, a new radiative pathway is formed when the dye molecule is in proximity to a metal nanoparticle. Taking this into account, Eqn.(2.6) can be modified to include new radiative, k_r^{NP}, and non-radiative, k_{nr}^{NP}, de-excitation rates due to the nanoparticle:

$$\Phi^{NP} = \frac{k_r + k_r^{NP}}{k_r + k_{nr} + k_r^{NP} + k_{nr}^{NP}} \tag{2.16}$$

The rate of k_r^{NP} and k_{nr}^{NP} are at a maximum when the resonance wavelength of the particle is equal to the emission peak wavelength of the fluorescent dye [17].

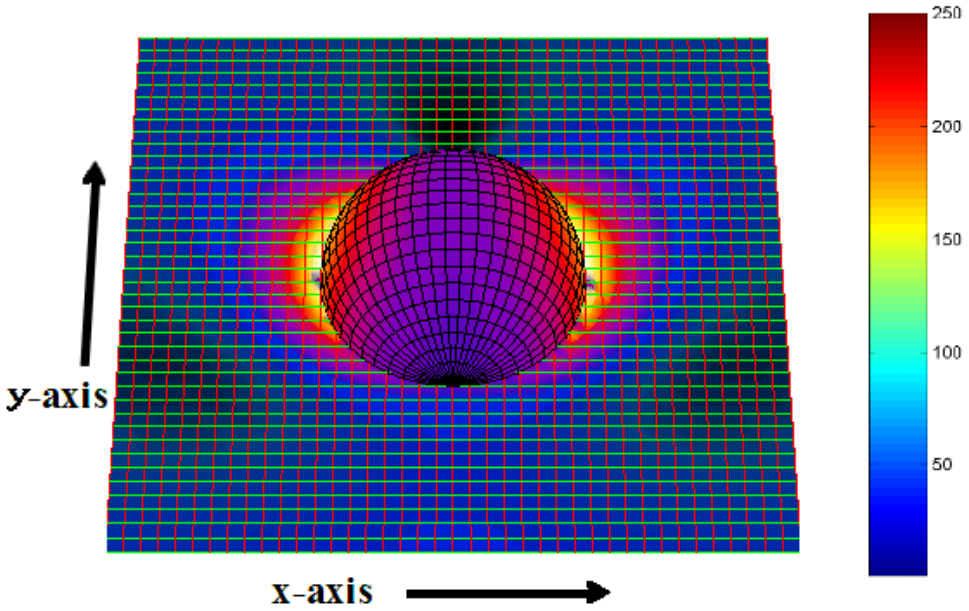

Figure 2.8: Localised enhancement of the electric field around a metal nanoparticle modeled using MaX-1. Polarization is along the x-axis and illumination is along the y-axis (λ520nm).

Fluorescent dyes with a low quantum efficiency receive the greatest enhancement, whereas dyes with a high quantum efficiency are not considerably improved. A decrease in the quantum efficiency of the dye can be seen if the dye is too close to the metal nanoparticle, typically within 5nm. This is due to non-radiative de-excitation of the dye due to the proximity of the metal [18, 19]. There is also an impact on the fluorescence lifetime of the dye due to its proximity to the nanoparticle, causing it to decrease [20]. This is shown in the modification of Eqn.(2.8), which now becomes

$$\frac{1}{\tau^{NP}} = k_r + k_{nr} + k_r^{NP} + k_{nr}^{NP} \tag{2.17}$$

where τ^{NP} is the modified fluorescence lifetime. This shortening of the lifetime also leads to increased photostability of the dye since the fluorophore will spend less time in the excited state and therefore be less susceptible to photobleaching [21].

The second effect of the EM field on the dye, the increase in the excitation

rate of the dye, is caused by the intense EM field around the metal nanoparticle. The excitation rate, k_{ex}^{i}, is directly proportional to the square of the intensity of the incident E-field, $\overrightarrow{E_i}$.

$$k_{ex}^{i} \propto \varepsilon(\lambda)|\hat{p_{ex}} \cdot \overrightarrow{E_i}|^2 \tag{2.18}$$

where $\varepsilon(\lambda)$ is the molar absorptivity of the dye and $\hat{p_{ex}}$ is fluorescent dye modeled as an oscillating electric dipole. When the dye is placed close to the nanoparticle, the electric field increases and the excitation enhancement factor (R_{ex}) can be defined as

$$R_{ex} = \frac{|\hat{p_{ex}} \cdot \overrightarrow{E_1}|^2}{|\hat{p_{ex}} \cdot \overrightarrow{E_i}|^2} \tag{2.19}$$

where $\overrightarrow{E_1}$ is the electromagnetic field amplitude generated by the metal nanoparticle. The enhancement factor is greatest for small particles of approximately 10nm and decreases with increasing size [22]. It is also dependent upon distance from the nanoparticle as the EM field intensity decreases rapidly with increasing distance. The increase is at a maximum when the absorption peak wavelength of the fluorescent dye coincides with the resonance wavelength of the particle [17]. This phenomenon will be discussed further in Chapter 4.

2.4.1 Fluorescence Enhancement of Silver and Gold Nanoparticles

The composition of the NP has a large influence on the induced metal-enhanced fluorescence (MEF) [23, 24]. Gold and silver NPs are the most commonly used NPs in MEF, with silver being the most dominant. One of the reasons for this is that silver NPs have a larger extinction cross section, C_{ext}, than gold NPs and therefore have a larger absorbance [22]. The extinction coefficient of a NP is the sum of the scattering cross section and the absorbing cross section and is related to the absorption (A) as shown in Eqn.(2.20).

$$A = 0.434\rho.C_{ext}.l \tag{2.20}$$

where ρ is the density of the particles and l is the pathlength.

Silver, however, is susceptible to etching from buffers containing salt and this is not desirable in biochip devices which tend to use biomolecules in a buffer solution. Some work has been carried out on preventing the silver from etching by using protective coatings [25]. Gold NPs do not suffer from the same degree of etching as silver. They also have a high chemical stability, the surface chemistry and surface modification is well understood and binding of biomolecules is accomplished easily [26]. In this work both gold and silver NPs are used. Chapter 4 describes the experimental work carried out using silver NPs, both spherical and triangular in shape, while Chapter 5 describes experimental work involving both gold and silver NPs.

2.5 DNA

Deoxyribonucleic acid (DNA) strands have been used in FRET-based biosensors as discussed in Chapter 1, where they are used as spacers between FRET dye pairs. DNA is a nucleic acid that not only contains genetic coding but is also used in a large range of biosensors. It is comprised of two long polymer strands and repeating units called nucleotides (or bases). There are four types of bases, and they are Adenine (A), Thymine (T), Guanine (G) and Cytosine (C), as shown in Fig. 2.9. Each base on one polymer strand forms a hydrogen bond with only one type of base on the other strand. A only bonds to T and G only bonds to C. This is known as complementary base pairing [27, 28]. The bases lie horizontally between the two spiraling polymer strands.

DNA does not exist as a single strand in living organisms but as two long interwinding strands in the shape of a double helix, as shown in Fig. 2.10. However the hydrogen bonds can be broken and rejoined relatively easily either by high temperatures (90°C) or mechanical force [29]. The rejoining of two complementary DNA strands is known as hybridisation.

DNA strands can be chemically synthesised to form relatively short fragments of nucleic acids with defined chemical structure or sequence, and are known as oligonucleotides. The sequence can be tailored to any given set of bases, and a

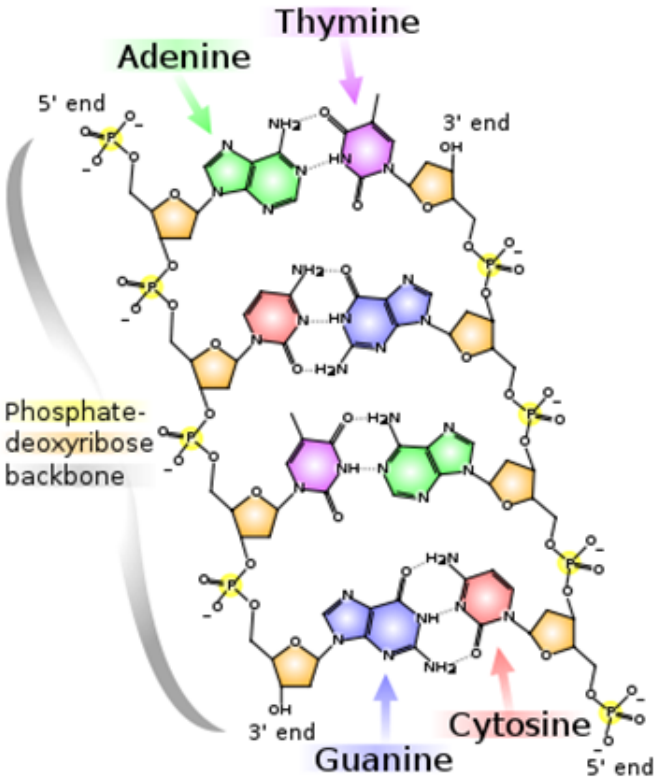

Figure 2.9: Chemical structure of the DNA.

Figure 2.10: A section of DNA. The bases lie horizontally between the two spiraling strands.

complementary or non-complementary strand can be used to test for comparability. The distance between each base pair (bp) is 0.34nm. This can be used to calculate the length of the desired strand. The oligonucleotides can also be labeled at either end with different functional groups or dye molecules. This can facilitate the attachment of the strands to surfaces and their chemical interaction monitored by fluorescence for example [30, 31]. In this work, DNA strands are used as spacers to control the distance between the FRET dye pair, and this is discussed further in Chapter 4 and Chapter 5.

2.6 Summary

This chapter describes the theory governing the interaction of electromagnetic radiation with fluorescent dyes and metal nanoparticles. The first section explained photoluminescence using energy level diagrams and the differences between fluorescence and phosphorescence. Next, the concept of fluorescence resonance energy transfer was introduced and the equations associated with this interaction were defined. The plasmonic enhancement of fluorescent dyes in proximity to a metal nanoparticle was then outlined. Two pathways of enhancement were described; emission enhancement via an increased quantum yield and excitation enhancement. The dependence on nanoparticle size and dye properties for this enhancement was also discussed. The interaction between FRET and the plasmonic enhancement of fluorescence in the presence of adjacent metal nanoparticles is the focus of the work in the following chapters. Finally, a short overview of the structure and properties of DNA was provided due to the fact that DNA was employed as a spacer in the FRET experiments described in Chapters 4 and 5.

References

[1] D. C. Giancoli. *Physics : principles with applications*. Prentice Hall, Upper Saddle River, N.J., 1998.

[2] G. Shenk. *Absorption of Light and Ultraviolet Radiation: fluorescence and phosporescence emission*. Allyn and Bacon chemistry series. Allyn and Bacon, Inc, Boston, 1973.

[3] L. D. S. Yadav. *Organic spectroscopy*. Kluwer ; Anamaya Publishers, Dordrecht [Netherlands]; Boston; New Delhi, 2005.

[4] D. Rendell and D. J. Mowthorpe. *Fluorescence and phosphorescence spectroscopy*. Published on behalf of ACOL, London by Wiley, Chichester [West Sussex]; New York, 1987.

[5] J. R. Lakowicz. *Principles of fluorescence spectroscopy*. Kluwer Academic/Plenum Publishers, New York, 1999.

[6] T. Förster. Intermolecular energy transfer and fluorescence. *Ann. Physics*, 2:55–75, 1948. [Translated by R. S. Knox].

[7] R. Rudolf, M. Mongillo, R. Rizzuto, and T. Pozzan. Looking forward to seeing calcium. *Nat Rev Mol Cell Biol*, 4(7):579–586, 2003.

[8] B. K-K. Fung and Lubert Stryer. Surface density determination in membranes by fluorescence energy transfer. *Biochemistry*, 17(24):5241–5248, 1978.

[9] D. S. Wang and M. Kerker. Absorption and luminescence of dye-coated silver and gold particles. *Physical Review B*, 25(4):2433–2449, 1982.

[10] G. Mie. Beitrage zur optik trueber medien speziell kolloidaler metalloesungen. *Ann. Phys.*, 25:377–445, 1908.

[11] C. F. Bohren and D. R. Huffman. *Absorption and scattering of light by small particles.* Wiley, New York, 1983.

[12] U. Kreibig and M. Vollmer. *Optical properties of Metal Clusters.* Springer Series in Materials Science. Springer-Verlag Berlin Heidelberg, 1995.

[13] D. L. Feldheim and C. A. Foss. *Metal nanoparticles - Synthesis, Characterization and Application.* Marcel Dekker, Inc., 2002.

[14] K. L. Kelly, A. A. Lazarides, and G. C. Schatz. Computational electromagnetics of metal nanoparticles and their aggregates. *Computing in Science & Engineering*, 3(4):67–73, 2001.

[15] D. G. Myszka. Analysis of small-molecule interactions using biacore s51 technology. *Analytical Biochemistry*, 329(2):316–323, 2004.

[16] D. D. Evanoff, R. L. White, and G. Chumanov. Measuring the distance dependence of the local electromagnetic field from silver nanoparticles. *Journal of physical Chemistry B*, 108:1522–1524, 2004.

[17] J. Kummerlen, A. Leitner, H. Brunner, F. R. Aussenegg, and A. Wokaun. Enhanced dye fluorescence over silver island films - analysis of the distance dependence. *Molecular Physics*, 80(5):1031–1046, 1993.

[18] T. Huang and R. W. Murray. Quenching of [Ru(bpy)3]2+ fluorescence by binding to Au nanoparticles. *Langmuir*, 18:7077–7081, 2002.

[19] R.R. Chance, A. Prock, and R. Silbey. Molecular fluorescence and energy transer near interfaces. *Adv. Chem. Phys.*, 60:1–65, 1978.

[20] J. R. Lakowicz, B. Shen, and I. Gryczynski. Intrinsic fluorescence from DNA can be enhanced by metallic particles. *Biochem. Biophis. Res. Commun.*, 286:875–879, 2001.

[21] J. R. Lakowicz. Radiative decay engineering: Biophysical and biomedical applications. *Analytical Biochemistry*, 298(1):1–24, 2001.

[22] O. Stranik. *Plasmonic enhancement of fluorescence for biomedical diagnostics*. PhD thesis, 2007.

[23] K. Aslan, M. Wu, and J. R. Lakowicz. Metal enhanced fluorescence solution-based sensing platform 2: Fluorescent core-shell Ag@SiO2 nanoballs. *Journal of Fluorescence*, 17:127–131, 2007.

[24] K. Aslan, M. Wu, J. R. Lakowicz, and C. D. Geddes. Fluorescent core-shell Ag@SiO2 nanocomposites for metal-enhanced fluorescence and single nanoparticle sensing platforms. *Journal of the American Chemical Society*, 129(6):1524–+, 2007.

[25] J. Zhang, J. Malicka, I. Gryczynski, and J. R. Lakowicz. Oligonucleotide-displaced organic monolayer-protected silver nanoparticles and enhanced luminescence of their salted aggregates. *Analytical Biochemistry*, 330(1):81–86, 2004.

[26] J. R. Lakowicz and J. Zhang. Metal-enhanced fluorescence of an organic fluorophore using gold particles. *Optical Express*, 15(5):2598–2606, 2007.

[27] J. D. Watson and F. H. C. Crick. Molecular structure of nucleic acids: A structure for deoxyribose nucleic acid. *Nature*, 171(4356):737–738, 1953.

[28] W. Saenger. *Principles of nucleic acid structure*. Springer advanced texts in chemistry. Springer-Verlag, New York, 1984.

[29] H. Clausen-Schaumann, M. Rief, C. Tolksdorf, and H. E. Gaub. Mechanical stability of single DNA molecules. *Biophysical Journal*, 78(4):1997–2007, 2000.

[30] J. Malicka, I. Gryczynski, and J. R. Lakowicz. DNA hybridization assays using metal-enhanced fluorescence. *Biochemical and Biophysical Research Communications*, 306(1):213–218, 2003.

[31] N. Mathur, A. Aneja, P. K. Bhatnagar, and P. C. Mathur. A new FRET-based sensitive DNA sensor for medical diagnostics using PNA probe and water-soluble blue light emitting polymer. *Journal of Sensors*, 2008.

Chapter 3

Materials and Methods

3.1 Introduction

This chapter focuses on the materials and methods that are common to the two experimental chapters, Chapters 4 and 5. Other techniques and methods that are specific to particular investigations are presented in the relevant chapters. This chapter begins with a description of the donor and acceptor dyes used to demonstrate the FRET interaction and why these dyes were chosen. The Layer-by-Layer deposition technique for ultra thin deposition of polyelectrolyte layers is also discussed and its versatility explored. Additionally, metal nanoparticles, whose size, shape and composition are tailored to the spectroscopic properties of the donor and acceptor molecules are described. Finally, the general experimental procedures and characterisation techniques are presented.

3.2 Fluorescence Dyes

In the first part of the work presented here, FRET was achieved using a donor ruthenium complex (Bis(2,2'-bipyridine)-5-isothiocyanato-phenanthroline)ruthenium bis(hexafluorophosphate)) whose fluorescence band at 610nm overlaps sufficiently with the absorption band of the Cy5 acceptor dye, which occurs at 650nm. The ruthenium dye complex (Ru-complex) has many benefits including its strong absorption, high quantum efficiency, and large Stokes shift. Cy5 is one of the most widely used fluorescent dyes for labeling biological molecules in immunoassays

and biochip arrays. The absorption and the emission wavelengths are in the visible red spectral region, which is sufficiently removed from the intrinsic fluorescence of most biological tissues, to suppress the background noise [1]. As a FRET pair, these two dyes have a very large Stokes shift, which reduces cross talk and improves the accuracy of the results. Table 3.1 gives the donor (Ru-complex) and acceptor (Cy5) dye properties while Fig. 3.1 shows the absorption and emission spectra of the donor and acceptor dyes. The overlap between the donor emission and the acceptor absorption is highlighted in grey. The extent of overlap contributes to the rate of energy transfer as described in Section 2.3.1. Both of these dyes can also be conjugated to a polyelectrolyte for deposition onto planar surfaces, as will be discussed in Section 3.5. One of the drawbacks to these dyes is that they are photosensitive and can photobleach easily when irradiated continuously, making them harder to handle. Photobleaching results in the loss of the dyes' ability to absorb light of a particular wavelength, due to photo degradation of the dye molecules, thus reducing their emission. This can be reduced by keeping the dye samples in the dark and limiting their exposure to ambient light [2].

	Excitation λ	Emission λ	Quantum Yield	Lifetime
Donor (Ru)	450nm	620nm	0.042	∼900ns
Acceptor (Cy5)	650nm	670nm	0.28	∼1.0ns

Table 3.1: Donor and acceptor dye properties.

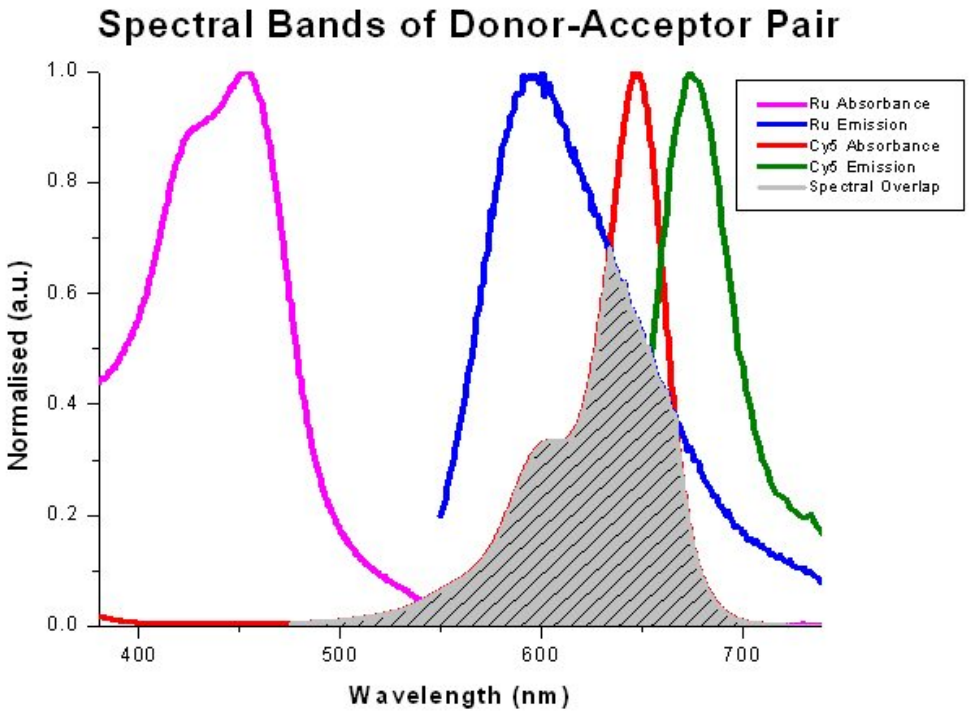

Figure 3.1: Absorption and emission spectra of the donor and acceptor dyes.

3.3 Layer-by-Layer Deposition of Polyelectrolytes

A model planar FRET system was designed, which was compatible with disposable biochips, in order to investigate the FRET-plasmonic interaction. As discussed previously, the FRET interaction is very sensitive to D-A separation. Highly controlled nm-scale polyelectrolyte separation layers between D and A were engineered using the technique of Layer-by-Layer (LBL) deposition. LBL deposition consists of the formation of ultra thin layers on substrates, where the thickness is controlled with nanometer precision. This technique utilises polyelectrolytes (PELs) which are electrostatically charged water soluble polymers. The chemical structure of the PELs determines whether they are positively or negatively charged, at a certain pH. The polyelectrolytes used in this work were poly(styrene sulphonate) (PSS-polyanion) and poly(allylamine hydrochloride) (PAH-polycation) and their chemical structure is shown in Fig. 3.2. Also shown in Fig. 3.2 are the chemical structures of poly(acrylic acid) (PAC-polyanion) and poly(diallyldimethylammonium chloride) (PDAC-polycation) which are used in conjunction with PAH and PSS in Chapter 4 and Chapter 5.

By alternately adsorbing oppositely charged polyelectrolytes onto a surface it

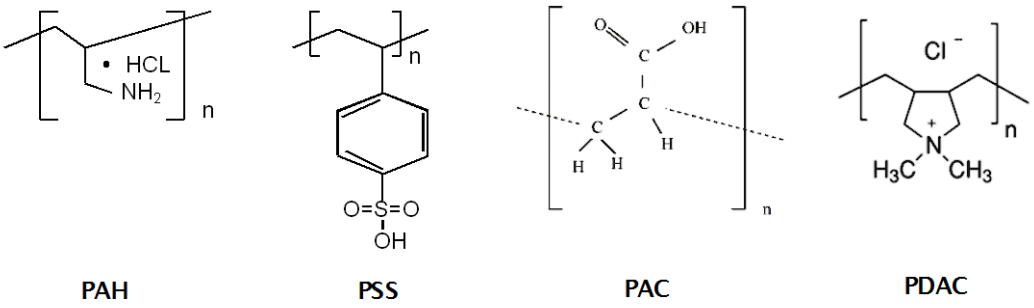

Figure 3.2: Chemical structure of the polyelectrolytes. PSS is negatively charged, PAH is positively charged at pH=7.

is possible to build up controlled multilayers of cross linked polyanion-polycation films. The thickness of these layers can be modified by pH and salt content. Reviews of this technique are given in references [3–6].

The steps involved in the LBL deposition are shown in Fig. 3.3. The process begins with a charged surface. Next a solution of oppositely charged polyelectrolyte is added Fig. 3.3(i). There is a strong electrostatic interaction between the charged substrate and the polymer which results in deposition of an ultra thin layer of polymer. The charge on the surface is converted to that of the PEL solution and this prevents further deposition of the polymer Fig. 3.3(ii). The substrate is washed repeatedly in deionised water to remove any excess polyelectrolyte. Next a solution of oppositely charged polyelectrolyte is added Fig. 3.3(iii). An ultra thin layer of polymer is deposited on the surface as before, causing a change in the charge on the substrate Fig. 3.3(iv). It is possible to build up multiple layers using this method, and the thickness and stability of the layer can be tailored by adjusting the pH and salt content of the PEL [7].

This PEL layering technique can be used to deposit a surface of known charge and thickness. It can also be used to immobilise fluorophores onto the surface. Dyes can be conjugated to one of the PELs and deposited easily upon the oppositely charged surface. Section 3.5 describes how the Ruthenium and Cy5 dyes were conjugated to a positively charged polymer, polyallylamine hydrochloride (PAH). PELs have also been used to deposit dyes at a controlled distance from nanoparticles [1, 8–10]. Both of these techniques were employed in the experiments reported in Chapter 4. The polyelectrolytes were used to space the donor

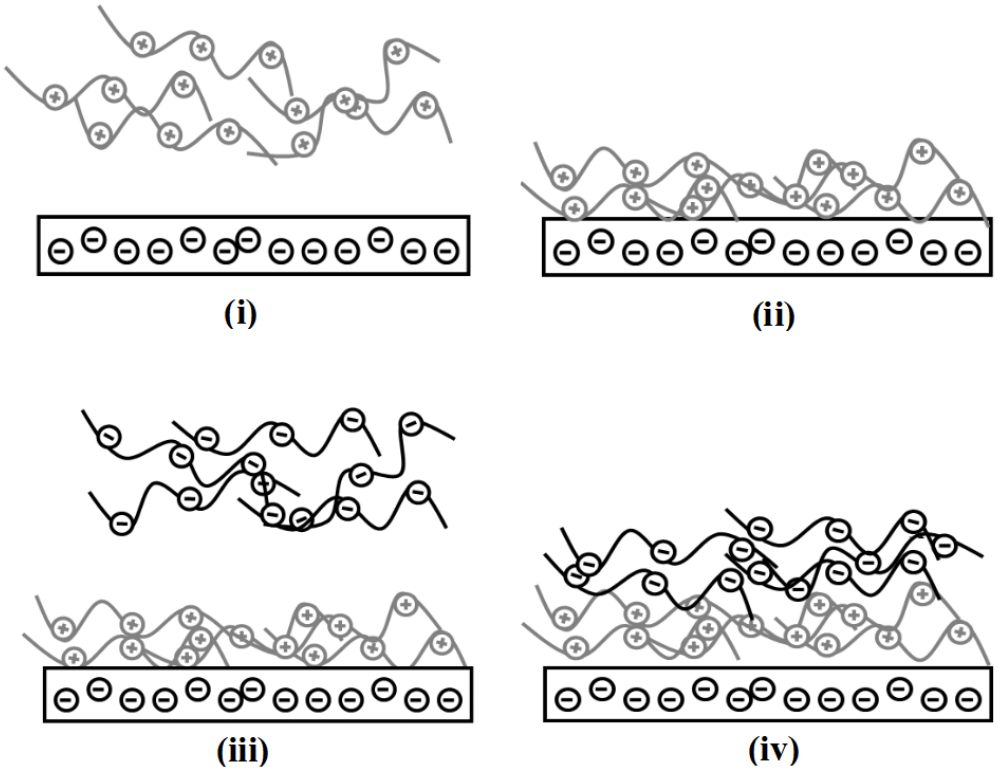

Figure 3.3: Layer-by-Layer deposition of polyelectrolytes.

and acceptor dyes a controlled distance apart. Fig.3.4 shows a schematic of the layering system used. To increase the donor-acceptor distance, more PEL layers were included between the two dye layers. Nanoparticles were added into the system and placed at different distances from the dyes. This is discussed further in Section 3.4.

3.4 Metal Nanoparticles

As discussed in Section 2.3 plasmonic enhancement of fluorescence has been extensively documented. The interaction results in significant enhancements in fluorescence when a fluorophore is in the vicinity of a metal NP [1]. It was proposed that using the plasmonic effect of metal NPs could increase the R_0 of the donor-acceptor pair, the details of which are discussed in Chapter 4. NPs were synthesised to correspond to the spectroscopic properties of the donor and acceptor molecules. Large spherical silver NPs with a diameter of 60nm with a

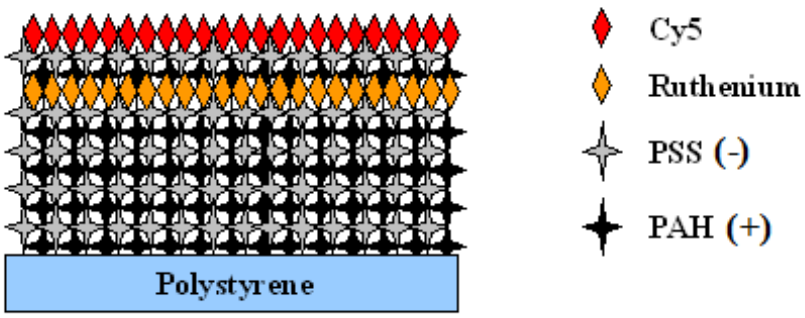

Figure 3.4: Schematic of PEL spacer layers.

plasmon resonance at 425nm corresponding to the donor absorption band and silver nanoprisms 163nm in size with a plasmon resonance at 650nm corresponding to the acceptor absorption were employed. Fig. 3.5 shows a Transmission Electron Microscope (TEM) image of the NPs, reproduced with permission [11].

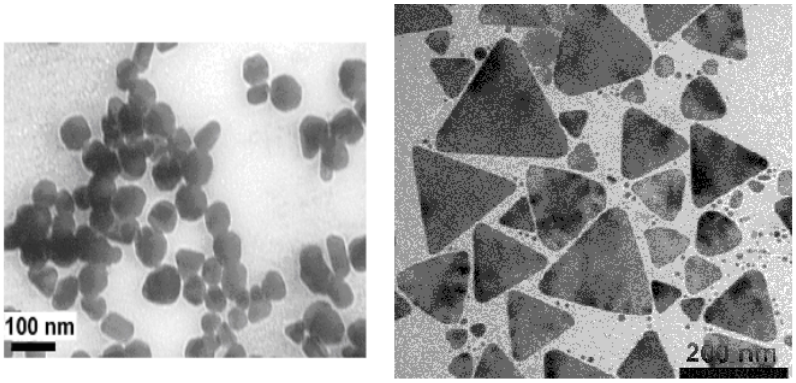

Figure 3.5: TEM of 60nm +/-11nm spherical silver NPs and 163nm triangular silver NPs [11].

It was possible to adjust the plasmon resonance of the nanoprisms by coating them with the polyelectrolytes. This blue-shifted the resonance peak to 600nm which corresponds to the centre of the spectral overlap of the dyes, see Fig. 3.6. This is caused by the change in refractive index of the medium around the NP, in accordance with Mie's theory of light scattering by spherical particles [12–14]. The metal NPs are all negatively charged and adsorb readily onto a positively charged polyelectrolyte. For this work the NPs were synthesised by Robert Nooney and Ondrej Stranik, two post doctoral researchers within the

Biomedical Diagnostics Institute (BDI). The spherical silver NPs were prepared by reducing silver nitrate with sodium citrate in the presence of aniline [15]. The triangular NPs were prepared by a photoconversion process, where 8nm silver NPs were illuminated with monochromatic light of the desired plasmon resonance for several hours, in order to form triangular NPs or nanoprisms [11].

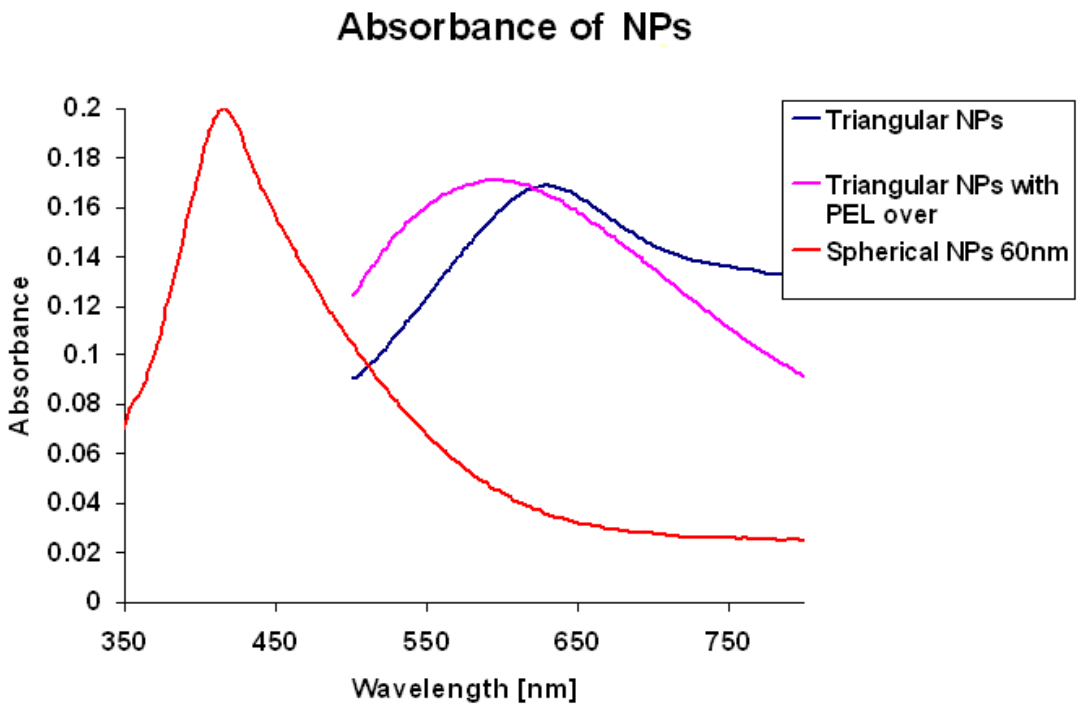

Figure 3.6: Absorption spectra of the NPs employed in the work presented here.

3.5 Experimental Procedures

There are numerous elements involved in the formation of the experimental system. Several of these experimental procedures are detailed below, including the deposition of the polyelectrolytes, the conjugation of the dye, the deposition of the NPs and the micropatterning of the dyes.

3.5.1 Polyelectrolyte LBL Technique

As indicated previously, PELs were used as a tool to create uniformly charged surfaces and as spacer layers. The first step in the LBL process was to activate the surface of the substrate in order to give it an initial charge. Two substrates were employed, a glass coverslip and a polystyrene microtiter plate. For glass surfaces activation was achieved by immersing the coverslip slides into a potassium hydroxide solution (1% KOH, 39% Water, 60% ethanol)and sonicated for 40 mins to remove any impurities. The slides were then rinsed in deionised water and dried in the oven for 15 mins at 35°C. Plasmas are ionised gases, which can be generated by applying strong electric or magnetic fields to a gas or by heating it to high temperatures [16]. The glass coverslips (Menzel Glaser) were placed in an oxygen plasma and exposed to a broad spectrum of ions, electrons, radicals and EM radiation. These species strongly interact with the first few nanometers of the polymer surface and in the case of glass and polystyrene, increase the negative charge density on the surface upon which the PELs could then be layered [17]. The plasma was generated using 5 sccm O_2 (standard cubic centimeters per minute), at 50W and 50mTorr for 1min. Later experiments were performed on clear bottomed microtiter plates (purchased from Greiner Bio-One International). Clear bottomed plates were used to allow for absorption measurements alongside fluorescence. The activation of the polystyrene microtiter plates was the same as described above - in an oxygen plasma. Each polyelectrolyte solution was prepared using 2mg/ml polyelectrolyte in deionised water (pH 7.4), with 0.5M NaCl. These concentrations yielded a deposited layer which was 1.5nm thick [11]. The PEL solution was then sonicated for 40mins at room temperature. The prepared glass coverslips were then immersed in the PEL solutions using a coverslip rack.

The surface of the microtiter plates was coated in PELs by the addition of 250μl of solution. In both cases the surfaces were left to incubate for 15mins. The surfaces were then washed with deionised water five times to ensure adequate removal of unbound PEL. The process was repeated with the oppositely charged PEL. Eight layers of alternating PELs were placed on top of the substrate to generate a uniformly charged surface for the attachment of PAH conjugated dyes or metal NPs in the sequence $[PSS/PAH]_x$, where x is the number of bilayers ($x = 4$ in this case). Any fewer layers than eight leads to non-uniformity in the layer and ambiguous charge on the surface [17].

3.5.2 Conjugation of Dyes to PEL

PELs were also conjugated to the donor and acceptor dyes in order to facilitate the deposition of reproducible fluorescence films. Both Ruthenium and Cy5 were conjugated to the positively charged polyallyamine hydrochloride (PAH). The Ruthenium dye was conjugated via the amine group of the PAH and the isothiocyanate group of the Ruthenium complex. Firstly, 4.7mg of PAH (5x10^{-5} mols of monomer) and 2.1mg of sodium hydrogen carbonate (25x10^{-5} mols) were dissolved in 0.25mL of water. Then 4.9mg of Ru-ITC (5x10^{-6} mols) was dissolved in 1mL Dimethylformamide (DMF). The solutions were then mixed under rapid stirring at 4°C and left to age for 2hours in darkness. The addition of acetone then caused the Ru-PEL to precipitate and this was filtered out. The absorption and emission peaks for the Ru-PEL are 450nm and 620nm respectively, as shown on Fig. 3.7. Cy5 was conjugated using a slightly different method. 200mg PAH was dissolved in 4ml deionised water and left to dissolve overnight. The Cy5 Mono NHS ester (1mg) was mixed with 200μl of DMSO or DMF. The PAH solution was then placed on a stirrer and set at a speed of 300rpm. The dye solution was added to the stirring PAH solution 50μl at a time. The solution was then placed in aluminium foil and put on a bench rocker for 2hours. The dye solution was then placed into separating columns (Sigma Aldrich 30kDa), with 1ml in each column. The columns were centrifuged at 4,000rpm for 5mins, the filtrate was removed and 4ml of deionised water was added to the concentrate to buffer exchange. This water exchange was repeated 4 times. This concentration

of dye was the stock solution with a value of 1.0 and all future concentration values were diluted from this. The absorption and emission peaks for the Cy5-PEL were 650nm and 670nm respectively, see Fig. 3.7. Both dyes were later put through a series of dilutions to obtain the optimum FRET interaction.

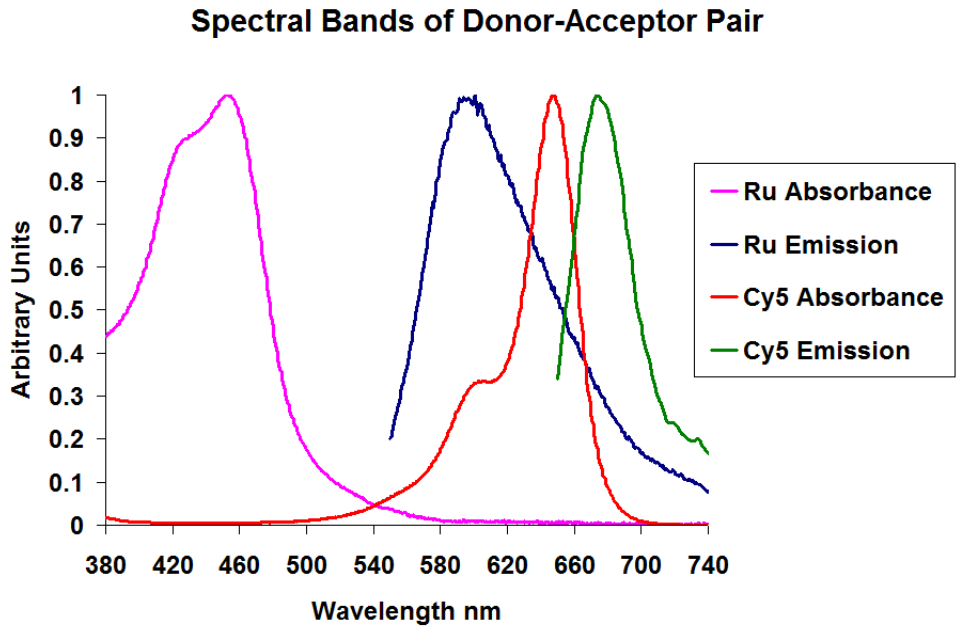

Figure 3.7: Absorption and emission spectra of the Ru-PEL and Cy5-PEL fluorescence dyes

3.5.3 Dye and NP Deposition

The Ru-PEL deposition onto the PEL surface was confirmed using fluorescence emission. This was performed on both glass and polymer substrates. After plasma treatment of the substrate, $[PAH/PSS]_4$ layers were deposited, generating a uniformly charged negative surface. Next a Ru-PEL layer was deposited and left to incubate for 15mins. The surface was then washed in deionised water 5 times. Fig. 3.8 shows an image of the Ruthenium emission on a glass coverslip. (A) shows the edge of a full deposited layer and (B) shows a line grid of Ru-complex. This was generated by adapting the stamp printing method described in [18], and is detailed below. Fig. 3.9 shows the emission spectrum of Ru-PEL obtained from a spectrophotometer, using the polystyrene microtiter plates. There is a

linear relationship between concentration of Ru-PEL and fluorescence intensity and this is shown in Fig. 3.10.

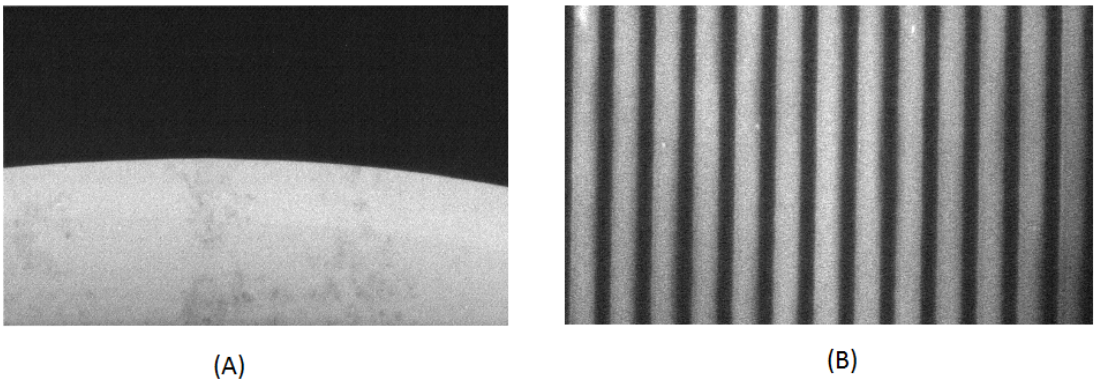

Figure 3.8: Ru-complex emission on a glass coverslip (A) shows the edge of a circular overlayer and (B) shows a line grid.

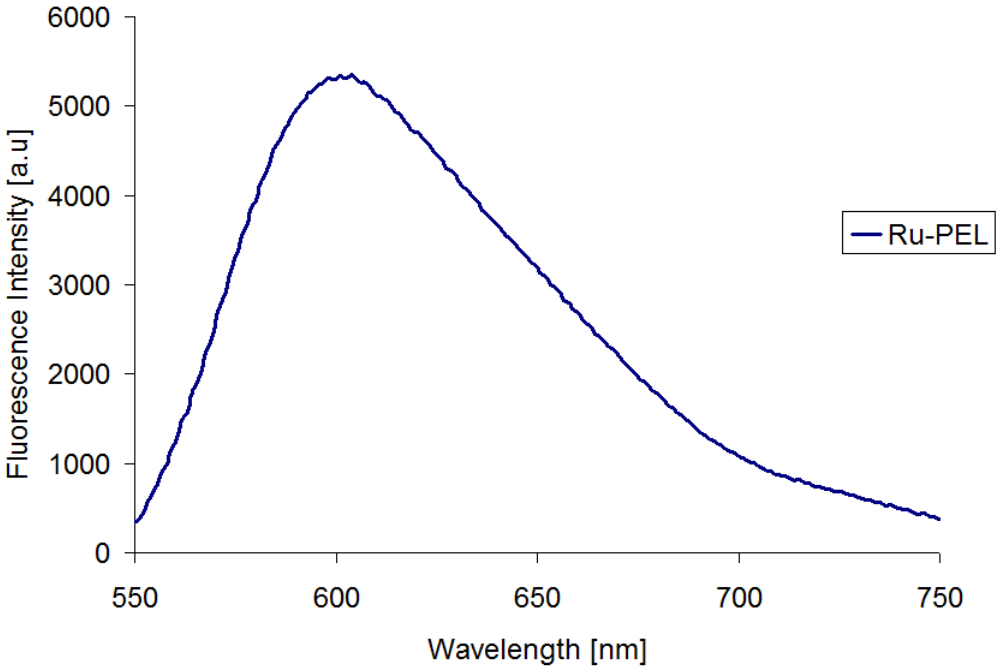

Figure 3.9: Ru-PEL emission spectrum on polystyrene (excitation λ450nm).

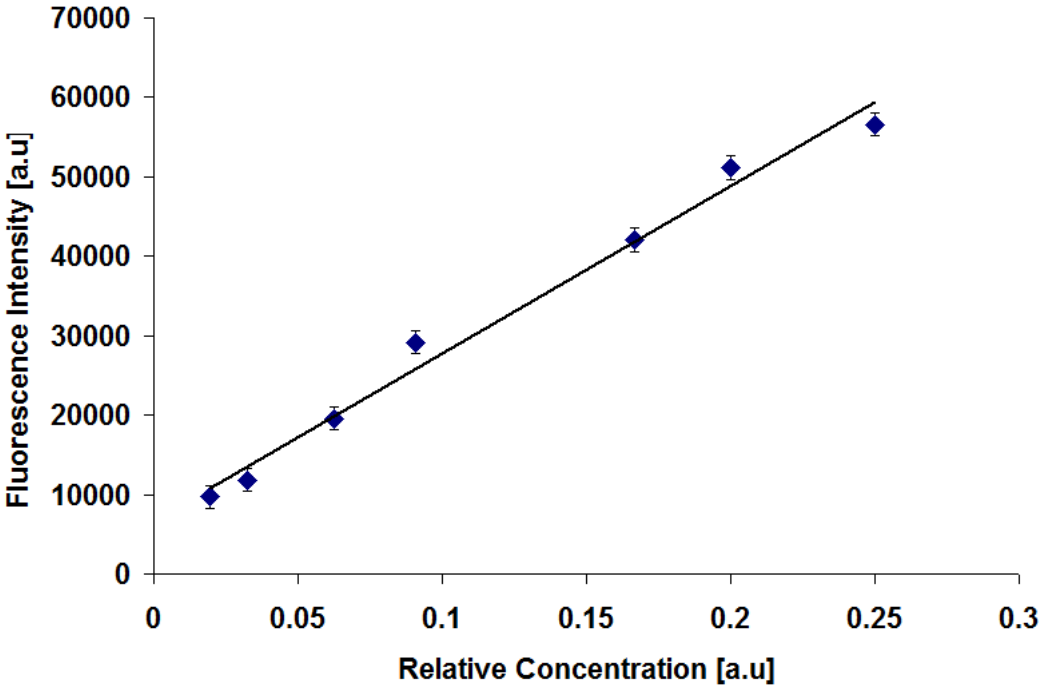

Figure 3.10: Fluorescence intensity variation of Ru-PEL with concentration.

Cy5 was attached to the PEL substrate using the same protocol as above. Evidence of the attachment on both glass and polystyrene is shown in Fig. 3.11 and Fig. 3.12 respectively. The fluorescence intensity dependence of Cy5 on the concentration is shown in Fig. 3.13. At high concentrations there is quenching of the fluorescence due to homo-FRET, the fluorescence peaks at the optimum concentration and then decreases with decreasing concentration.

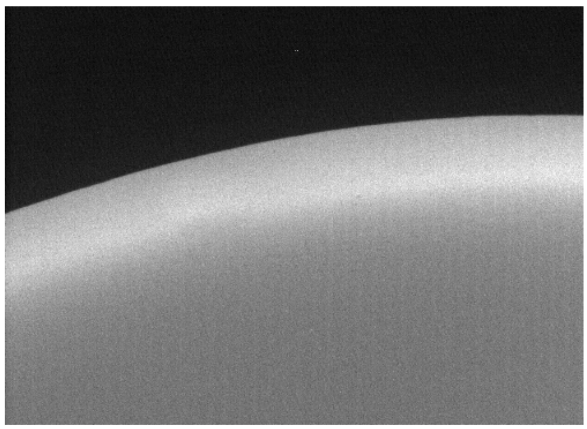

Figure 3.11: Cy5 emission on a glass coverslip. Edge of the circular overlayer can be seen.

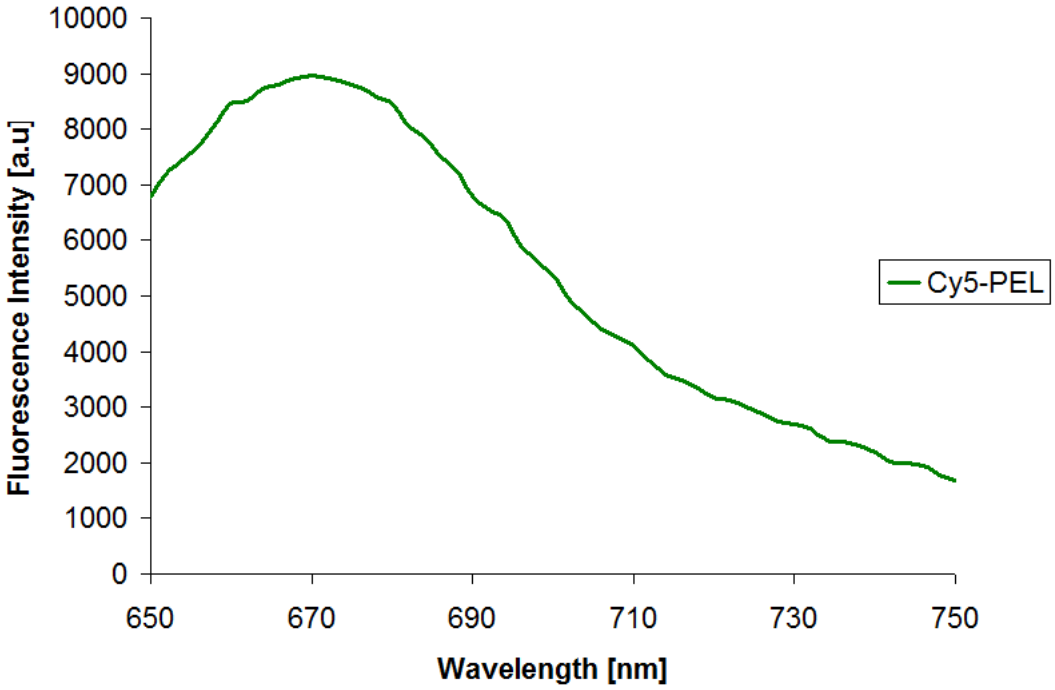

Figure 3.12: Cy5-PEL emission spectrum on polystyrene (excitation λ610nm).

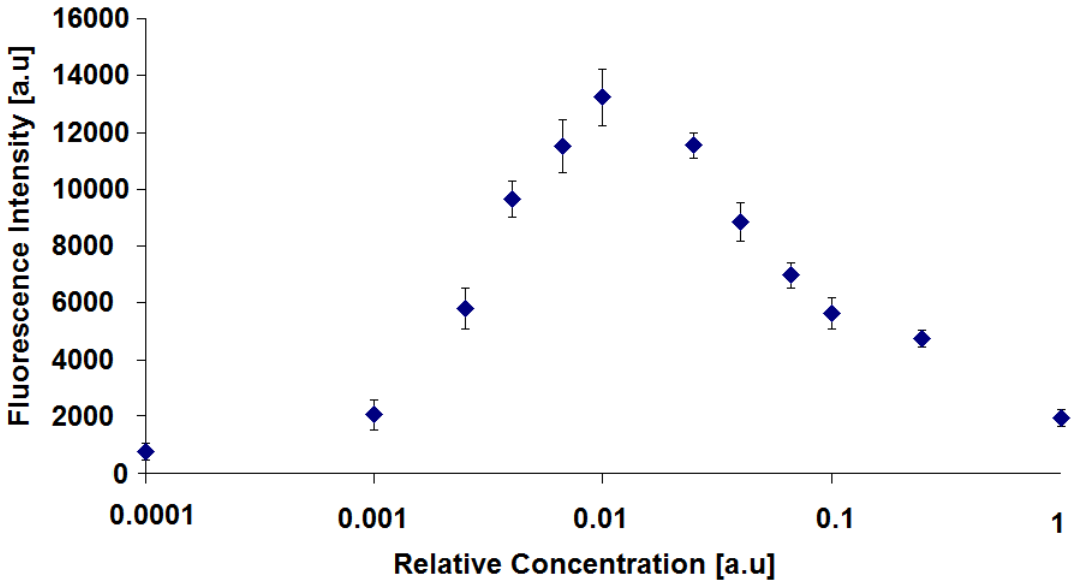

Figure 3.13: Fluorescence intensity variation of Cy5 with concentration.

The metal nanoparticles, which are negatively charged, were electrostatically attached to a positively charged PEL surface. Unlike spin coating or ink jet printing, where the NPs are physisorbed onto the surface quickly [11, 19], the NPs take a longer time to attach, and so are left in solution on the surface for up to 12 hours. Fig. 3.14 shows the upturned image of a microtiter plate after NP attachment and subsequent PEL layering. Each colour corresponds to a different number of PEL layers over the NPs. This colour change is due to the refractive index change around the NP, which alters the plasmon resonance wavelength. Fig. 3.15 shows the image of a microtiter plate with gold and silver NPs, again with their colour corresponding to their plasmon resonance wavelength.

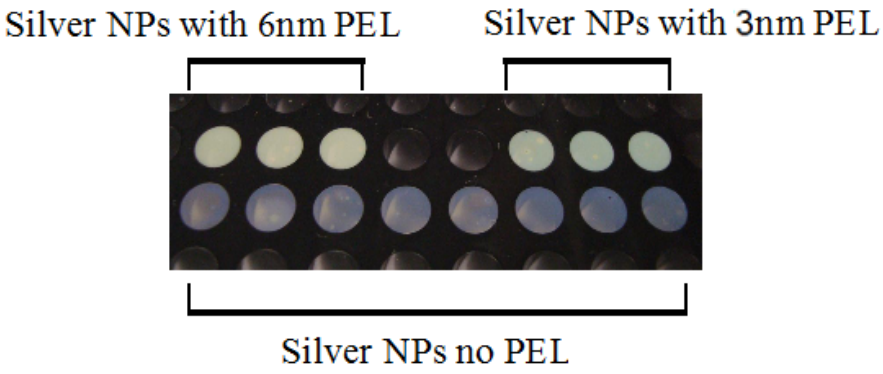

Figure 3.14: NPs with and without PEL overlayers.

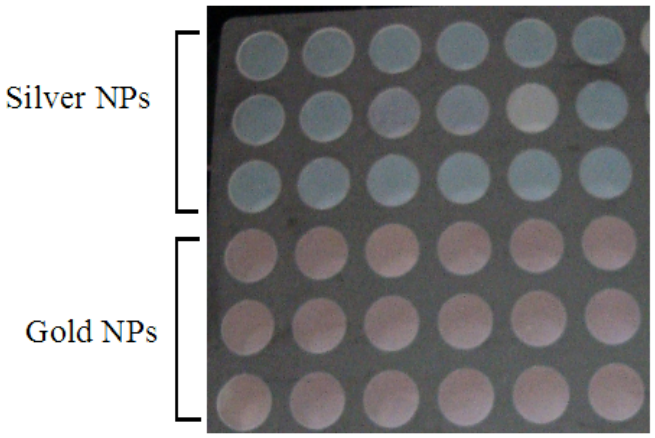

Figure 3.15: Gold and silver NPs.

The NPs were placed at increasing distance from a Ru-PEL layer. Fig. 3.16 shows that at distances <6nm the metal NP quenches the dye and at distances >6nm the dye is too far away from the NP to experience enhancement. The optimum distance to place the dye is at 6nm.

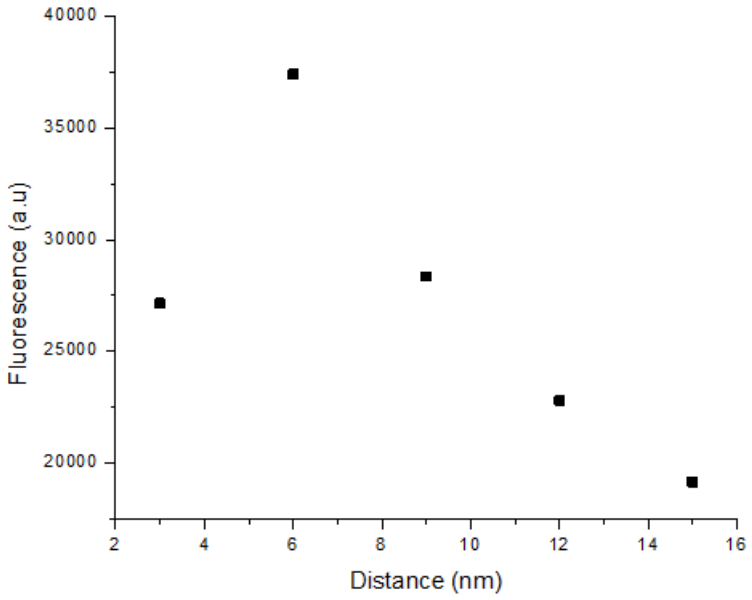

Figure 3.16: Distance dependence of the MEF of Ru-PEL dye with 60nm silver NPs.

3.5.4 Micropatterning Polymers

The micropatterning of polymers has been extensively investigated [20–23] and is a useful tool for patterning polymer surfaces. In this work, surfaces were patterned with dye using polymer stamps made from poly(dimethylsiloxane) (PDMS) in order to facilitate lifetime imaging of the surface, whereby specific areas could be located using the pattern. This is discussed in more detail in Chapter 4. PDMS is a silicone rubber formed from liquid prepolymer and a curing agent. The stamps were fabricated by adding 67.02g of PDMS elastomer base (Sylguard 184) to 6.702g of the curing agent and stirring. The mixture was then placed in a desiccator for 15mins to remove all of the bubbles. A silicon master,

which had parallel lines 10μm wide, 10μm high with 10μm spacing was cleaned and placed in an aluminium foil tray. The elastomer was then poured onto the silicon wafer. The mould was placed in an oven for 8 hours at 60°C. The wafer was removed carefully from the tray and the PDMS peeled off [18]. The stamps were cut out of the mould using a scalpel. This concept is illustrated in Fig. 3.17.

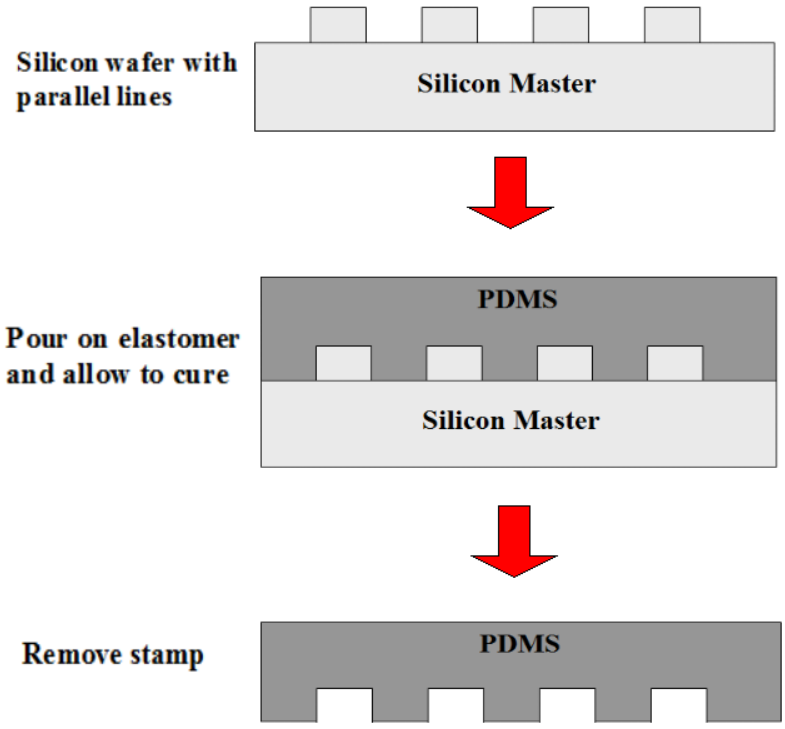

Figure 3.17: Illustration of the fabrication of a PDMS stamp.

In order to successfully micropattern the Ru-complex, an inking solution was developed. This inking solution consisted of 2.5g 20% poly(diallyldimethylammonium chloride) PDAC in H_2O which was added to 7.5ml H_2O and 10ml ethanol. The solution was sonicated for 15 mins and 200μl 10^{-5}M $Ru(dpp)_3$ was then added. The absorption and emission spectra of the Ru-dpp, as shown in Fig. 3.18, was similar to those for the Ru-PEL, however some adjustments had to be made to the theoretical predictions of the Förster Radius due to the change in the overlap between the donor and acceptor. This is discussed further in Chapter 4.

The process of micropatterning the coverslip surface involved preparing the

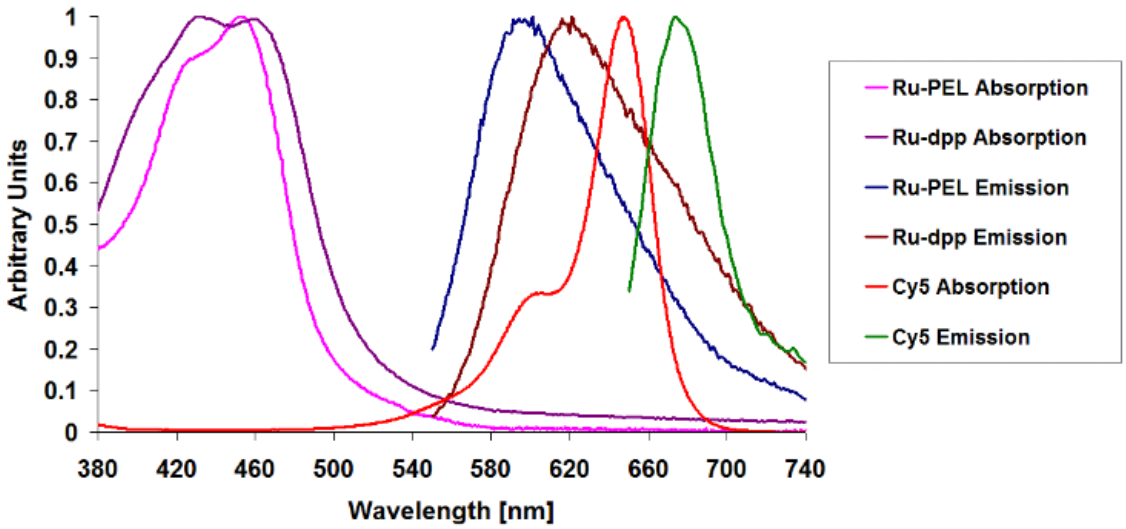

Figure 3.18: Absorption and emission spectra of the Ru-dpp dye

surface of the coverslip with a uniform charged PEL, as discussed in Section 3.5.1. The stamps were then washed in deionised water, dried in a nitrogen stream, and plasma treated to create a negative surface charge. The stamps were placed in the Ru-dpp inking solution for 10mins, washed briefly in a beaker of water to remove excess dye and placed in the oven to dry for 5mins at 40°C. The stamps were then placed carefully onto a negatively charged PEL layer on the coverslip. After 1 hour the coverslip was removed and washed in deionised water 3 times, sonicated for 2 seconds and dried in a nitrogen stream. Layers of PAH and then PSS were deposited immediately to prevent oxygen quenching of the Ru-dpp [24]. Fig. 3.19 illustrates the steps involved in the preparation of the dye micropatterned surfaces.

Fig. 3.20 shows the fluorescence of the Ru-dpp micropatterned lines. The deposition of Cy5 in clean lines was not as successful as with the Ru-dpp, as is shown in Fig. 3.21. For this reason, the Ru-dpp was micropatterned in the experiments, and the Cy5 was deposited in a circular overlayer.

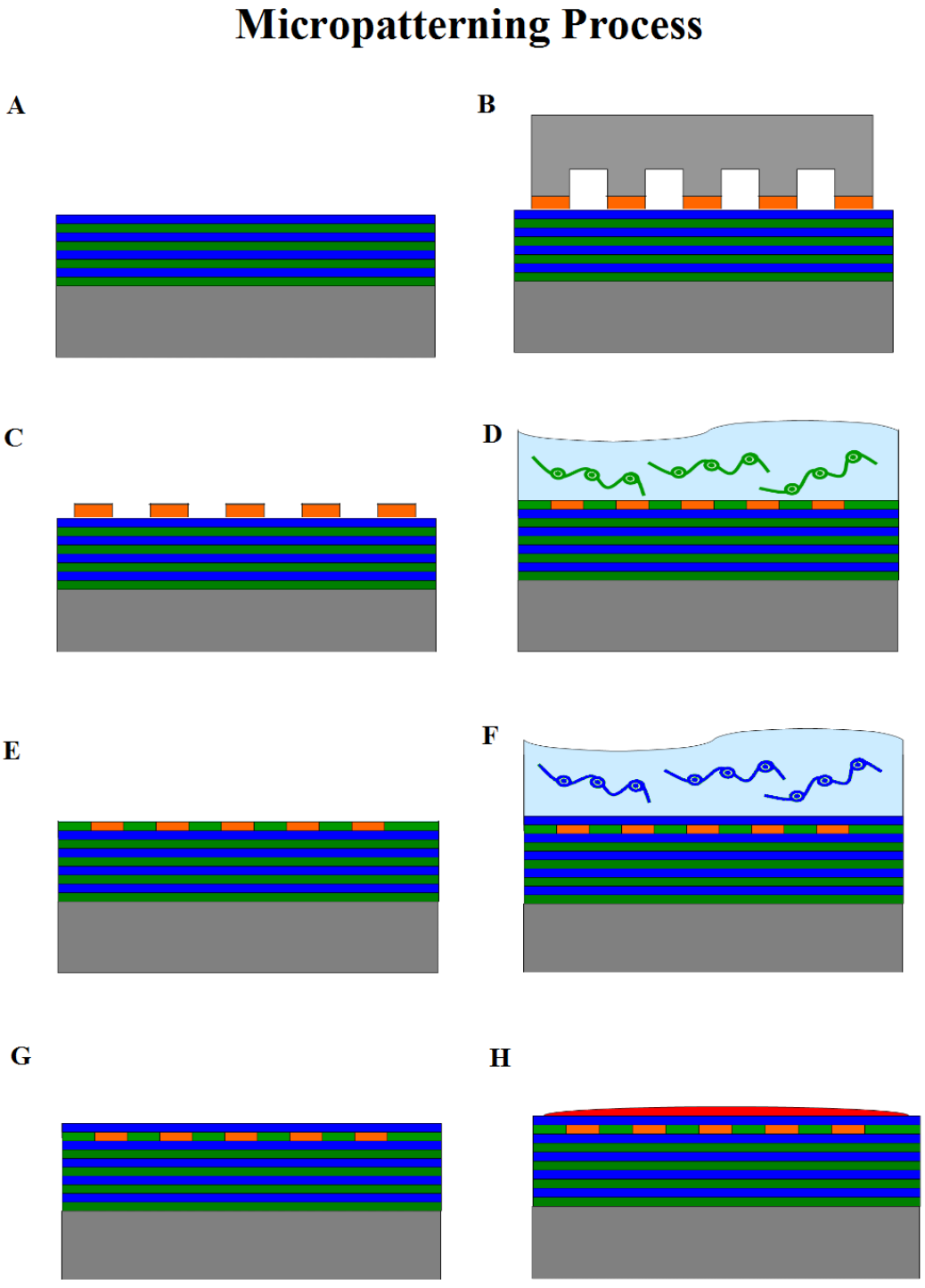

Figure 3.19: Illustration of the steps involved in the preparation of dye micropatterned surfaces. **A** - formation of PEL layers on glass coverslip **B** - stamp-printing of positively charged donor dye using PDMS stamp **C** - removal of stamp, leaving lines of donor dye on surface **D** - electrostatic adsorption of positive PEL **E** - washing of unbound PEL **F** - electrostatic absorption of negatively charged PEL **G** - washing of unbound PEL **H** - electrostatic absorption of circular accepter overlayer.

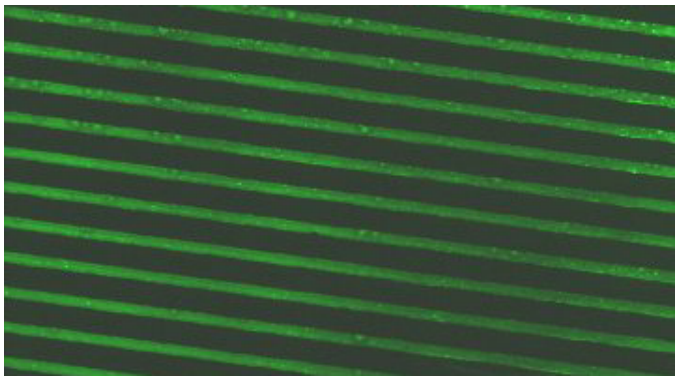

Figure 3.20: Ru(dpp) micropatterned lines (10μm) (excitation λ450nm).

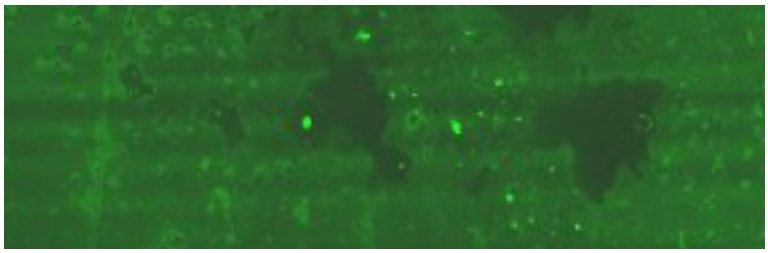

Figure 3.21: Cy5 micropatterned lines (10μm) (excitation λ610nm).

3.6 Instrumentation and Characterisation Techniques

Surface activation in plasma was performed on an Oxford Instruments PlasmaLab 80Plus (Abindon, Oxfordshire, UK) at 5 sccm O_2, 50 mTorr pressure, and 50 W power for 1 min.

The spectral analysis was performed on a Tecan Safire II Spectrophotometer. Light sources on this instrument are a high energy UV xenon flashlamp and light emitting diodes. The detector for fluorescence is an extended wavelength low dark current photomultiplier tube and for absorbance is a UV silicon photodiode. The UV-visible extinction spectra of the NPs and dyes in PAH solution were measured with a Cary 50 Scan UV-Visible Spectrophotometer (Varian) in transmission mode.

Fluorescence lifetime recordings were performed on a MicroTime 200 inverse time resolved fluorescence microscope (MT200, PicoQuant, Berlin, Germany). The microscope body comprised a modified Olympus IX71 equipped with a 60x water emersion lens (UPlanSApo 60x 1.2 water/CC1.48, Olympus). Sample illu-

mination was achieved using a horizontally polarised 440nm pulsed diode laser (LDH-P-C440, PicoQuant) operated at 500kHz, resulting in a 2μs pulse period. Fluorescence was separated from excitation using a 440/535nm dichroic filter (z440/535rpc, AHF/Chroma) and passed through a 550nm low pass emission filter (HQ550LP, AHF/Chroma). Emitted light passed through a 50/50 beam splitter (Olympus) and focused onto two single photon avalanche detectors (SPADs, Micro Photon Devices). Sections analysed were 40μm by 40μm in size and greater than 10000 counts were recorded for each sample. The resulting time correlated single photon counting lifetime histograms were fitted after the influence of the machine response function (IRF) using triple exponential fits. All data was analysed using SymPhoTime (PicoQuant).

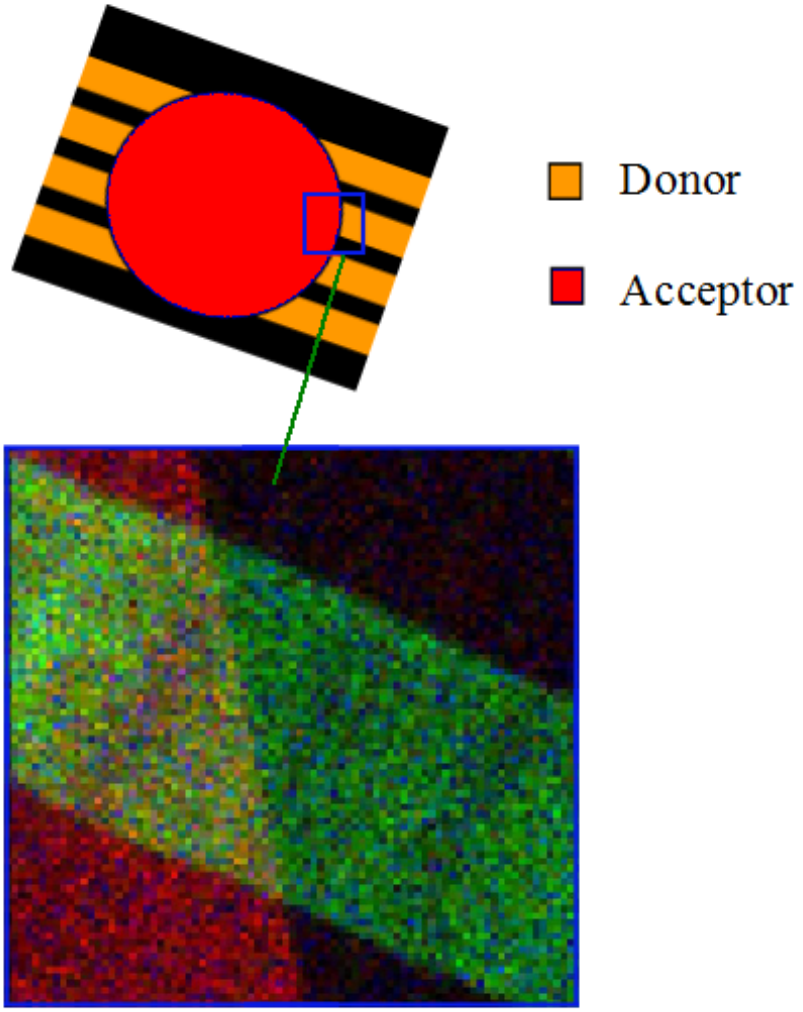

Figure 3.22: Area measured with FLIM (40μm x 40μm).

3.7 Summary

This chapter described the common processes and materials used in the two experimental chapters. The FRET dye pair used in Chapter 4 and the layer-by-layer deposition of ultra thin polyelectrolyte layers were described. The procedure for deposition of dye conjugates and nanoparticles was also explained. A micropatterning technique was also described which can print nanostructures onto surfaces with dyes or nanoparticles. Finally, the instrumentation used to characterise each of these processes was also introduced.

References

[1] O. Stranik, H. M. McEvoy, C. McDonagh, and B. D. MacCraith. Plasmonic enhancement of fluorescence for sensor applications. *Sensor and Actuators B*, 107(1):148–153, 2005.

[2] J. R. Lakowicz. *Principles of fluorescence spectroscopy.* Kluwer Academic/Plenum Publishers, New York, 1999.

[3] P. T. Hammond. Form and function in multilayer assembly: New application at the nanoscale. *Advanced Materials*, 16(15, August 4):1271–1293, 2004.

[4] M. Schonhoff. Self-assembled polyelectrolyte multilayers. *Current Opinion in Colloid and Interface Science*, 8:86–95, 2003.

[5] X. Shi, M. Shen, and H. Mohwald. Polyelectrolyte multilayer nanoreactors toward the synthesis of diverse nanostructructured materials. *Progress in polymer science*, 29:987–1019, 2004.

[6] P. Bertrand, A. Jonas, A. Laschewsky, and R. Legras. Ultrathin polymer coating by complexation of polyelectrolytes at interfaces: suitable materials, structure and properties. *Macromolecular Rapid Communications*, 21:319–348, 2000.

[7] M. Salomaki, P. Tervasmaki, S. Areva, and J. Kankare. The hofmeister anion effect and the growth of polyelectrolyte multilayers. *Langmuir*, 20:3679–3683, 2004.

[8] K. Ray, R. Badugu, and J. R. Lakowicz. Polyelectrolyte layer-by-layer assembly to control the distance between fluorophores and plasmonic nanostructures. *Chem. Mater.*, 19(24):5902–5909, 2007.

[9] Y. Lvov and G. Sukhorukov. Assembly of thin films by means of successive depostition of alternate layers of DNA and poly(allylamine). *Macromolecules*, 26:5396–5399, 1993.

[10] O. Stranik, R. Nooney, C. McDonagh, and B. D. MacCraith. Optimization of nanoparticle size for plasmonic enhancement of fluorescence. *Plasmonics*, 2(1):15–22, 2007.

[11] O. Stranik. *Plasmonic enhancement of fluorescence for biomedical diagnostics*. PhD thesis, 2007.

[12] C. F. Bohren and D. R. Huffman. *Absorption and scattering of light by small particles*. Wiley, New York, 1983.

[13] D. L. Feldheim and C. A. Foss. *Metal nanoparticles - Synthesis, Characterization and Application*. Marcel Dekker, Inc., 2002.

[14] U. Kreibig and M. Vollmer. *Optical properties of Metal Clusters*. Springer Series in Materials Science. Springer-Verlag Berlin Heidelberg, 1995.

[15] Y. Tan, Y. F. Li, and D. Zhu. Preparation of silver nanocrystal in presence of aniline. *Journal of colloid and interface science*, 258:244–251, 2003.

[16] J. G. A. Terlingen. *Introduction of functional groups at polymer surfaces by glow discharge techniques*. PhD thesis, 1993.

[17] S. D. Spillman, H. M. McEvoy, and B. D. MacCraith. Fabrication of substrate-independent protein microarrays using polyelectrolyte scaffolding. *Langmuir*, 25(3):1403–1411, 2008.

[18] O. Stranik, D. Iacopino, R. Nooney, C. McDonagh, and B. D. MacCraith. Optical properties of micro-patterned silver nanoparticle substrates. *Journal of Fluorescence*, 20(1):215–223, 2010.

[19] Y. K. Hong, H. Kim, G. Lee, W. Kim, J. I. Park, J. Cheon, and J. Y. Koo. Controlled two-dimensional distribution of nanoparticles by spin-coating method. *Applied Physics Letters*, 80(5):844–846, 2002.

[20] X. Jiang, H. Zheng, S. Gourdin, and P. T. Hammond. Polymer-on-polymer stamping:? universal approaches to chemically patterned surfaces. *Langmuir*, 18(7):2607–2615, 2002.

[21] J. L. Tan, J. Tien, and C. S. Chen. Microcontact printing of proteins on mixed self-assembled monolayers. *Langmuir*, 18(2):519–523, 2001.

[22] M. C. Berg, J. Choi, P. T. Hammond, and M. F. Rubner. Tailored micropatterns through weak polyelectrolyte stamping. *Langmuir*, 19(6):2231–2237, 2003.

[23] S. Kidambi, C. Chan, and I. Lee. Selective depositions on polyelectrolyte multilayers:? self-assembled monolayers of m-dPEG acid as molecular template. *Journal of the American Chemical Society*, 126(14):4697–4703, 2004.

[24] B. D. MacCraith, C. McDonagh, G. O' Keeffe, E. T. Keyes, J. G. Vos, B. O' Kelly, and J. F. McGilp. Fibre optic oxygen sensor based on fluorescence quenching of evanescent-wave excited ruthenium complexes in sol-gel derived porous coatings. *Analyst*, 118:385–388, 1993.

Chapter 4

Planar FRET and Plasmonic Interactions

4.1 Introduction

This chapter describes the design and characterisation of a model FRET system that is compatible with planar optical biochips arrays. The motivation for this approach was two-fold, (i) to demonstrate FRET in a 2-D layer configuration that uses methods and techniques that are similar to those used for development of fluorescence-based biochips, such as those already developed in the Biomedical Diagnostics Institute and (ii) to assess the theory of FRET in 2-D and to compare it with experimental results. The distance dependence of FRET, as well as the concentration dependence, were measured experimentally and compared to the theory already established in Chapter 2. A long-lifetime fluorescent ruthenium complex was chosen as the donor and the widely used fluorescent label, Cy5, as the acceptor. Both donor and acceptor were conjugated to polyelectrolytes (PELs), which enabled controlled deposition of a 2-D layered FRET system. Layer-by-Layer (LBL) deposition of PELs, as described in the previous chapter, was also used to define a highly controllable D-A separation. FRET from a donor to multiple acceptors in the 2-D layers was modeled using MATLAB. Both intensity and lifetime FRET measurements were carried out and there was good agreement between experimental results and the theoretical model. The use of DNA strands of different lengths as D-A spacers is also presented in this chapter,

as is the interaction between FRET and the LSPR of metal NPs in the planar configuration.

4.2 Experimental Planar FRET

The remainder of this chapter presents results on (i) the demonstration of FRET in the 2-D planar configuration, (ii) the investigation of the distance dependence (iii) investigation of the concentration dependence and (iv) investigation of the planar plasmonic-FRET interaction. As explained in Section (2.3), energy transfer occurs due to dipole-dipole interactions and these are limited to distances of 0.5nm-10nm. The Förster Radius (R_0) for the Ruthenium complex and Cy5 was calculated in MATLAB using Eqn.(2.10) and Eqn.(2.11) (see Appendix 2) and was found to be 3.48nm. This is the distance at which the energy transfer is reduced to 50%. To establish the FRET distance dependence, the two dyes had to be placed at controlled distances apart, which encompassed the R_0. Both DNA and PELs were used to distance the donor and acceptor from each other and were also used to separate the nanoparticles from the donor and acceptor in the work described in Section 4.3.

4.2.1 Distance Dependence of FRET Interaction using DNA

The first part of the work involved designing a D-A system to demonstrate the occurrence of FRET. To investigate how the transfer efficiency was dependent upon the separation distance, the two dyes had to be placed at controlled distances apart. Initially different lengths of DNA oligonucleotide spacers were used to achieve this, as discussed in Chapter 2. A primary DNA strand was labeled with an amino group at one end and was attached to a donor surface. Secondary DNA strands, complementary in sequence and of increasing lengths were labeled with the acceptor, Cy5. These were hybridised to the primary strand. In an ideal case, these DNA strands would protrude perpendicularly from the surface separating the donor dye molecule from the acceptor dye molecule as illustrated in Fig. 4.1. The theoretically predicted transfer efficiency is shown in Fig. 4.2 for a R_0=3.48nm.

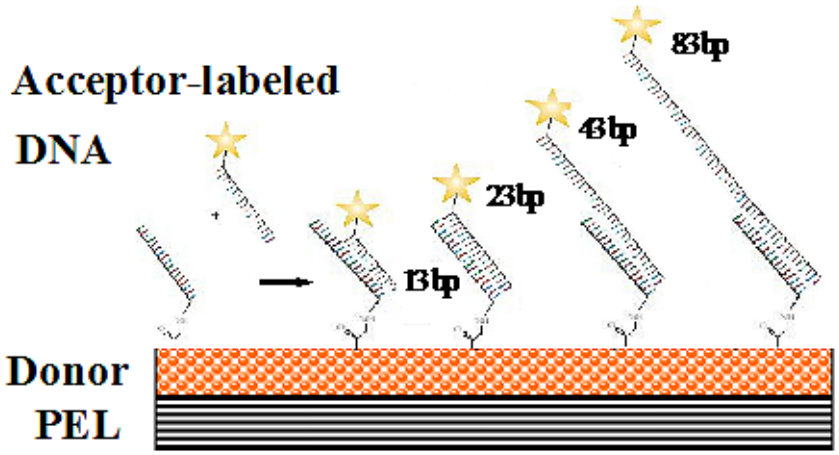

Figure 4.1: Schematic of varying separation distances using different lengths of DNA.

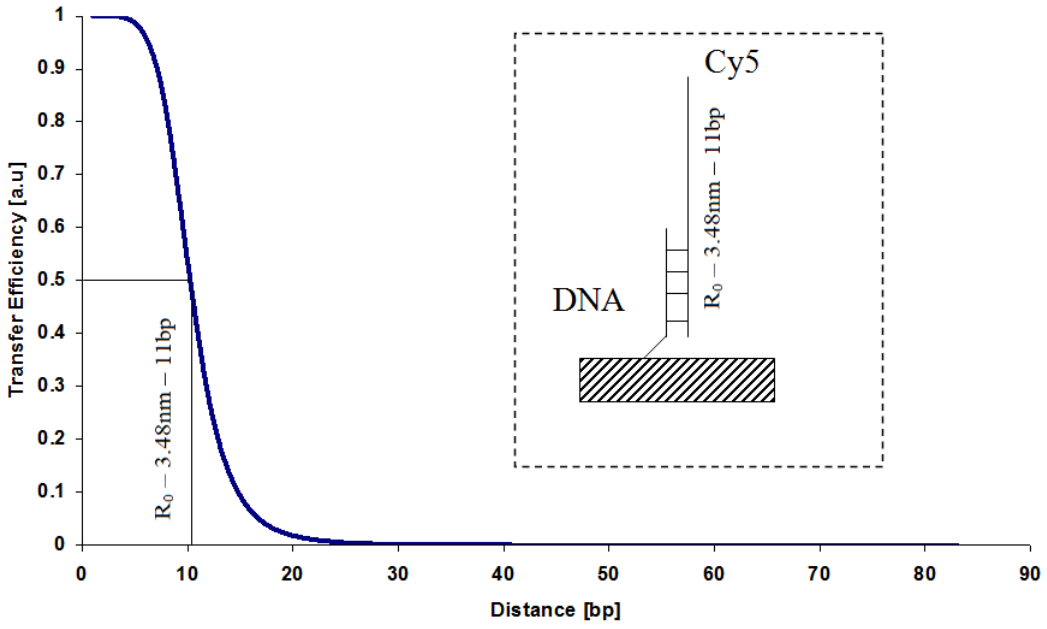

Figure 4.2: The theoretical energy transfer efficiency of the system.

The experiment was performed in transparent-bottomed microtiter plates made of polystyrene. As described in Chapter 3, the plate was plasma-treated in oxygen to functionalise the surface. This creates a negative surface charge on top of which the layers could be deposited. Positively and negatively charged poly-electrolytes were alternately deposited onto the surface. Each layer was 1.5nm thick and this alternated deposition was continued until a homogeneous charged surface was created (approximately eight layers) [1]. The donor layer (Ru-PEL) was then deposited, followed by a layer of PAC. The carboxyl groups (COOH) on the PAC layer provided sites for the attachment of the amine group (NH_2) on the primary DNA strand. The PAC surface and the secondary DNA strands were both negatively charged, leading to low non-specific binding of the acceptor labeled strand directly on to the donor surface [2]. This is illustrated in Fig. 4.3.

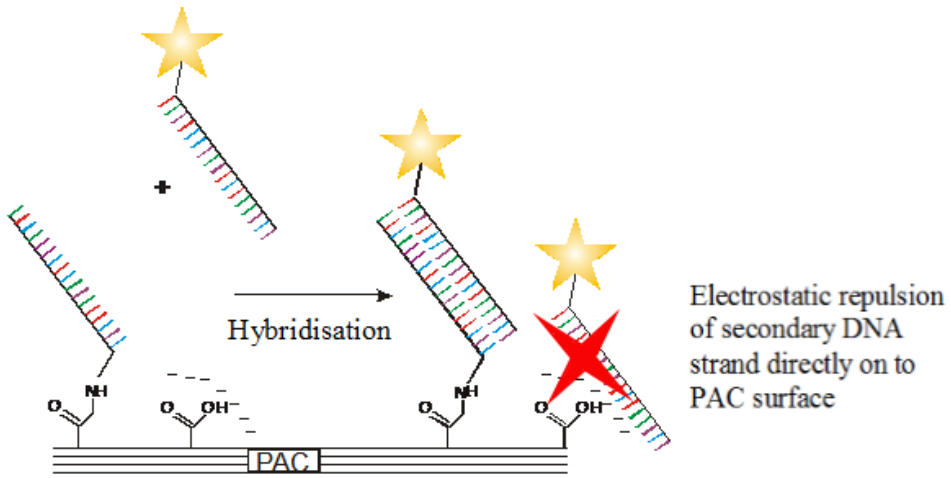

Figure 4.3: Schematic describing how there is reduced non-specific binding of acceptor labeled DNA.

The amino-labeled primary DNA was covalently bound to the carboxyl groups by carbodiimide activation. This involved the use of a crosslinking agent, 1-[3-(dimethyl-amino)propyl]-3-ethylcarbodiimide- hydrochloride (EDC). First 50mM EDC was dissolved in 10mM 2-(N-morpholino)ethanesulfonic acid buffer (MES buffer, pH 6.00). The amino-labeled DNA was diluted to 10^{-6} Mbp in a reaction buffer. The reaction buffer was obtained by mixing 10μl of 1M $MgCl_2$ solution

with 100 μl of EDC solution and 890μl of 0.01 MES buffer. The DNA was pipetted into the reaction wells of the microtiter plate and left to incubate overnight. The wells were then washed with deionised water three times and dried with nitrogen flow. The complementary secondary DNA strands labeled with the acceptor, were diluted using hybridisation buffer to a concentration of 10^{-6} Mbp, added to the wells and left to hybridise for 2 hours. The wells were then washed with deionised water three times and dried with nitrogen flow.

Results

The FRET efficiency was calculated using fluorescence intensities measured using a spectrophotometer as discussed in Chapter 3, and Eqn.(4.1). The samples were first excited at the acceptor excitation wavelength, 610nm, in order to confirm that the acceptor-labeled DNA had hybridised. Fig. 4.4 shows the emission spectra of the acceptor, confirming hybridisation of the primary and secondary DNA strands.

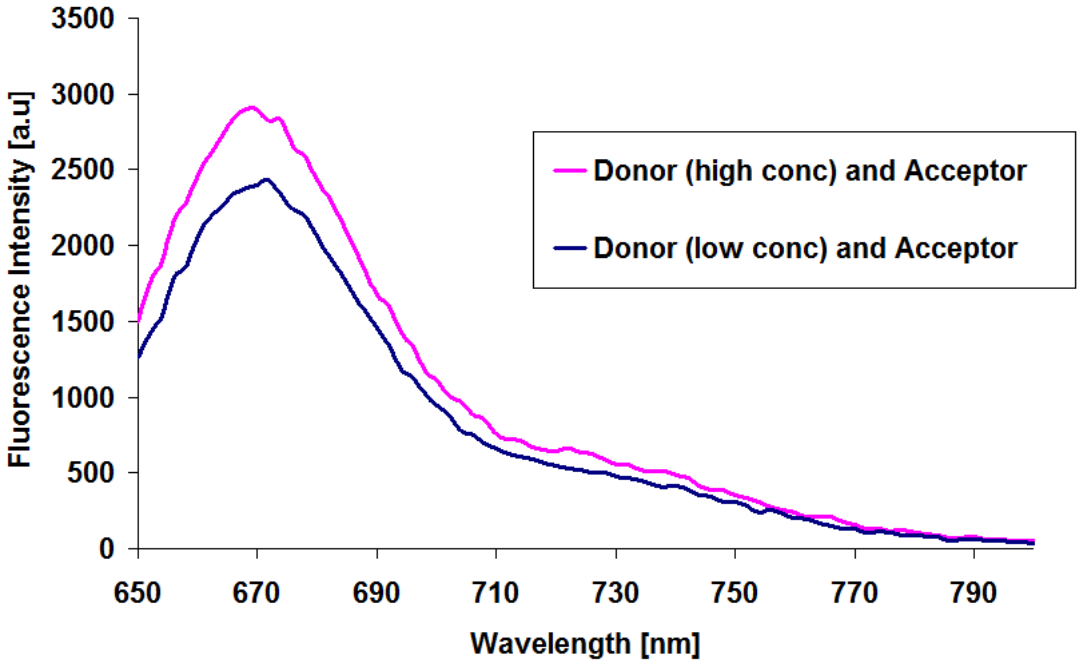

Figure 4.4: Emission spectra of the acceptor-labeled DNA (excitation λ610nm).

The samples were then excited at the donor excitation wavelength, 452nm,

and the emission spectra were recorded. Two different concentrations of the donor were used in order to find the optimum ratio of dye molecules. Fig. 4.5 shows the emission spectra of the donor in the presence and absence of the acceptor.

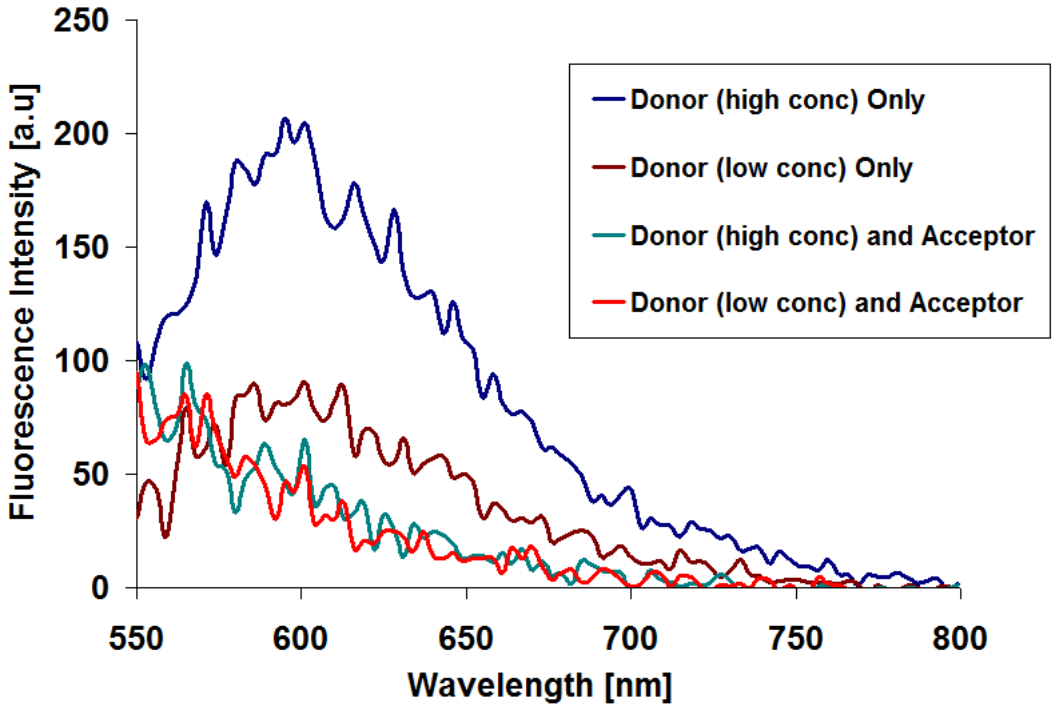

Figure 4.5: Emission spectra of the donor and acceptor, excited at 452nm

The emission spectra shown in Fig. 4.5 confirmed that FRET was occurring between the two dyes. In order to investigate the hybridisation process, a comparison study was carried out between two different PEL surfaces. The first was the original PAC layer with the primary amino-labeled DNA being covalently bound to the surface and the secondary acceptor-labeled DNA strand being hybridised. The second surface was a PAH layer which was positively charged. The secondary acceptor-labeled DNA strand was electrostatically bound to this layer. Fig. 4.6 shows the results of the PAC layer for two different lengths of DNA, 13bp and 23bp. It can be seen that the donor emission has decreased in the presence of the acceptor and that there is a small increase in the acceptor emission at 670nm, due to energy transfer. No significant difference was recorded for the different lengths of DNA. This was most likely due to the orientation of the DNA strands, which may not have behaved like the ideal case protruding perpendicularly from the surface. It was more likely that the strands orientated themselves horizontally,

diagonally or non-linearly distorting the anticipated D-A distance.

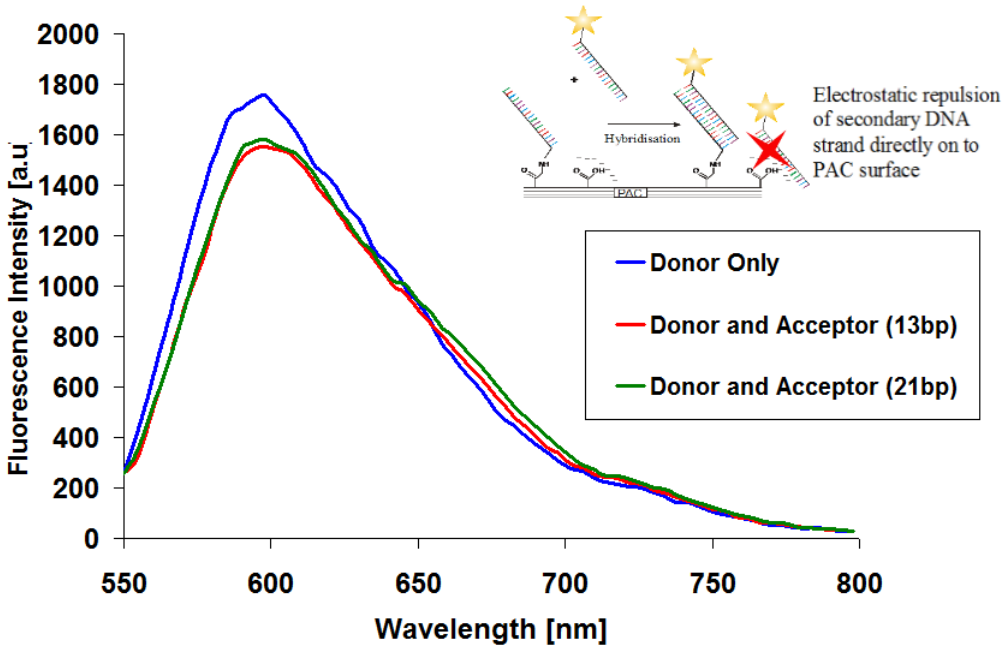

Figure 4.6: Emission spectra of the donor and acceptor, over a layer of PAC, excited at 452nm.

Fig. 4.7 shows the results of DNA strands electrostatically bound to the PAH layer, again for the two different lengths of DNA. It can be seen that the donor emission is decreased when the acceptor is present due to energy transfer. There appears to be greater energy transfer occurring with the 21bp DNA strand, and this could be due to a higher density of 21bp DNA strands attaching to the surface. This different approach does give a greater FRET effect, however the density of acceptor molecules on the surface is not controllable.

This investigation showed the ability to achieve FRET in a planar configuration using acceptor-labeled DNA. The system was not reliable for increasing the distances between the D-A pair due to the non-ideal orientation of the DNA strands. Omitting the hybridisation step and electrostatically binding the acceptor-labeled DNA to the surface gave much more promising results. However, as this system does not allow for the controlled distance separation of D and A, another approach using PELs as spacers to increase the distance was investigated.

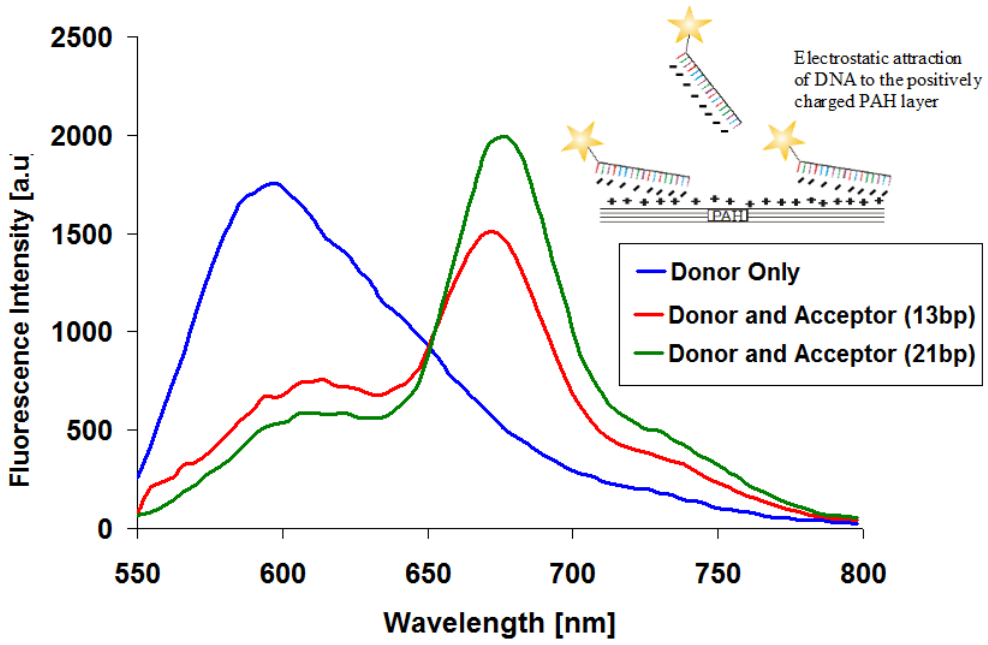

Figure 4.7: Emission spectra of the donor and acceptor, over a layer of PAH, excited at 452nm.

4.2.2 Distance Dependence of FRET Interaction using Polyelectrolytes

The previous section demonstrated FRET in a planar configuration for one D-A distance. To investigate how the transfer efficiency was dependent upon the separation distance, the two dyes had to be placed at controlled distances apart. The polyelectrolyte layer-by-layer technique used to deposit the donor layer, was employed to achieve this. The experimental design was similar to the one described previously, however the acceptor-labeled DNA strands were replaced with acceptor conjugated polyelectrolyte. This was a more robust, reproducible deposition technique and less expensive. A schematic of the experimental design is shown in Fig. 4.8.

The spectral analysis was performed on a Tecan Saffire II Spectrophotometer as discussed in Section 3.5. The acceptor (Cy5) shows little or no emission when excited at 450nm. However, when it is in close proximity to the donor and excited again at 450nm it fluoresces at 670nm due to energy transfer. A narrow excitation bandwidth was used to ensure minimal direct excitation of the acceptor. The Förster Radius for the FRET dye pair was 3.48nm, as calculated in the model,

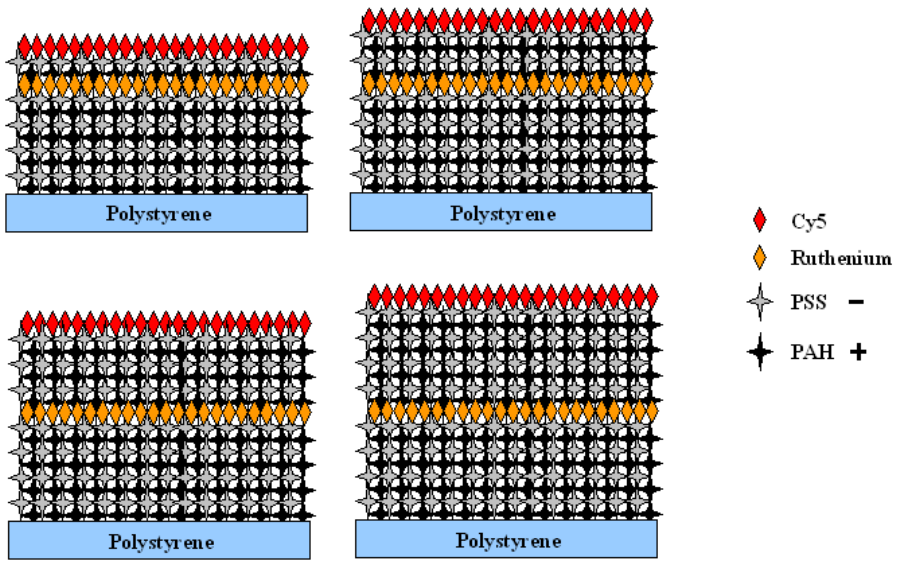

Figure 4.8: Schematic of varying separation distances using PEL layers.

therefore the dyes were placed at separation distances of 1.5nm, 4.5nm, 7.5nm, 10.5nm and 13.5nm in order to achieve a good spread of the transfer efficiency.

The spectral response of the FRET system, as shown in Fig. 4.9, confirmed the success of the system as a model system for demonstrating FRET and controlling the D-A distance. The transfer efficiency was measured and, as shown in Fig. 4.10, it was determined that for the smallest D-A distance, the transfer efficiency was greatest and that the donor fluorescence was at a minimum when the acceptor fluorescence was at a maximum. It can be seen that, as the D-A distance increased there was less energy transfer occurring and the donor fluorescence increased when the acceptor fluorescence decreased. The ratio of the acceptor peak to the donor peak for the closest distance, the FRET ratio (R_{DA}), was calculated to be $R_{DA} = 2.3$. The greater the ratio the more energy transfer is occurring and, hence, the higher transfer efficiency.

Fig. 4.10 shows the experimental versus theoretical transfer efficiency (E_T) of the system. This was found using Eqn.(4.1) with the values of the donor fluorescence intensity found from the spectral analysis.

$$E_T = 1 - \frac{F_{DA}}{F_D} \tag{4.1}$$

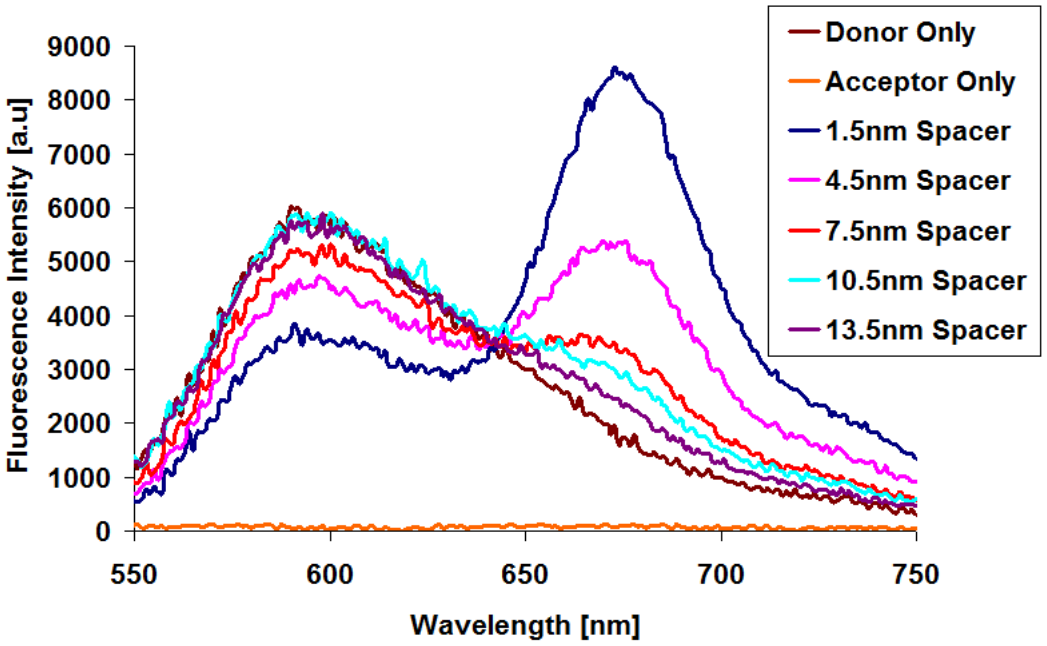

Figure 4.9: FRET spectral response with varying distances.

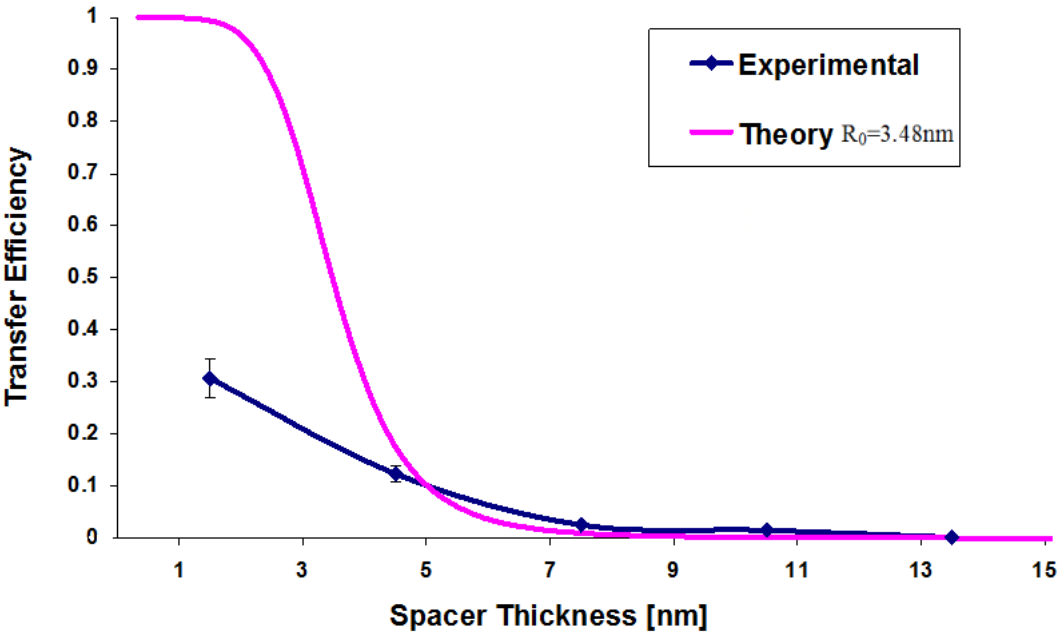

Figure 4.10: Comparison of transfer efficiencies.

As expected, the experimental and theoretical results both showed a decrease in the transfer efficiency with distance. However there was a large discrepancy between the results and the theory. Therefore, a more rigorous investigation into the theoretical model for 2-D FRET was undertaken.

4.2.3 Modeling Planar FRET

The FRET interaction between the Ruthenium complex and Cy5 dye layers was modeled using MATLAB. Fluorescing molecules are electric dipole emitters, therefore initially a single oscillating dipole was modeled using Maxwell's equations as described by Enderlein [3] and Eqn.(4.2).

$$E(r) = {k_0}^2 k \left[\left(-1 - \frac{3i}{kr} + \frac{3}{(kr)^2} \right) \hat{\mathbf{r}}(\hat{\mathbf{r}} \cdot \mathbf{p}) + \left(1 + \frac{i}{kr} - \frac{1}{(kr)^2} \right) \mathbf{p} \right] \frac{exp(ikr)}{kr} exp(-i\omega t) \tag{4.2}$$

where k is the wavenumber, $\mathbf{r}$ is the position vector, $\hat{\mathbf{r}}$ is the unit directional vector, $\mathbf{p}$ is the dipole orientation vector, ω is the angular frequency of the wave and t is time. Fig. 4.11 shows the contours of constant field amplitude $|E(r)|$ for a vertical dipole orientation.

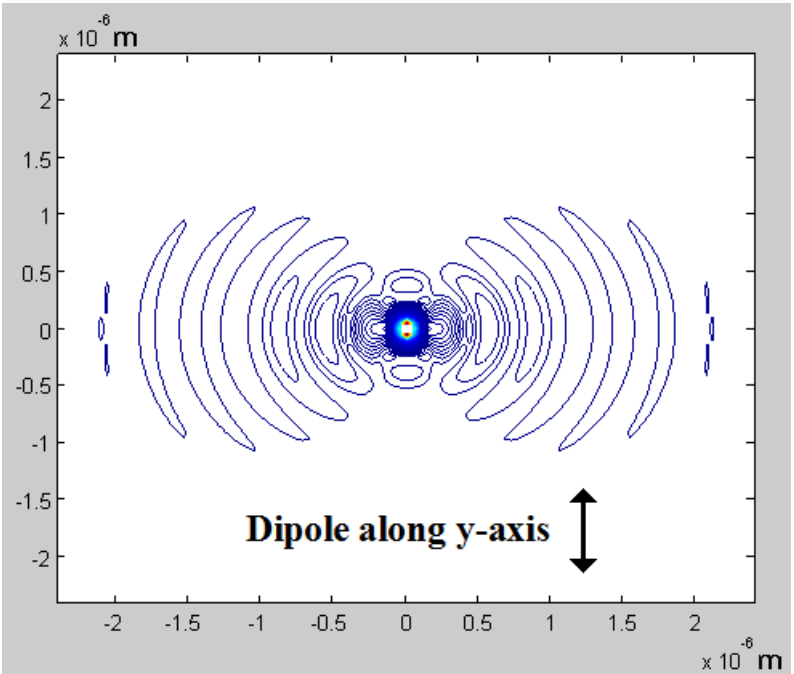

Figure 4.11: Single oscillating dipole

The fundamental FRET equations are based on a single donor to single acceptor design (see Chapter Two). Due to the planar dye layers in the experimental set up, the equations were therefore adjusted to account for donor to multiple acceptor energy transfer, as illustrated in Fig. 4.12. The equations were modified as described in Shaklai et al [4] and outlined below.

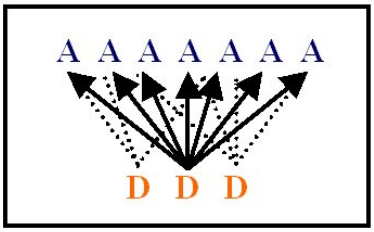

Figure 4.12: FRET theory applied to bi-layers.

The calculation of the FRET efficiency between two planar surfaces begins by letting $p_D(t)$ be the probability that a donor molecule excited at a time $t = 0$ is still excited at time t, i.e., $p_D(t) = n(t)/n(0)$ where $n(0)$ and $n(t)$ are the number of excited molecules at time zero and time t respectively. The fluorescence intensity (I) of the donor when excited with a continuous excitation beam is found by integrating $p_D(t)$ (Eqn.(4.4)). In the absence of any acceptor molecules this intensity is at a maximum. As acceptor molecules are introduced into the system, energy transfer occurs, and the probability of a donor molecule still being excited after time t is decreased. In turn this means that the donor fluorescence intensity is decreased. Donor fluorescence intensity continues to reduce with increasing numbers of acceptor molecules (s).

$$I = \int_0^\infty p_D(t)dt \tag{4.3}$$

where

$$p_D(t) = e^{-t/\tau_D} e^{s.L(t)} \tag{4.4}$$

$p_D(t)$ can be calculated where $L(t)$ is defined by:

$$L(t) = \int_{R_M}^\infty (1 - e^{-k(r)t}).2\pi.r(dr) \tag{4.5}$$

and

$$k(r) = \frac{1}{\tau_D}\left(\frac{R_0}{r}\right)^6 \tag{4.6}$$

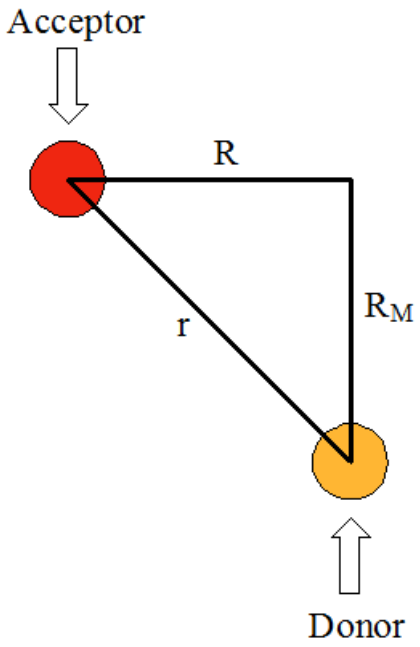

Figure 4.13: Coordinate system showing the distance r between donor and acceptor, the position R of an acceptor molecule from the point immediately above the donor molecule, and R_M the closest distance to which the acceptor can approach the donor [4].

The transfer efficiency can then be calculated using the values found for the fluorescence intensity

$$E = 1 - \frac{I}{I_0} \tag{4.7}$$

where I_0 is the fluorescence intensity of the donor in the absence of the acceptor. This is the same as Eqn.(4.1) in Section 2.3.1.

To account for energy transfer to multiple acceptors on the same layer, MATLAB was programmed to integrate over an acceptor distance from R_M to $r = 100nm$ for each donor molecule. 100nm was chosen due to the fact that at this distance it was certain that the FRET efficiency had been reduced to 0. The program then calculated how the energy transfer decreased as the donor and acceptor layer distance R_M was increased.

The model showed how the transfer efficiency was dependent upon the separation distance of the two dyes and also the concentration of the dyes as seen in Fig. 4.14. As the concentration of acceptor molecules increased so did the transfer efficiency. This was later verified experimentally. The results from section 4.2.2 (Fig. 4.10) were then compared to this modified theory, and is shown in Fig. 4.15.

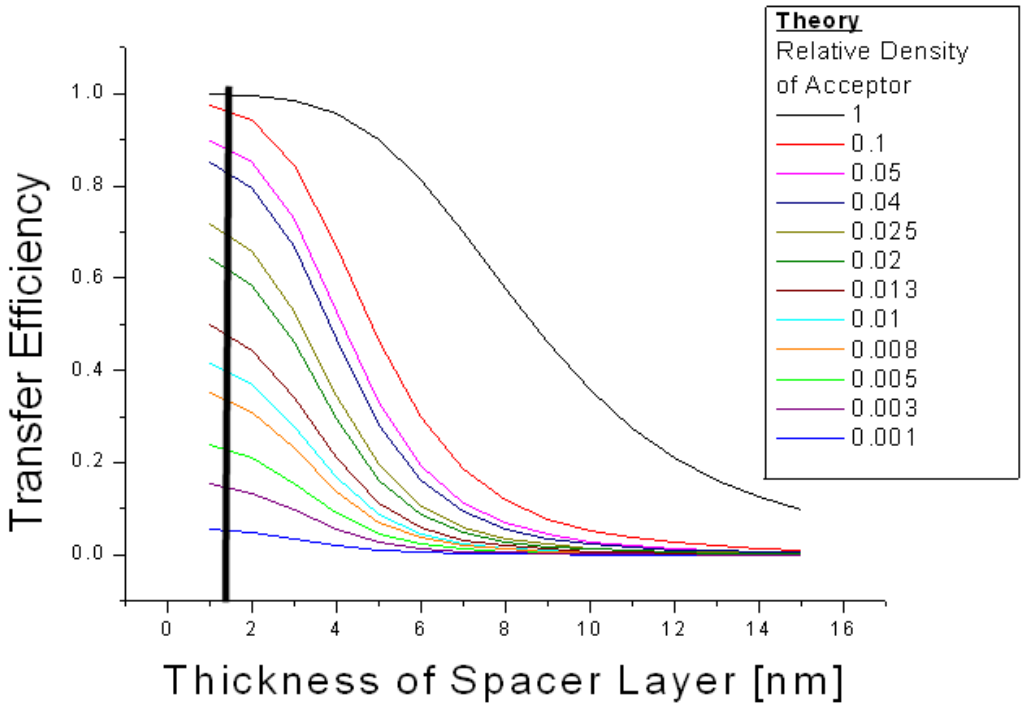

Figure 4.14: Theoretical transfer efficiency dependence on spacer layer thickness

There was good agreement between the modified theory and the experimental results. An explanation for any discrepancies was the possible migration of the dye molecules into the PEL layers leading to inaccuracies. As the polyelectrolytes are not solid films but are slightly porous, some of the dye molecules could have migrated through the layers giving different effective dye separation to that assumed in Fig. 4.8.

It was also observed that the number of PEL overlayers had an influence on the fluorescence intensity of the donor. The donor fluorescence intensity increased with an increasing thickness of the spacer layer, as shown in Fig. 4.16. This could be attributed to the shielding of the Ru-complex from the oxygen in the air, and thus oxygen quenching as discussed in Chapter 3.

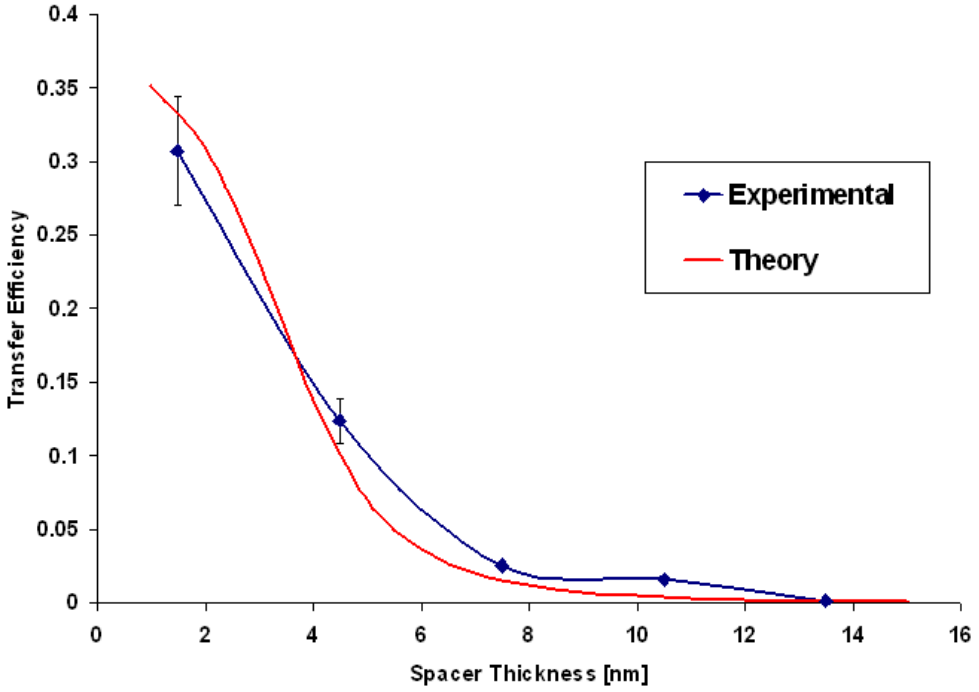

Figure 4.15: Comparison of transfer efficiencies

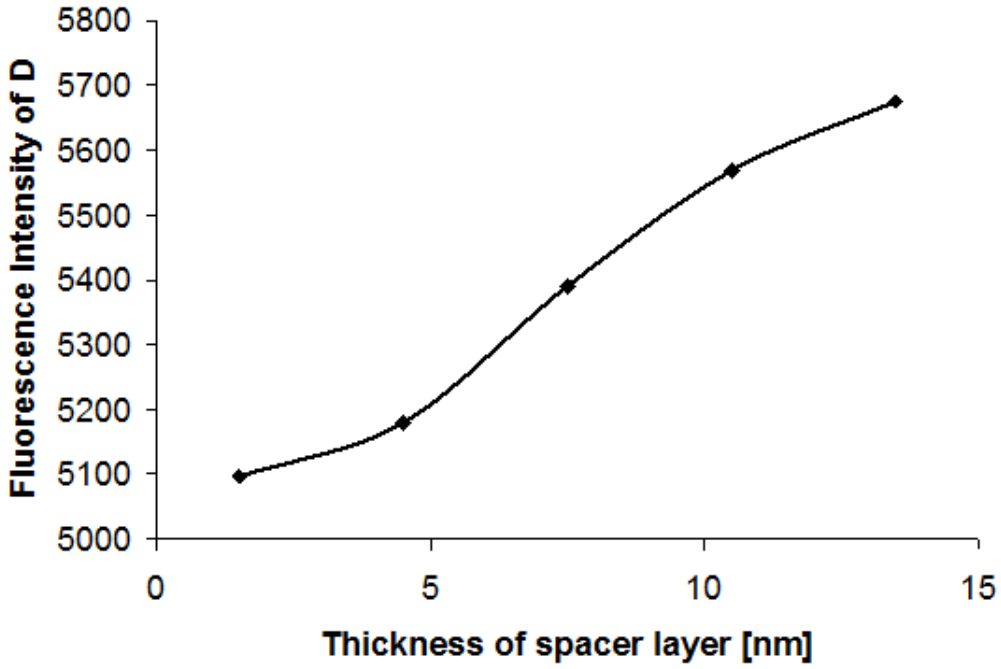

Figure 4.16: Increase in donor intensity with thickness of spacer layer.

Another issue was that the concentration of acceptor molecules in the dye layer increased with the number of PEL underlayers, as shown in Fig. 4.17. Therefore, for larger separations, the concentration of acceptor is slightly higher than predicted and therefore the transfer efficiency is increased. A revision of the experimental set up was carried out in order to take these suggestions into account and further optimise the model system.

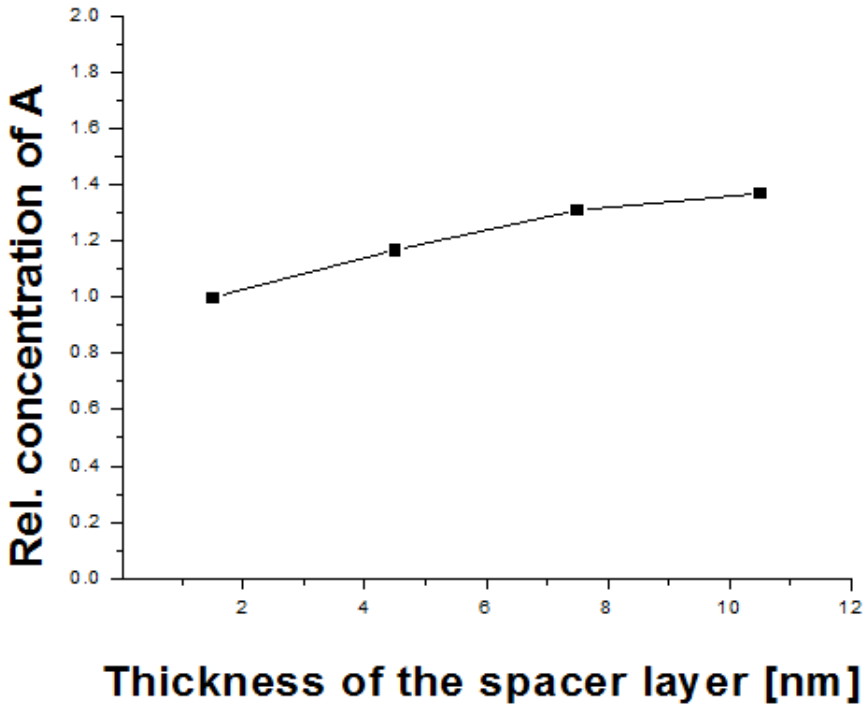

Figure 4.17: Increase in acceptor concentration with thickness of spacer layer.

It was proposed to keep the two dyes the same distance apart, but to vary the concentration of acceptor dye instead, as is shown in the model in Fig. 4.14. This is discussed in the next section.

4.2.4 FRET as a Function of Acceptor Concentration

An optimised experimental model was developed to minimise dye migration and keep the D-A separation distance constant. The donor molecules were immobilised onto a PEL substrate and the acceptor layer was then placed at a distance from it, using additional polyelectrolyte layers, as shown in Fig. 4.18. Due to the positive charge of both dyes and the nature of the PEL layering system, the distance between the D and A could only be a multiple of the bilayer structure as described in Chapter 3. This meant that they could be placed at separation distances of 1.5nm, 4.5nm, 7.5nm, 10.5nm and so on. The separation distance of 1.5nm was chosen for all subsequent experiments to ensure high transfer efficiency and compatibility with the model. Reducing the concentration of acceptor molecules in the layer, in turn reduced the transfer efficiency, as seen in the model in Section 4.2.3.

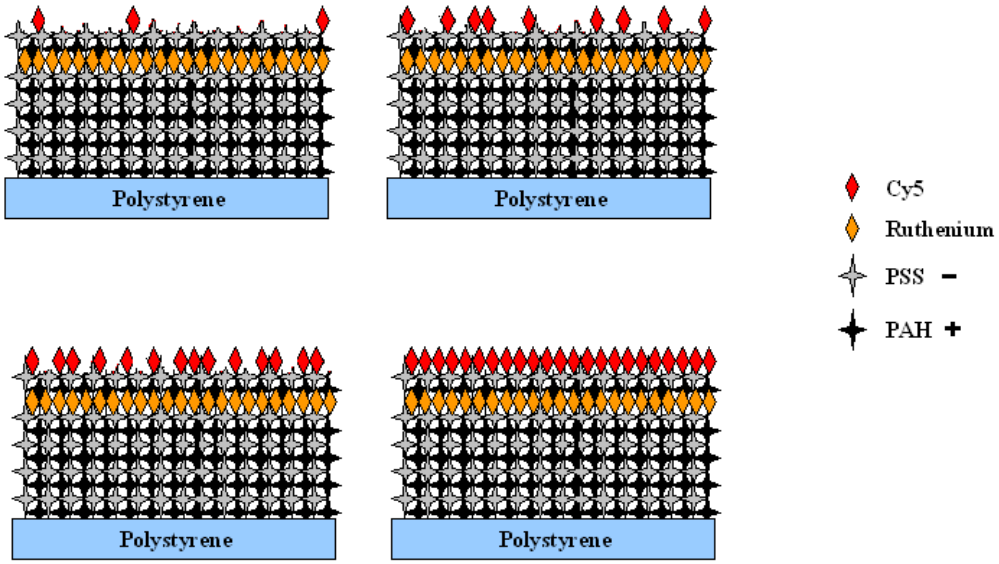

Figure 4.18: Schematic of varying acceptor concentrations in dye layer

Fluorescence Intensity Results

The FRET efficiency was measured using fluorescence intensity and fluorescence decay, as discussed in Chapter 2. FRET was successfully demonstrated using fluorescence intensity measurements from spectral analysis. This method of planar

FRET demonstration agreed well with the theoretical modeling. Fig. 4.19 shows that excitation of the donor at 450nm resulted in fluorescence of the acceptor at 670nm due to energy transfer between the two dye layers. The higher the concentration of acceptor the more transfer occurred, which resulted in less donor emission. As the acceptor concentration was reduced, less energy transfer took place and in turn the donor emission increased. The results were also analysed using filter sets to account for cross talk between the two dyes, as described by Gordon et al [5]. The difference between the two analysis techniques was minimal, due to the large Stokes shift of the dye pair, which reduced the level of cross-talk.

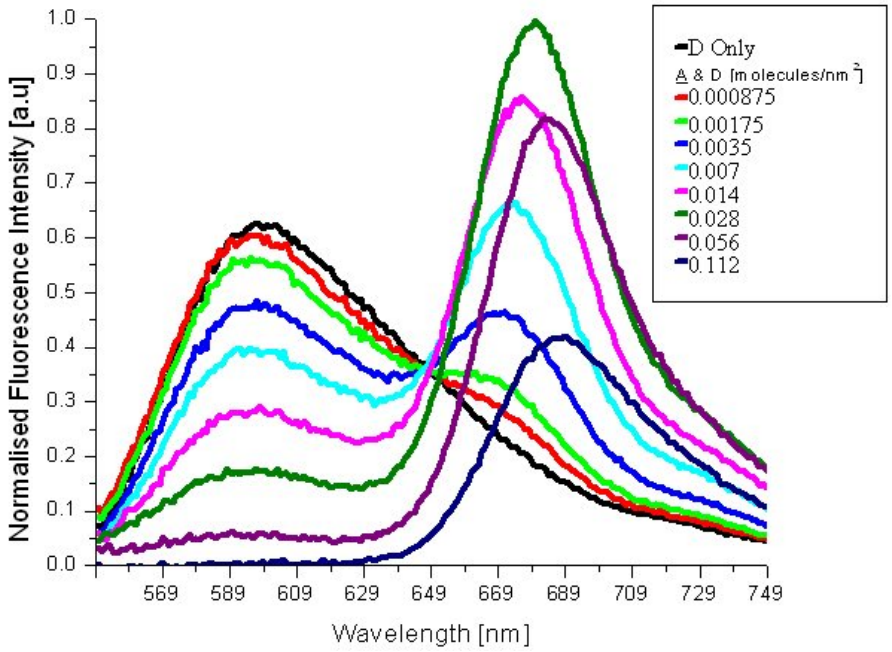

Figure 4.19: FRET as a function of acceptor concentration-spectral response (excitation λ450nm)

Fig. 4.20 shows the experimental versus theoretical transfer efficiency (E_T) of the system. This was found using Eqn.(4.1) with the values of the donor fluorescence intensity found from the spectral analysis. The transfer efficiency showed very good agreement with theory with low standard deviations of $\pm 5\%$, validating the use of the experimental model.

Due to the success of the experimental design, it was then used as the standard model for the next set of experiments, which incorporated metal nanoparticles to test for plasmonic-FRET interactions. Using the previous design in Section 4.2.2,

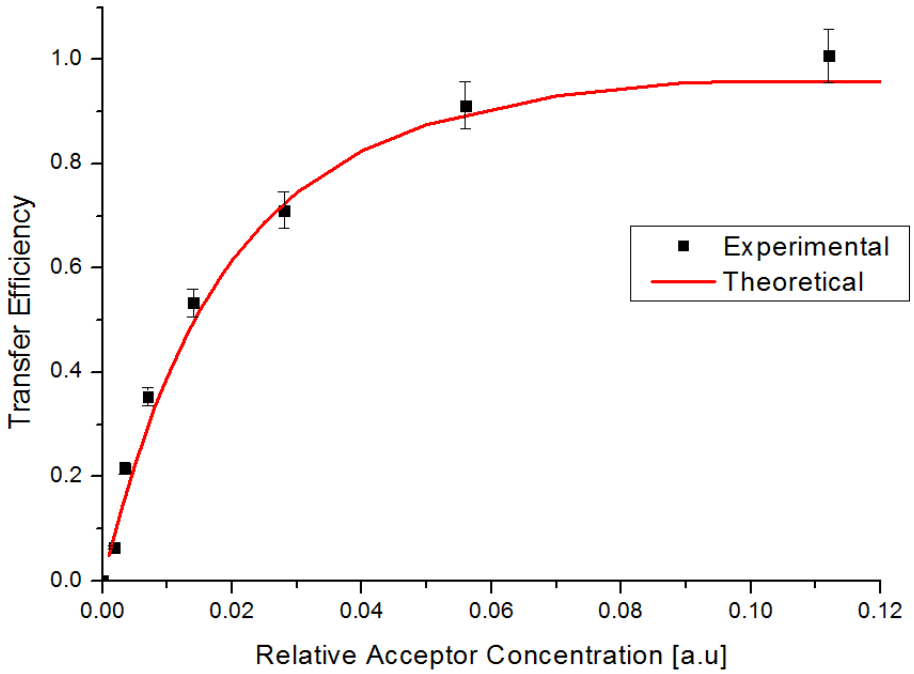

Figure 4.20: Theory vs Experimental

where the separation distance was varied, the NPs would have been at different distances from the donor dye layer but with this design they are always at the same distance, as shown in Fig. 4.21. The design also allowed for NPs to be placed above, below or in the centre of the FRET dye pair.

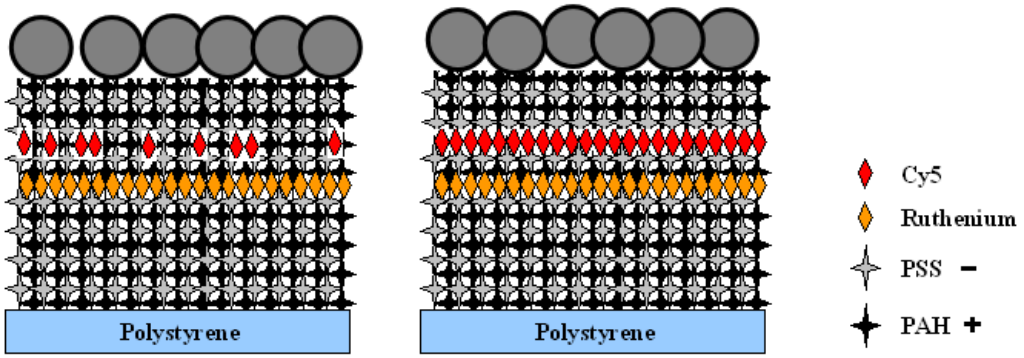

Figure 4.21: Schematic of varying concentration plus NPs

Lifetime Results

The FRET efficiency can also be calculated using fluorescence decays and Eqn.(2.14). A PicoQuant FLIM system was used to measure the lifetimes of the donor in the absence and presence of the acceptor. In order to measure the lifetime decays, the system needs to optically focus on the surface under investigation. The previous experiments were performed in a microtiter plate and had no surface structures upon which to focus. Micropatterning of the FRET layer was used to facilitate fluorescence lifetime imaging [6–10]. Section 3.5 describes the micropatterning process that was used to produce the samples initially. The donor was stamp printed onto glass cover slips and coated with a layer of negatively charged poly-electrolyte, to give a spacer layer of 1.5nm. As explained in Section 3.5, it was not possible to produce sharp Cy5 grid lines. Therefore a large circular Cy5 overlayer was used instead, as shown in Fig. 4.22.

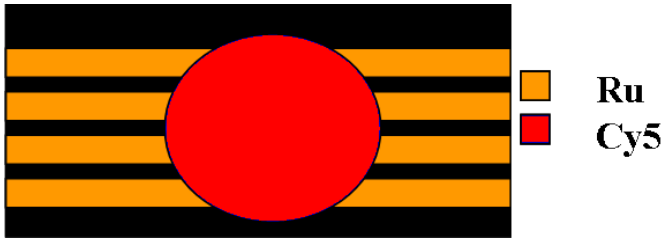

Figure 4.22: Stamped donor lines with acceptor droplet at a distance of 1.5nm.

The lifetimes of the donor and acceptor were measured at the edge of the droplet, to ensure that the area measured by the FLIM had a section of donor only, acceptor only and donor with acceptor. Fig. 4.23 shows an example of the fluorescence lifetime decay fit for the donor and Fig. 4.24 is a colour fit of the lifetimes, where green represents the donor lifetime and red represents the acceptor lifetime. The overlap area between the donor and acceptor is similar to the donor only area, and this was confirmed in the lifetime results when sections were scanned individually. The donor only lifetime was 904ns and the acceptor only lifetime was 1ns. The section with the donor and acceptor gave a lifetime of 880ns, which was much less than anticipated, giving a transfer efficiency of 0.02.

To eliminate the possibility that there was a thin layer of acceptor covering the entire slide that was leading to a reduced donor only lifetime, a small section of

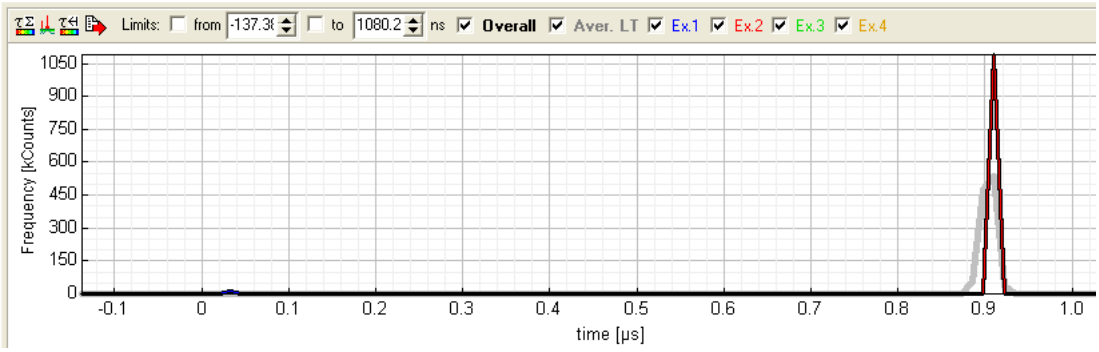

Figure 4.23: Fluorescence lifetime decay trace for donor only.

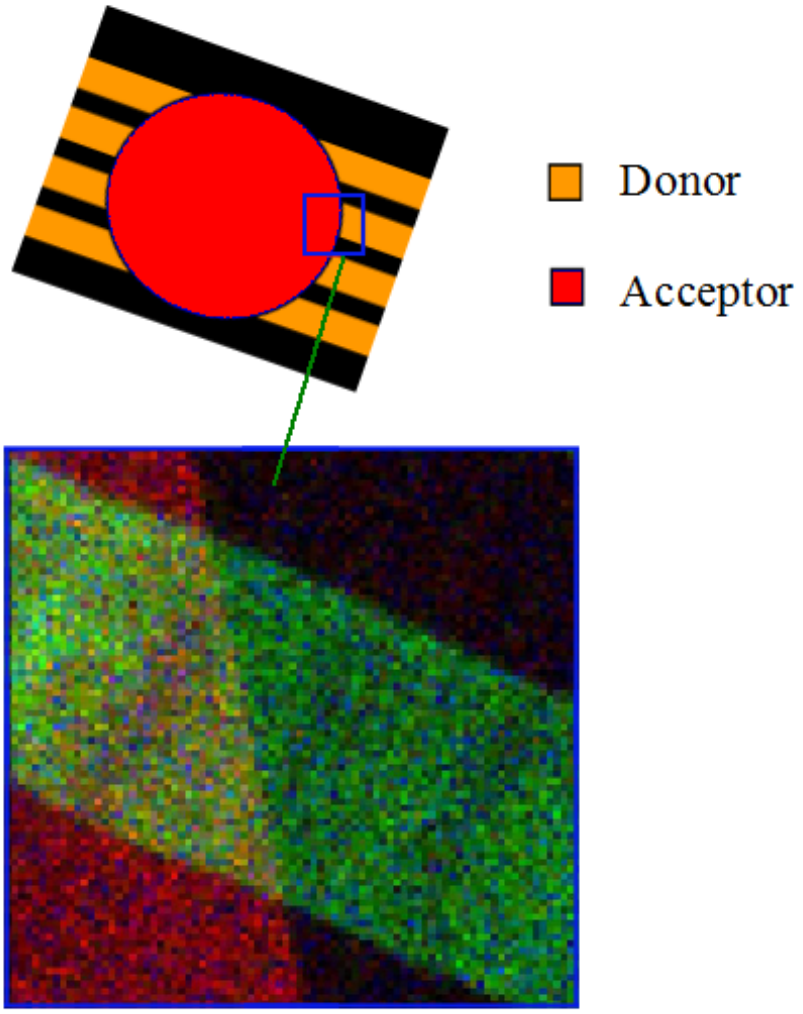

Figure 4.24: Colour fit of the donor and acceptor, area marked on schematic.

the circular overlayer was irradiated with an intense excitation beam of 640nm to photobleach the acceptor molecules, but leave the donor molecules intact. This would ensure that the donor molecules underneath would have no acceptor to transfer energy to. Fig. 4.25 shows the image of the lifetimes, A - shows the lifetimes before photobleaching and B - shows the lifetimes after photobleaching. The photobleached section is marked with a blue square. There was no significant difference found in the FLIM image and the lifetime values after photobleaching.

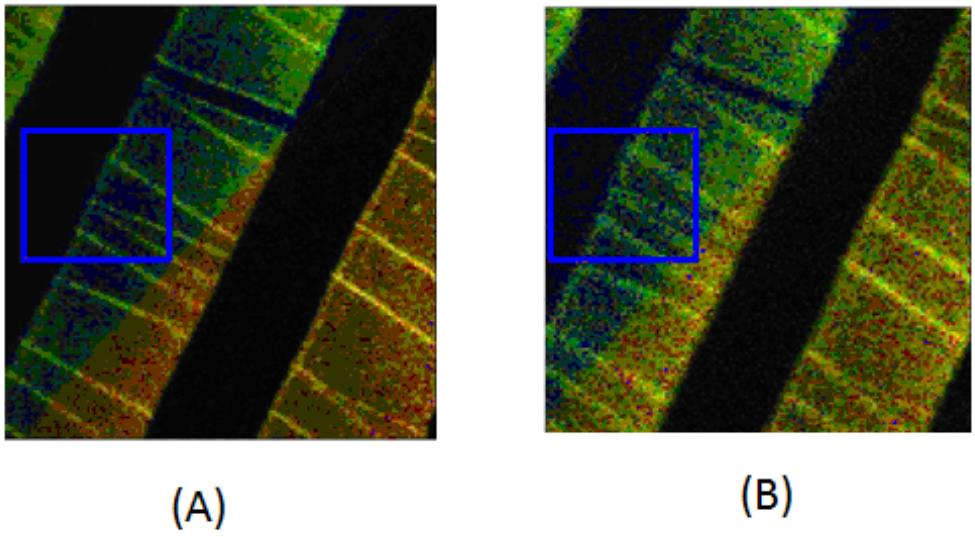

Figure 4.25: Fluorescence lifetime image. A - Donor and acceptor lifetimes before photobleaching and B - Donor and acceptor lifetimes after photobleaching.

The system could take images of the donor and acceptor emission and this is shown in Fig. 4.26, to confirm that the acceptor section was photobleached. A - shows the donor and acceptor emission and B - shows the acceptor emission after photobleaching a section of the circular overlayer.

A low concentration of acceptor molecules could explain the lack of change in the donor lifetime and emission, resulting in very little energy transfer. A small 'coffee ring' effect was observed in depositing the circular overlayer. This was manifest as a migration of dye towards the edge of the droplet. In order to reduce this, the sample was sonicated briefly after deposition, which may have removed many of the acceptor molecules. Another approach was therefore taken

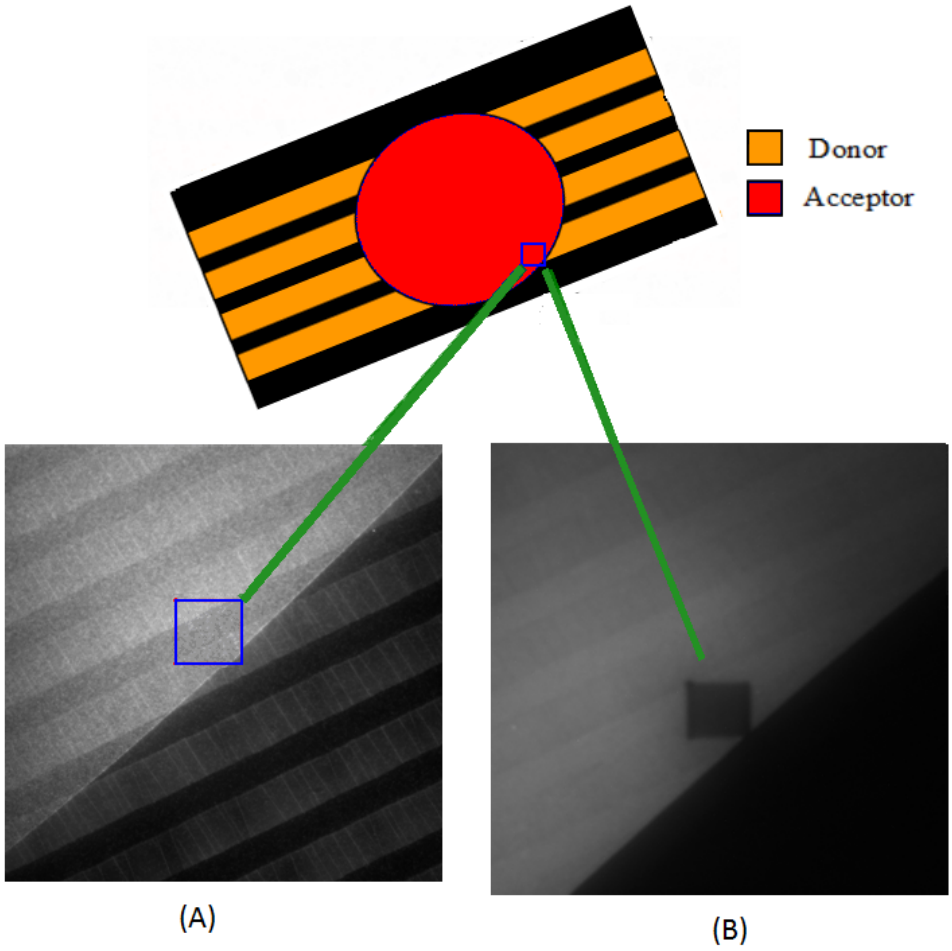

Figure 4.26: Fluorescence intensity image. A - Donor and acceptor emission and B - Acceptor emission after photobleaching a section.

to measure the lifetimes of the FRET pair.

The experiments in Section 4.3.1 showed energy transfer occurring between the donor and the acceptor using intensity measurements from layers inside microtiter plate wells. This experimental design was re-employed here and the acceptor concentration in the individual wells was varied. The edge of the microtiter plate was removed to allow the plate to lie within the focal plane of the FLIM optics. The lifetime of the donor only was measured and compared to the donor lifetime in the wells with both acceptor and donor. It was observed that as the concentration of the acceptor increased, there was a decrease in the donor lifetime. The transfer efficiency for each concentration of acceptor was calculated using Eqn.(2.14).

Fig. 4.27 shows the transfer efficiency as a function of the acceptor concentration in a 2-D configuration. There is a mismatch between the theoretical model

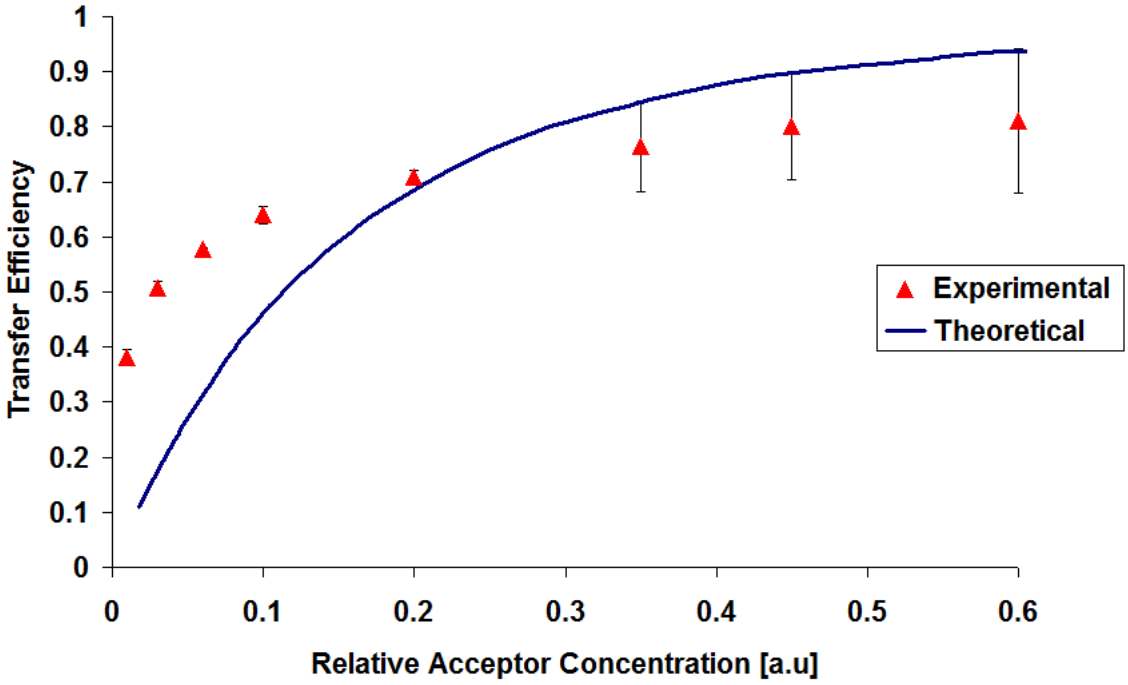

Figure 4.27: FRET as a function of acceptor concentration-lifetime response

and the experimental results, compared to that found using fluorescence intensities in Fig. 4.20. One of the drawbacks of this design was that there were no features on the surface of the well upon which to focus, i.e. grid lines, and so the focal position on each well had to be determined using the scattered light from the upper and lower surfaces. This may explain the discrepancies seen in the results. This method of calculating the FRET efficiency while successful, is more complex and time consuming than using fluorescence intensities. The FLIM system is complex and not conducive to using in POC devices, therefore this method of calculating FRET was not continued.

4.3 FRET-Plasmonic Interaction

Metal-enhanced fluorescence (MEF) for single dyes has been well established where the dye fluorescence in the presence of metal NPs can be enhanced by up to 10-15 times depending on the dye, dye-NP separation and/or NP size, as discussed in Chapter 2 [11–15]. This plasmonic effect is due to the localized surface plasmon resonance (LSPR) at the surface of the metal NP. The LSPR modifies the intensity of the electromagnetic field around the fluorophore, and this can lead to an increase in the emitted fluorescence intensity, as discussed in Section 2.4. While some groups have found this interaction to be at the expense of the Förster transfer rate in FRET systems [16, 17], recently there have been a few reports in the literature where this plasmonic effect has been shown to increase the efficiency of FRET by allowing FRET to occur at longer separation distances [18, 19]. Zhang et al have shown a 75% increase in the value of the Förster Radius (R_0) by attaching hybridised donor and acceptor labeled oligonucleotides to a silver NP [20]. They also found that the MEF-FRET increases with increasing size of the metal NP [21]. Lessard-Viger et al have also shown MEF-FRET using metal core NPs surrounded by concentric silica layers containing donor and acceptor molecules at controlled distances from the core [22]. They have reported an increase in the transfer efficiency by a factor of 4 and an increase in the Förster Radius by 30%. Fig. 4.28 shows the experimental designs used by these two groups.

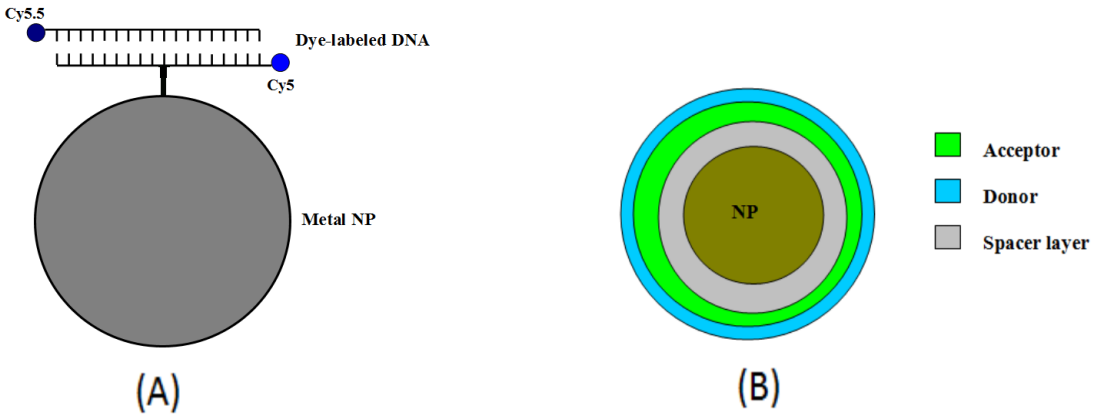

Figure 4.28: Metal-enhanced fluorescence combined with FRET. A - Zhang et al. B - Lessard-Viger et al. [20, 22]

A drawback of both of these experimental designs is the limitation in the positioning of the NP relative to the dye. The flexibility of the 2-D FRET platform allows different configurations and NPs to be investigated with ease. The enhancement of FRET using MEF is investigated here using two approaches; linear D-A-NP combinations are investigated in this chapter and a configuration where the FRET dye pair is equidistant from the NP in investigated in Chapter 5. As discussed in Section 4.2.4, the experimental design where the acceptor concentration was varied allows easy incorporation of the plasmonics and ensures that the NPs are the same distance from each of the dye layers for a set experiment. The highly adaptable polyelectrolyte LBL technique allowed the dye layers and NPs to be placed in different configurations. NPs were placed above, below and in the centre of the two dye layers. NPs were then also placed a set distance from a mixed dye layer that, ensured equidistance of the NP from the D-A pair, as this was designed to be equivalent to the configuration used in the demonstration of FRET enhancement by Zhang et al [20]. Only three different acceptor concentrations were used to increase the throughput time of the experiments and to reduce material consumption. Fig. 4.29 shows the spectral response of the FRET system for the three different acceptor concentrations without any NPs (as shown in Fig. 4.18). The fluorescence ratio (R_{DA}) is the acceptor emission divided by the donor emission. In this case for the maximum concentration of acceptor used, $R_{DA} = 1.7$.

4.3.1 Nanoparticles Above

Firstly, the silver metal nanoparticles were placed above the D-A pair. Both spherical and triangular NPs were tested. Motivation for using two different types of NPs was to take into consideration the two possible plasmonic enhancement mechanisms (see Section 2.3). The spherical NPs had a plasmon resonance at 425nm matching the absorbance of the ruthenium complex. The triangular NPs had a plasmon resonance at 600nm, which matched the overlap area of the ruthenium emission and Cy5 absorbance. A spacer layer of 6nm was deposited between the uppermost dye and the NPs. This was the optimum distance as shown in Chapter 3 and reported by [23]. The NP solutions were deposited into

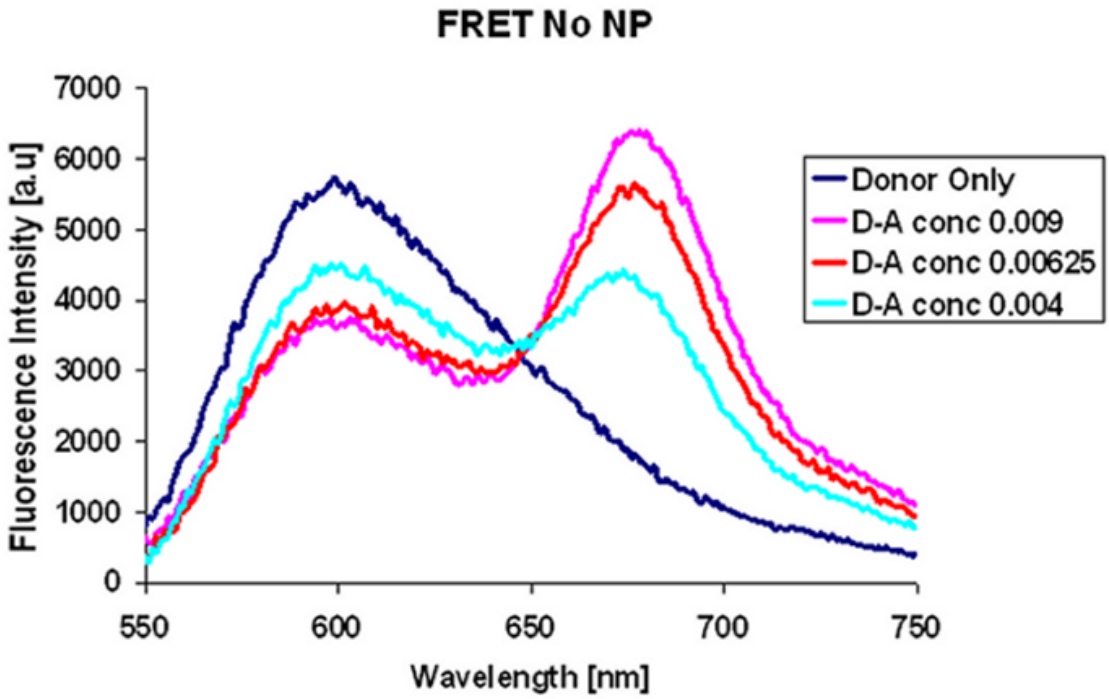

Figure 4.29: FRET spectral response without any NPs (excitation λ450nm).

the wells of the microwell plate and left overnight at room temperature to form a monolayer on the surface. This design meant that the NPs were closer to the acceptor layer than the donor layer, as shown in Fig. 4.30.

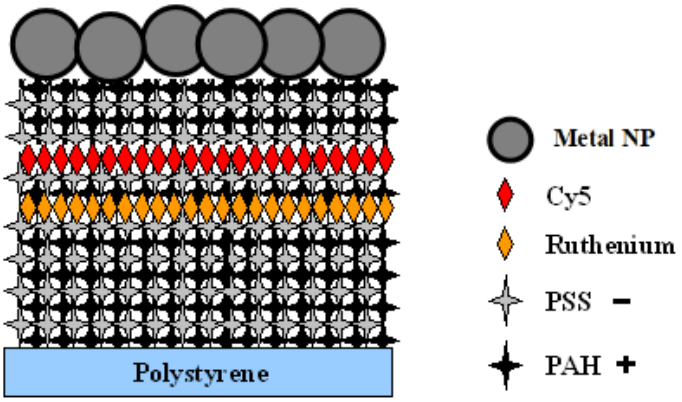

Figure 4.30: Schematic of dye layers and NPs above.

Fig. 4.31 shows the spectral response of the system with the triangular NPs. FRET was observed with NPs positioned above the D-A pair. For the triangular NPs with a 600nm plasmon resonance, the overall fluorescence from both the

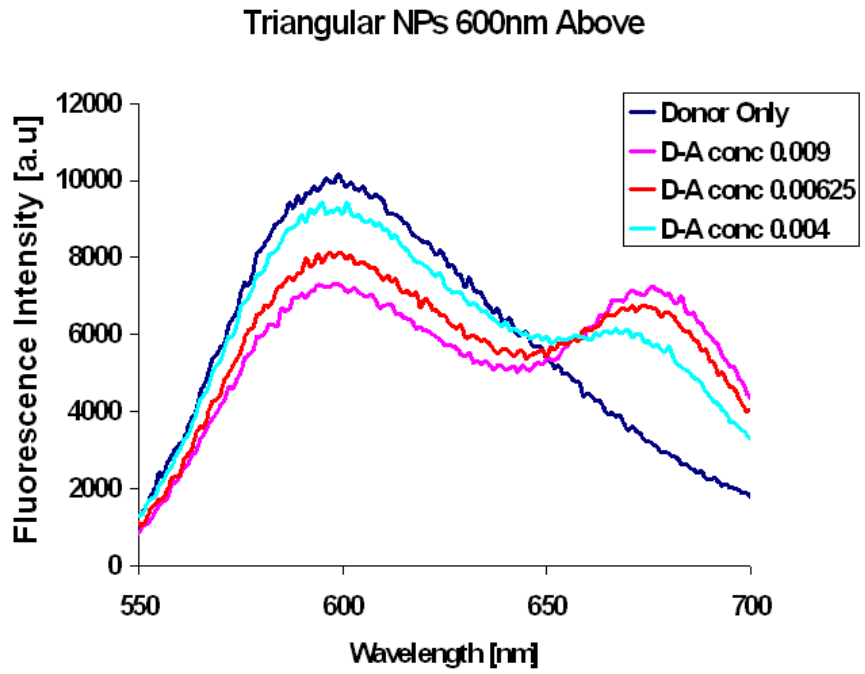

Figure 4.31: FRET spectral response with 600nm triangular NPs above (excitation λ450nm).

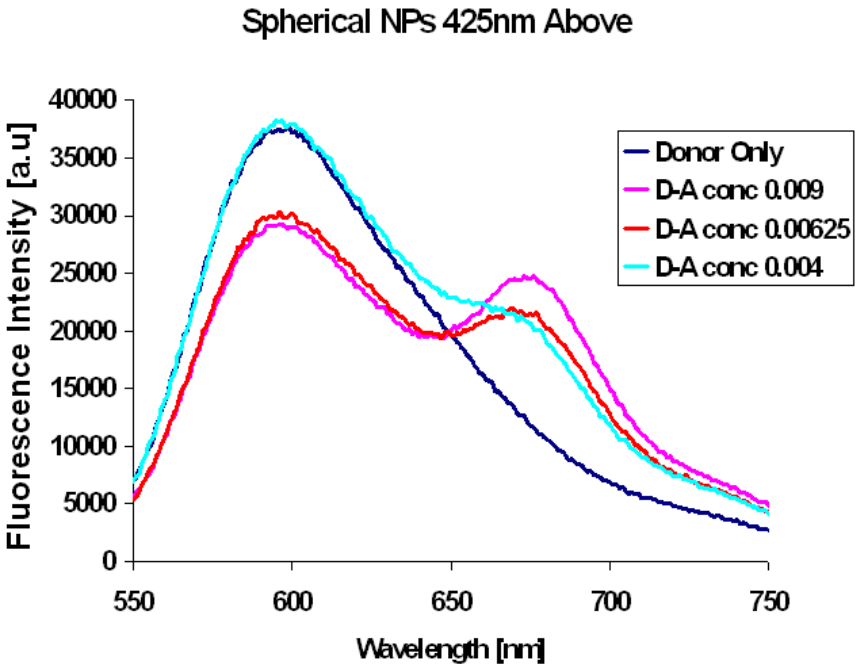

Figure 4.32: FRET spectral response with 425nm spherical NPs above (excitation λ450nm).

donor and the acceptor increased compared to the system without NPs, and the fluorescence ratio reduced $R_{DA} = 0.99$. For the spherical NPs (Fig. 4.32) with a 425nm plasmon resonance, the overall fluorescence from both the donor and the

acceptor has increased dramatically. However the ratio of the D-A peaks dropped from $R_{DA} = 1.7$ to $R_{DA} = 0.86$. This is shown in Fig. 4.33. Negative values in the transfer efficiency can be caused by the statistical error from sample to sample when very little FRET is occurring or a reduction in the donor intensity due to photobleaching or oxygen quenching prior to measurement. Metal enhanced fluorescence is occurring for the individual donor and acceptor. The fact that the overall transfer efficiency is reduced for both NP types indicated the dominant enhancement channels in this configuration are NP-D and NP-A and the FRET D-A channel is less dominant. It also appears that the excitation channel of MEF (where the LSPR is matched to the absorbance of the donor) is the most dominant. This is consistent with previous work on single dye enhancement [11, 23–25].

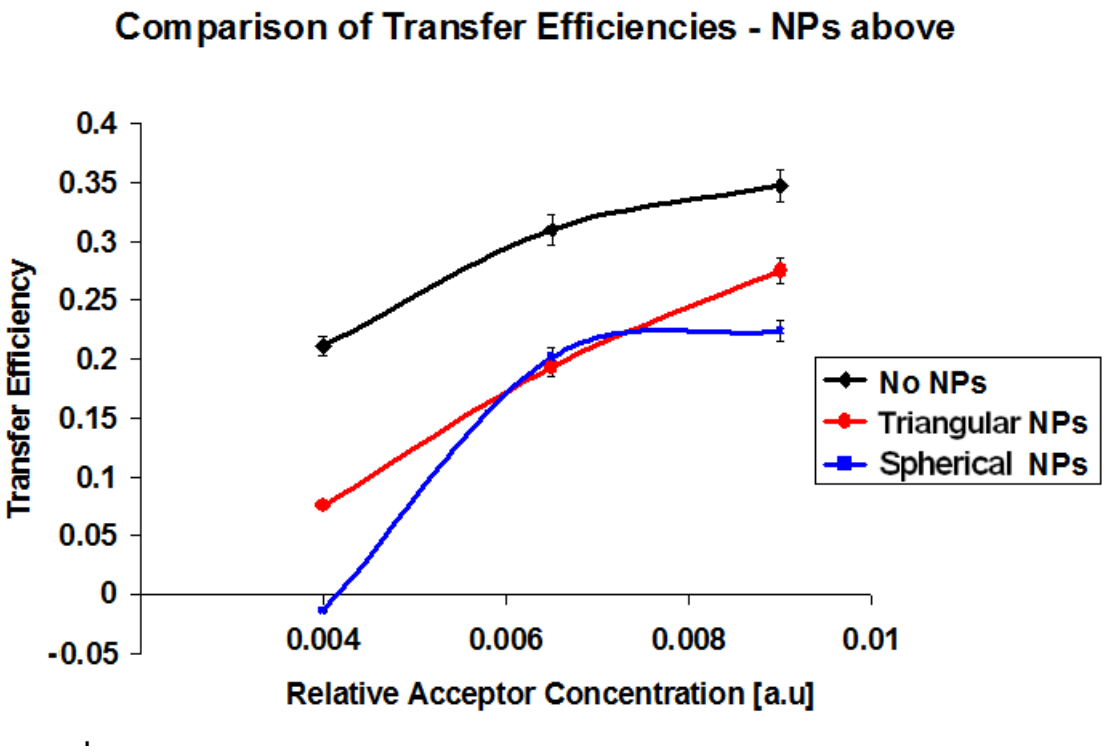

Figure 4.33: Comparison of transfer efficiencies for NPs above the two dye layers.

4.3.2 Nanoparticles in Centre

Next the silver metal nanoparticles were placed in the centre of the D-A pair. Again both spherical and triangular NPs were tested. This design meant that the NPs were equidistant from the acceptor layer and donor layer. However, as the NPs are quite large, the polyelectrolyte and dye layers placed on top of them can wrap around them forming a rough monolayer. This rough monolayer has a higher concentration of acceptor dye molecules due to the increased surface coverage, see Fig. 4.34.

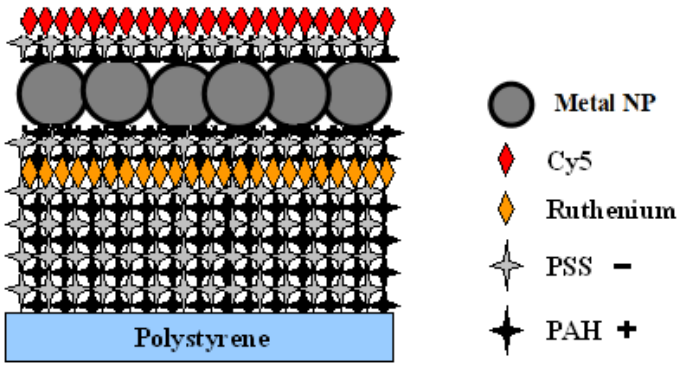

Figure 4.34: Schematic of dye layers and NPs in centre.

Fig. 4.35 shows the spectral response of the triangular NPs while Fig. 4.36 shows the spectral response of the spherical NPs.

Practically all FRET effects have disappeared with this configuration for both types of nanoparticles. It is probable that the donor and acceptor pair are too far apart for dipole-dipole interactions to take place. This interaction is limited at approximately 10nm and the triangular NPs were 15nm in diameter and the spherical NPs were 60nm in diameter. There was no transfer of energy across the NP between the dye molecules. Fig. 4.37 shows the reduction in transfer efficiency when the NPs are placed between the two dye layers. The negative values on the graph are due to the donor plus acceptor peaks being greater than the donor only peaks. This occurs when the donor only sample has been quenched, for example by oxygen or photobleached by light. It can also be caused by statistical error from sample to sample as was discussed earlier, and which is the probable cause

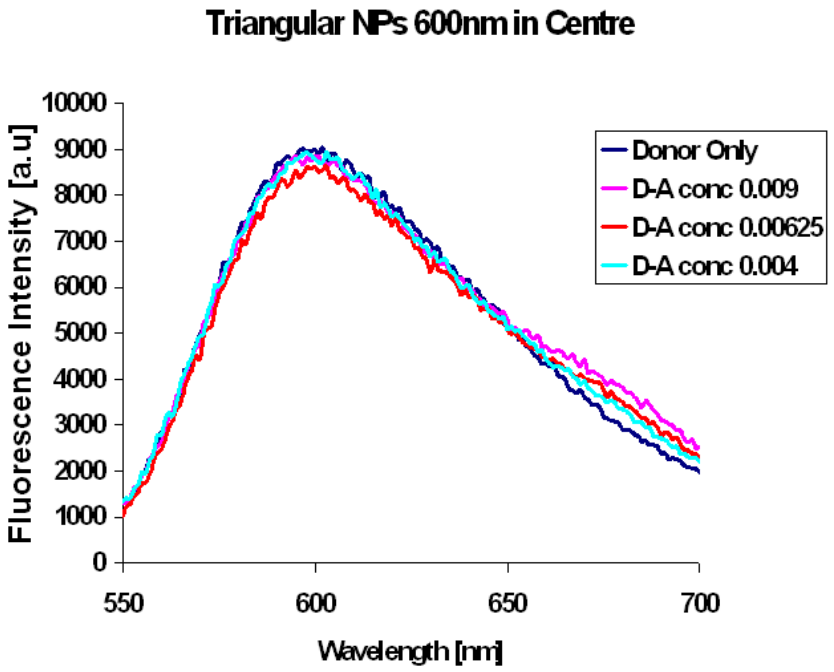

Figure 4.35: FRET spectral response with 600nm NPs in centre (excitation λ450nm).

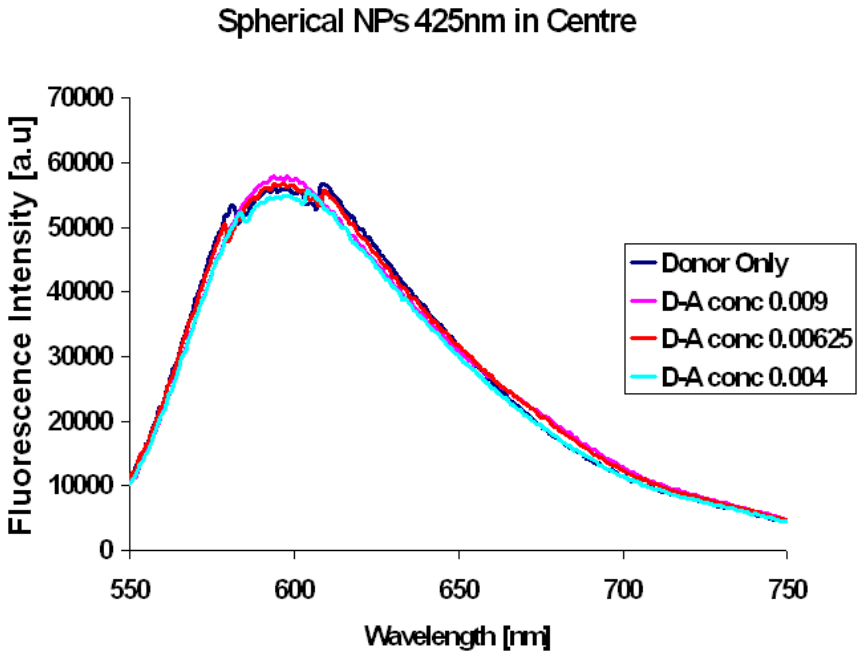

Figure 4.36: FRET spectral response with 425nm NPs in centre (excitation λ450nm).

here.

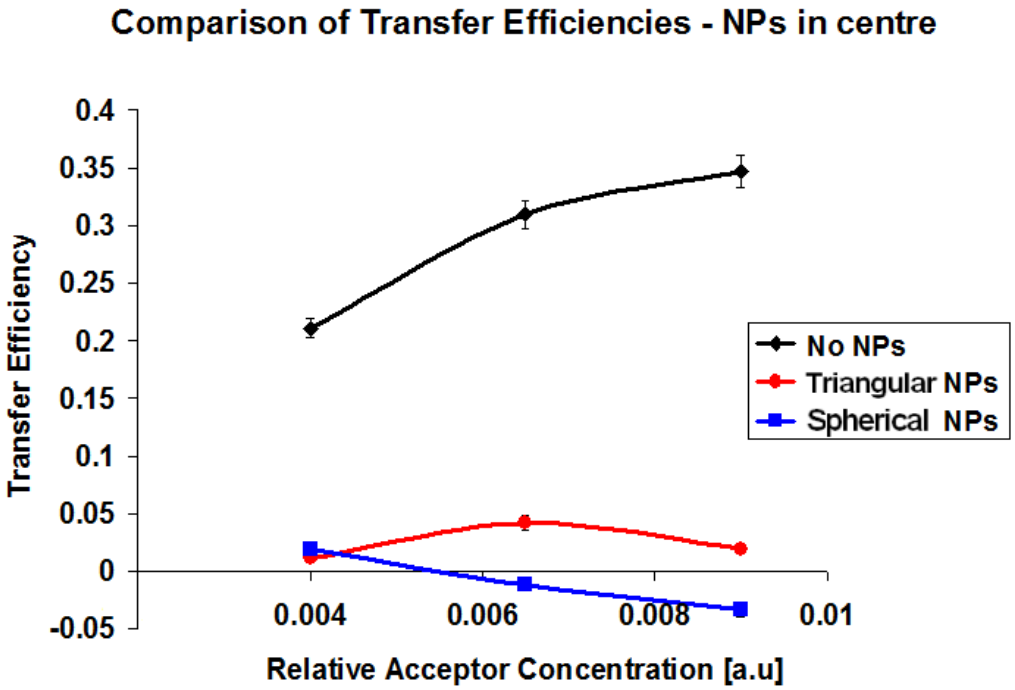

Figure 4.37: Comparison of transfer efficiencies for NPs in the centre of the two dye layers.

Although there is no FRET, it is to be noted that there is still some individual dye fluorescence enhancement, again the larger effect observed for spherical NPs with 425nm LSPR which is resonantly matched to the donor absorption. This is consistent with previous results shown in Section 4.3.1.

4.3.3 Nanoparticles Below

The metal nanoparticles were then placed below the D-A pair. Again both spherical and triangular NPs were tested. This design meant that the NPs were closer to the donor layer than the acceptor layer. The polyelectrolyte and dye layers placed on top of the NPs wrap around them, forming a rough monolayer with a higher surface area, see Fig. 4.38. However as both the donor and acceptor dye are wrapped around, their relative concentrations are unaffected.

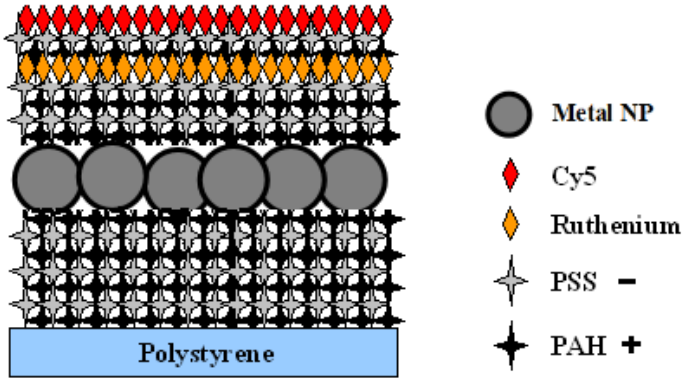

Figure 4.38: Schematic of dye layers and NPs below.

Fig. 4.39 and Fig. 4.40 show the spectral response of the triangular NPs and spherical NPs respectively.

FRET is still occurring with NPs below the D-A pair. For the triangular NPs with a 600nm plasmon resonance, the overall fluorescence from both the donor and the acceptor has increased slightly, but the FRET ratio has dropped from $R_{DA} = 1.7$ to $R_{DA} = 1.2$. For the spherical NPs with a 425nm plasmon resonance, the overall fluorescence from both the donor and the acceptor has increased dramatically. However FRET ratio has also decreased to $R_{DA} = 0.68$ resulting in less energy transfer occurring. There appears to be direct plasmonic enhancement of the individual donor and acceptor, but no enhancement of the energy transfer. Fig. 4.41 shows the reduction in transfer efficiency when the NPs are placed below the two dye layers.

In this configuration although no FRET enhancement is observed, the transfer efficiency is generally lower for both NP types than for NPs above. The

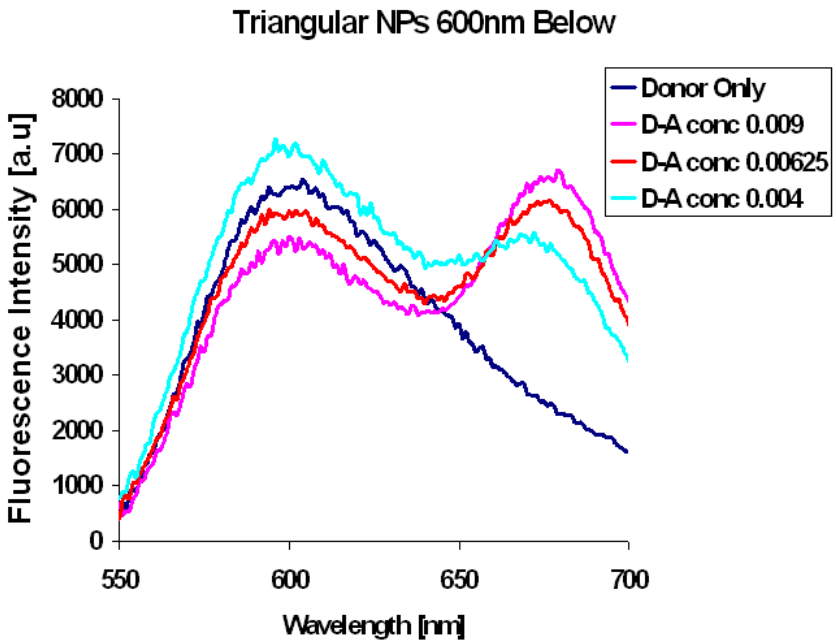

Figure 4.39: FRET spectral response with 600nm NPs below (excitation λ450nm).

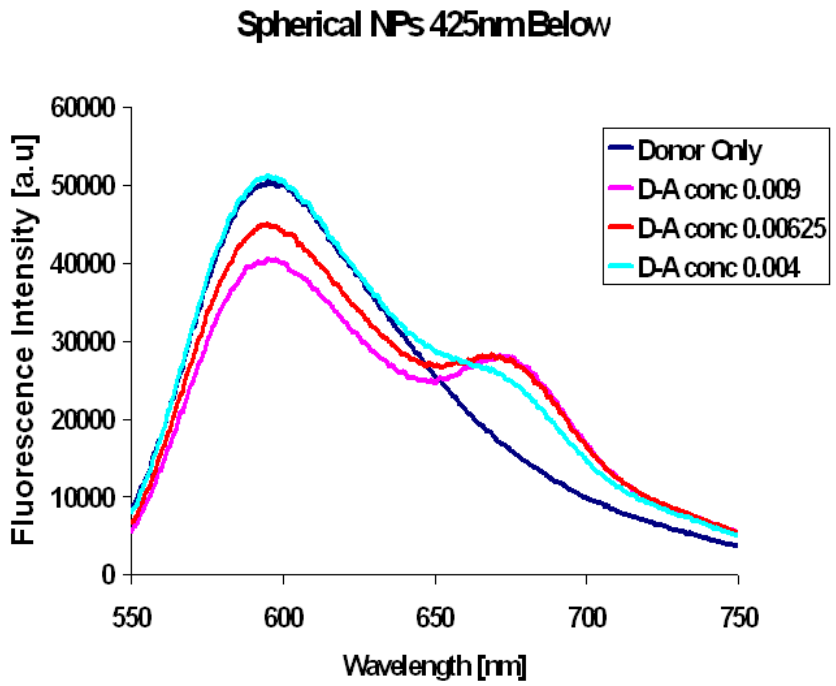

Figure 4.40: FRET spectral response with 425nm NPs below (excitation λ450nm).

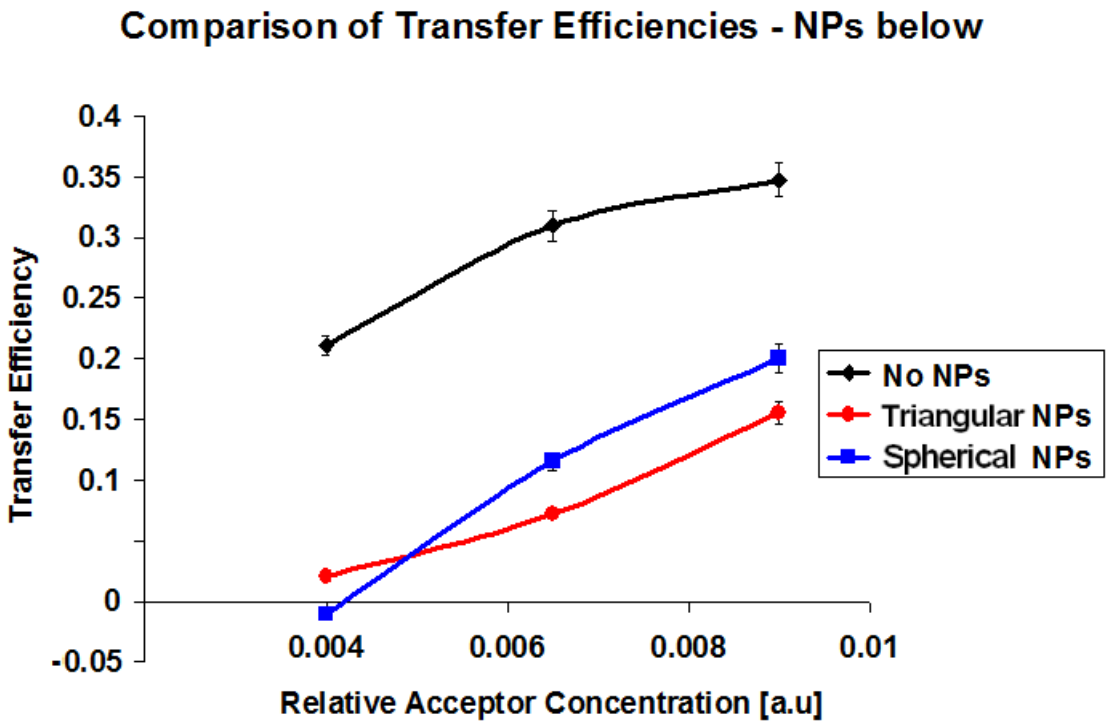

Figure 4.41: Comparison of transfer efficiencies for NPs below the two dye layers.

enhancement of the donor by the triangular NPs, which is matched to the acceptor absorption, is relatively lower. The enhancement of the donor by the spherical NPs, which is matched to the donor absorption, is relatively higher. The spherical NPs are closer to the donor and therefore they produce a larger MEF. It was considered that the issue with no FRET enhancement was the linear placement of the dyes, D-A-NPs. In this configuration the FRET pair was not equidistant from the NPs, as in Zhang et al [20]. Lessard-Viger et al [22] had shown this equidistant configuration to show enhancement. It was therefore decided to take a different approach to ensure equidistance of the FRET dye pair from the NPs.

4.3.4 Nanoparticles with a Mixed Dye Layer

So far, none of the experimental configurations resulted in an increase of the transfer efficiency due to plasmonic interactions. Zhang et al [20] showed that they had achieved an increase in the FRET efficiency using metal nanoparticles and dye conjugated to ss-DNA in solution as depicted in Fig. 4.42.

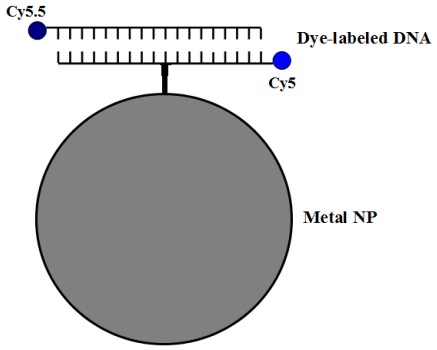

Figure 4.42: Schematic of metal NP with DNA FRET pair [20].

The single donor and acceptor pair in these experiments were equidistant from the NP. As the donor and acceptor were too far apart to have a FRET interaction in the experiments in Section 4.3.3, a combined dye layer was tested. This combined dye layer was a mixture of donor and acceptor molecules deposited on the surface, over an NP layer, as shown in Fig. 4.43. It was considered that an average FRET-plasmonic effect would be observed under these conditions, as a proportion of the D-A pairs would be equidistant and at the optimal distance from the NP.

Fig. 4.44 shows the spectral response of the combined D-A dye layer without any NPs. There is a small FRET effect. It is less than previous experiments due to lower concentration of the dyes as there is competition between the donor and acceptor molecules for surface coverage on the one layer. It is also due to an average D-A spacing as opposed to the controlled spacing in previous experiments.

Fig. 4.45 shows the spectral response of the combined D-A dye layer with spherical NPs below. Practically all FRET effects have disappeared with this configuration with and without spherical nanoparticles. The FRET ratio has been reduced from $R_{DA} = 0.68$ without the presence of NPs to $R_{DA} = 0.47$ in

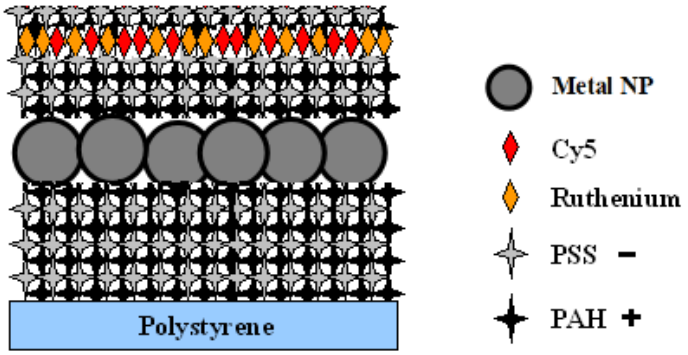

Figure 4.43: Schematic of mixed dye layer and NPs below.

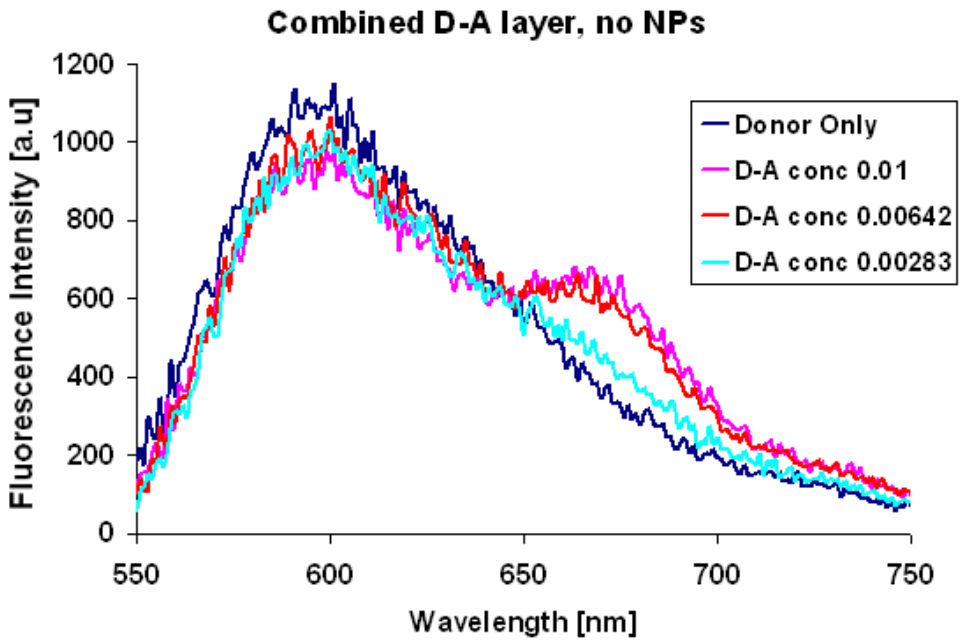

Figure 4.44: FRET spectral response of combined D-A dye layer without NPs (excitation λ450nm).

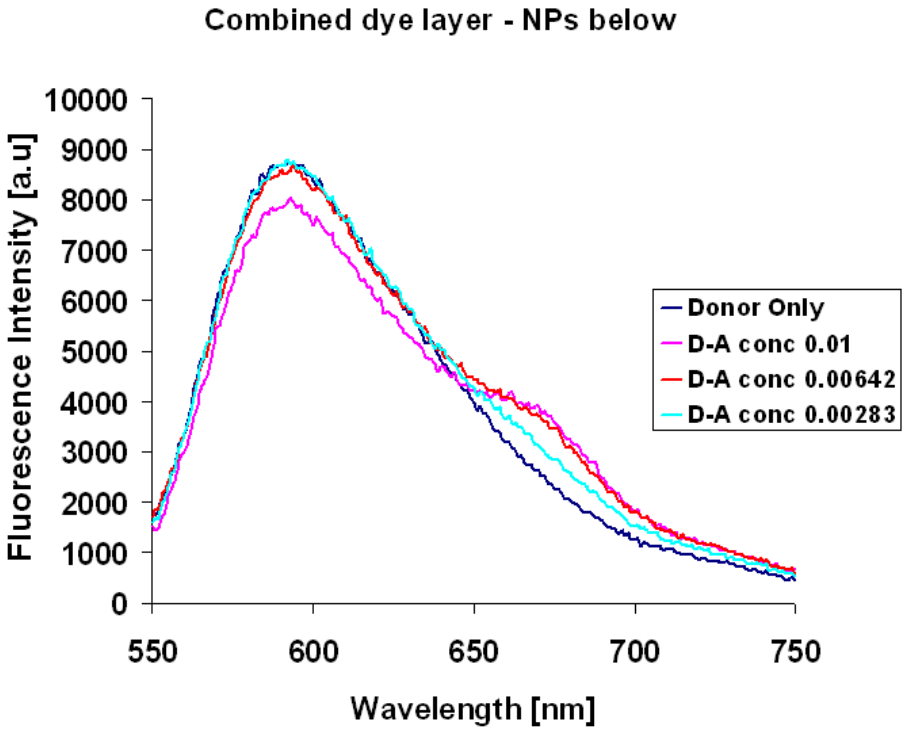

Figure 4.45: FRET spectral response with spherical 425nm NPs below a mixed dye layer (excitation λ450nm).

the presence of NPs. This could be due to the dye-NP de-excitation channel dominating the system and therefore no enhancement is seen in the FRET-NP channel. Fig. 4.46 shows the impact on FRET transfer efficiency with spherical nanoparticles placed below a combined D-A dye layer. The transfer efficiency is reduced.

No FRET enhancement has been observed using the planar FRET approach. It was decided to attempt the single NP-FRET approach as described in the paper by Zhang et al, as part of the investigation in Chapter 5.

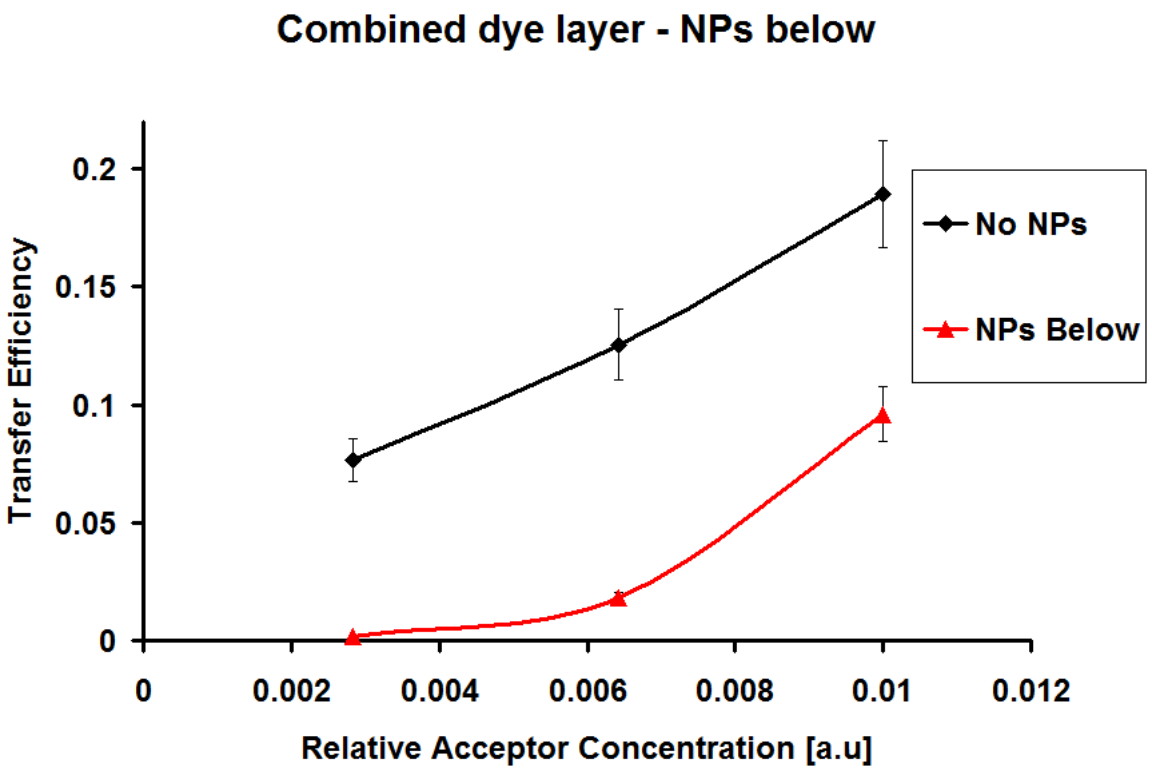

Figure 4.46: Comparison of transfer efficiencies with a combined dye layer.

4.4 Summary

The objective of designing a model system that allows FRET analysis was achieved. In the first part of this chapter, planar FRET was investigated using a number of different configurations. The first configuration allowed variation of the separation of the donor and acceptor via the use of PEL layers. FRET was successfully demonstrated using this configuration. As the results did not sufficiently match the simple theoretical behaviour, a more rigorous theory was proposed where a donor to multiple acceptors model was developed. This new model resulted in a significant improvement in the agreement of the theoretical and experimental results. The remaining discrepancy between the results was most likely caused by dye migration through the PEL layers. To address this issue, the configuration was optimised by varying the effective distance of the donor and acceptor by varying the concentration of the acceptor rather than the number of PEL layers. As expected, this reduced the discrepancy and resulted in excellent agreement between the theoretical and experimental results.

Some recent work reported in the literature [20, 22] claimed that combin-

ing FRET with plasmonics, FRET could be obtained over longer distances and, therefore, enable the technique to be employed in a wide variety of biosensor applications. To investigate this claim, two different types of NPs were tested with resonance wavelengths of 425nm and 600nm. The NPs were placed above, below and in the centre of the donor and acceptor dye layers. NPs were then also placed a set distance from a mixed dye layer to ensure equidistance from the D-A pair. It was found that for all configurations and all NP types the transfer efficiency was reduced. However, plasmonic enhancement of the individual D and A dyes was observed, which was consistent with previous work carried out within the BDI [13, 14, 26] and seen in the FRET systems of Reil et al and Giorgetti et al [16, 17].

A summary of the results is shown in Table 4.1. The fluorescence measurements are the peak values at 600nm for the donor only and donor with acceptor (highest concentration of A). The FRET Ratio for NPs in centre was not possible to calculate because the acceptor peaks were not sufficiently evident.

	D Only Fluor.	D-A Fluor.	FRET Ratios	E_T
No NPs	5668	3692	1.7	0.35
NPs Above (450nm)	37292	29014	0.86	0.22
NPs Above (600nm)	9975	7243	0.99	0.27
NPs Centre (450nm)	55290	57427	-	-0.038
NPs Centre (600nm)	8991	8852	-	0.015
NPs Below (450nm)	50075	40035	0.68	0.200
NPs Below (600nm)	6383	5499	1.2	0.139
Combined No NPs	956	775	0.68	0.189
Combined NPs (450nm)	8418	7610	0.47	0.096

Table 4.1: Summary of FRET-plasmonic interactions.

References

[1] S. D. Spillman, H. M. McEvoy, and B. D. MacCraith. Fabrication of substrate-independent protein microarrays using polyelectrolyte scaffolding. *Langmuir*, 25(3):1403–1411, 2008.

[2] A. Krieg, T. Ruckstuhl, and S. Seeger. Towards single-molecule DNA sequencing: Assays with low nonspecific adsorption. *Analytical Biochemistry*, 349(2):181–185, 2006.

[3] J. Enderlein. Electrodynamics of Fluorescence - private correspondence, 2003.

[4] N. Shaklai, J. Yguerabide, and H. M. Ranney. Interaction of hemoglobin with red blood cell membranes as shown by a fluorescent chromophore. *Biochemistry*, 16(25):5585–5592, 1977.

[5] G. W. Gordon, G. Berry, X. H. Liang, B. Levine, and B. Herman. Quantitative fluorescence resonance energy transfer measurements using fluorescence microscopy. *Biophysical Journal*, 74(5):2702–2713, 1998.

[6] X. Jiang, H. Zheng, S. Gourdin, and P. T. Hammond. Polymer-on-polymer stamping:? universal approaches to chemically patterned surfaces. *Langmuir*, 18(7):2607–2615, 2002.

[7] J. L. Tan, J. Tien, and C. S. Chen. Microcontact printing of proteins on mixed self-assembled monolayers. *Langmuir*, 18(2):519–523, 2001.

[8] M. C. Berg, J. Choi, P. T. Hammond, and M. F. Rubner. Tailored micropatterns through weak polyelectrolyte stamping. *Langmuir*, 19(6):2231–2237, 2003.

[9] S. Kidambi, C. Chan, and I. Lee. Selective depositions on polyelectrolyte multilayers:? self-assembled monolayers of m-dPEG acid as molecular template. *Journal of the American Chemical Society*, 126(14):4697–4703, 2004.

[10] O. Stranik, D. Iacopino, R. Nooney, C. McDonagh, and B. D. MacCraith. Optical properties of micro-patterned silver nanoparticle substrates. *Journal of Fluorescence*, 20(1):215–223, 2010.

[11] K. Aslan, I. Gryczynski, J. Malicka, E. Matveeva, J. R. Lakowicz, and C. D. Geddes. Metal-enhanced fluorescence: an emerging tool in biotechnology. *Current Opinion in Biotechnology*, 16(1):55–62, 2005.

[12] J. Malicka, I. Gryczynski, and J. R. Lakowicz. DNA hybridization assays using metal-enhanced fluorescence. *Biochemical and Biophysical Research Communications*, 306(1):213–218, 2003.

[13] O. Stranik, H. M. McEvoy, C. McDonagh, and B. D. MacCraith. Plasmonic enhancement of fluorescence for sensor applications. *Sensor and Actuators B*, 107(1):148–153, 2005.

[14] R. Nooney, A. Clifford, X. LeGuevel, O. Stranik, C. McDonagh, and B. D MacCraith. Enhancing the analytical performance of immunoassays that employ metal-enhanced fluorescence. *Analytical and Bioanalytical Chemistry*, 396(3):1127–1134, 2010.

[15] Joanna Malicka, Ignacy Gryczynski, Zygmunt Gryczynski, and Joseph R. Lakowicz. Effects of fluorophore-to-silver distance on the emission of cyanine-dye-labeled oligonucleotides. *Analytical Biochemistry*, 315(1):57–66, 2003.

[16] F. Reil, U. Hohenester, J. R. Krenn, and A. Leitner. Forster-type resonant energy transfer influenced by metal nanoparticles. *Nano Letters*, 8(12):4128–4133, 2008.

[17] E. Giorgetti, S. Cicchi, M. Muniz-Miranda, G. Margheri, T. Del Rosso, A. Giusti, A. Rindi, G. Ghini, S. Sottini, A. Marcelli, and P. Foggi. Forster resonance energy transfer (FRET) with a donor-acceptor system adsorbed

on silver or gold nanoisland films. *Physical Chemistry Chemical Physics*, 11(42):9798–9803, 2009.

[18] J. Malicka, I. Gryczynski, J. Fang, J. Kusba, and J. R. Lakowicz. Increased resonance energy transfer between fluorophores bound to DNA in proximity to metallic silver particles. *Analytical Biochemistry*, 315(2):160–169, 2003.

[19] P. Andrew and W. L. Barnes. Energy transfer across a metal film mediated by surface plasmon polaritons. *Science*, 306(5698):1002–1005, 2004.

[20] J. Zhang, Y. Fu, M.H. Chowdhury, and J.R. Lakowicz. Enhanced forster resonance energy transfer on single metal particle. 2. dependence on donor-acceptor separation distance, particle size, and distance from metal surface. *J. Phys. Chem. C*, 111(32):11784–11792, 2007.

[21] J. Zhang, J. Malicka, I Gryczynski, and J R Lakowicz. Surface-enhanced fluorescence of fluorescein-labeled oligonucleotides capped on silver nanoparticles. *Journal of Physical Chemistry B*, 109:7643–7648, 2005.

[22] M. Lessard-Viger, M. Rioux, L. Rainville, and D. Boudreau. FRET enhancement in multilayer core-shell nanoparticles. *Nano Letters*, 2009.

[23] O. Stranik. *Plasmonic enhancement of fluorescence for biomedical diagnostics*. PhD thesis, 2007.

[24] P. Anger, P. Bharadwaj, and L. Novotny. Enhancement and quenching of single-molecule fluorescence. *Physical Review Letters*, 96:113002, 2006.

[25] E. Hutter and J. H. Fendler. Explotation of localized surface plasmon resonance. *Advanced Materials*, 16(19, October 4):16851706, 2004.

[26] C. McDonagh, O. Stranik, R. Nooney, and B. D MacCraith. Nanoparticle strategies for enhancing the sensitivity of fluorescence-based biochips. *Nanomedicine*, 4(6):645–656, 2009.

Chapter 5

Solution FRET and Plasmonic Interactions

5.1 Introduction

The concept of plasmonic enhancement of FRET was introduced in Chapter 4, where this effect was investigated for the planar FRET configuration. A new model to investigate the interaction of FRET and plasmonics in solution was designed, which would be compatible with next-generation solution-based biosensors. This chapter investigates FRET in solution using two complementary dye labeled oligonucleotides. FRET was achieved using Cy5 as the donor, whose emission band at 670nm overlaps with the absorption band of the acceptor Cy5.5 at 675nm. The distance between the donor and acceptor was controlled by the number of base pairs on the oligonucleotides. First the energy transfer was measured in solution for two different lengths of DNA. Next the FRET pair were chemically bound to metal NPs and the energy transfer measured again. Gold, silver and silica particles were used in this work. The distance between the dye pair and the metal NPs was controlled using spacer layers composed of proteins and polyelectrolytes. A similar experimental design was described by Zhang et al [1], and showed promising results for FRET enhancement. Another design by Lessard-Viger et al [2] using metal NPs surrounded by dye doped silica shells also achieved an apparent FRET enhancement.

5.2 Materials and Methods

5.2.1 Fluorescent Dyes

The FRET dye pair used during the experiments in Chapter 4 was a Ruthenium-complex donor and a Cy5 acceptor. In this work, Cy5 was chosen as the donor (D) and Cy5.5 was chosen as the acceptor (A) because of their compatibility with the oligonucleotides (TIB Molbiol). The Stokes shift for this pair is small and therefore the possibility of cross-talk and bleed-through is more prevalent in these experiments than in the previous ones. Cross-talk refers to when the acceptor is directly excited by the donor excitation light [3, 4]. Bleed-through refers to when the donor emission is detected within the range of acceptor emission. Table. 5.1 gives the donor and acceptor dye properties while, Fig.5.1 shows the absorption and emission spectra of the donor and acceptor dyes.

	Excitation λ	Emission λ	Quantum Yield	Lifetime
Donor (Cy5)	650nm	670nm	0.28	∼1.0ns
Acceptor (Cy5.5)	675nm	694nm	0.23	∼1.0ns

Table 5.1: Donor and acceptor dye properties.

The Förster Radius (R_0) for the D-A pair was 6.07nm (see Appendix 4). Two different lengths of complementary oligonucleotides were used in this work, as is shown in Fig.5.2. The first was 21 base pairs (bp), which was 7.14nm in length. The second was 43 base pairs, which was 14.62nm in length. These lengths were the theoretical calculations based on uncurled oligonucleotides. This meant that if the 21bp oligonucleotide spacer remained uncurled, some energy transfer should be observed as the dyes would be within the 10nm FRET limit. In addition, if the 43bp oligonucleotide spacer remained uncurled, FRET should not be observed, as the dyes would be beyond the FRET limit and the dipole dipole interactions would not be able to take place.

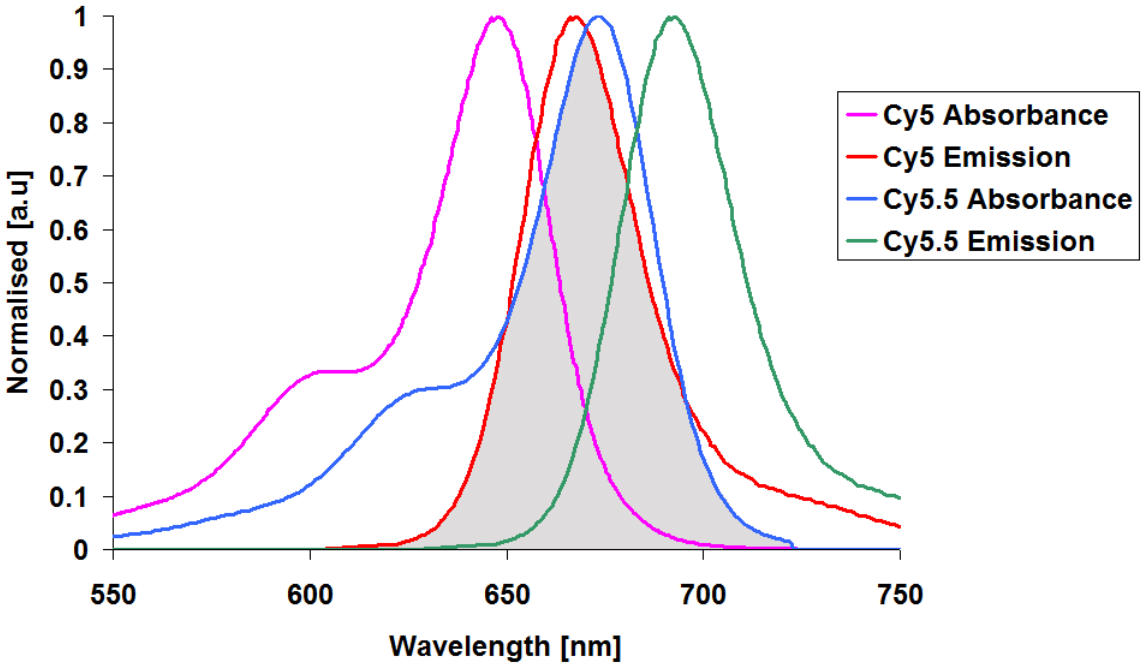

Figure 5.1: Absorption and emission spectra of the donor and acceptor dyes.

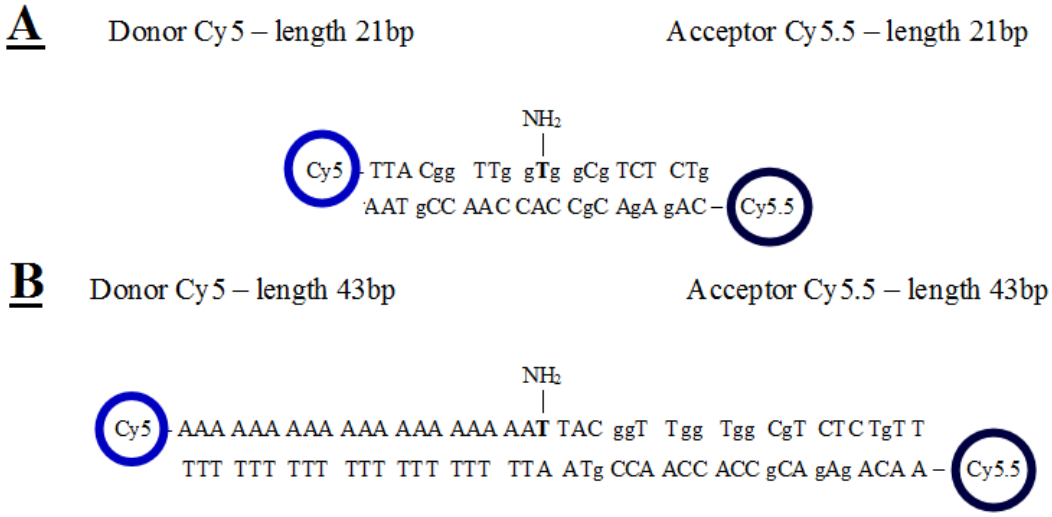

Figure 5.2: Oligonucleotide spacers used in the experiments. A - complementary oligonucleotide sequences 21 base pairs in length, labeled with D and A dyes. B - complementary oligonucleotide sequences 43 base pairs in length, labeled with D and A dyes.

5.2.2 Metal Nanoparticles

Gold and silver NPs were obtained from British Biocell International. Fig.5.3 shows the absorbance spectra of the two metal NP solutions, both NPs are 80nm in diameter. The silver NP plasmon resonance band is much broader than the gold NP band and this is due to the quadrupole and octupole resonances of the silver NP [5, 6]. The concentration of NPs was 10^9 particles/ml.

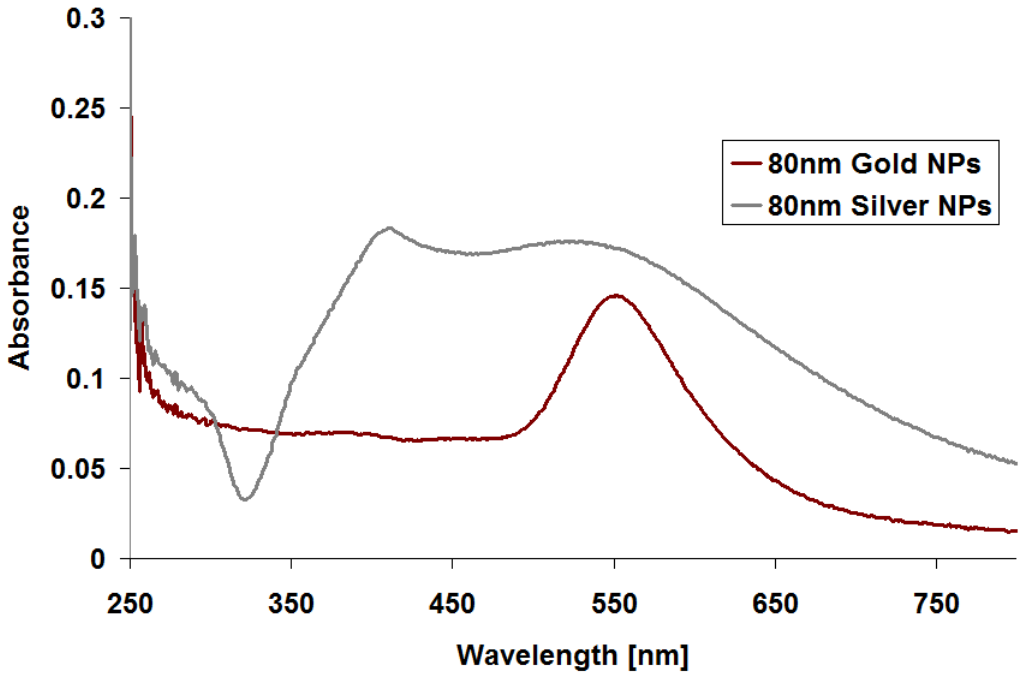

Figure 5.3: Gold and Silver NP plasmon resonance bands.

5.2.3 Experimental Procedures

Primary Spacer Layer

A spacer layer was required around the metal NPs in order to keep the donor and acceptor molecules outside the quenching zone. The metal NPs were coated with MHA (mercapto-hexadecanoic-acid - MW=288.5g), as illustrated in Fig. 5.4. For this process, 1ml of the original NP solution was buffer exchanged with water by centrifuging at 17,000 rpm for 5 minutes and re-suspending the NPs in 1ml of deionised water. This solution was then centrifuged at the same rate and 1ml of 50mM MHA activated in DMF (dimethylformamide) was added. The

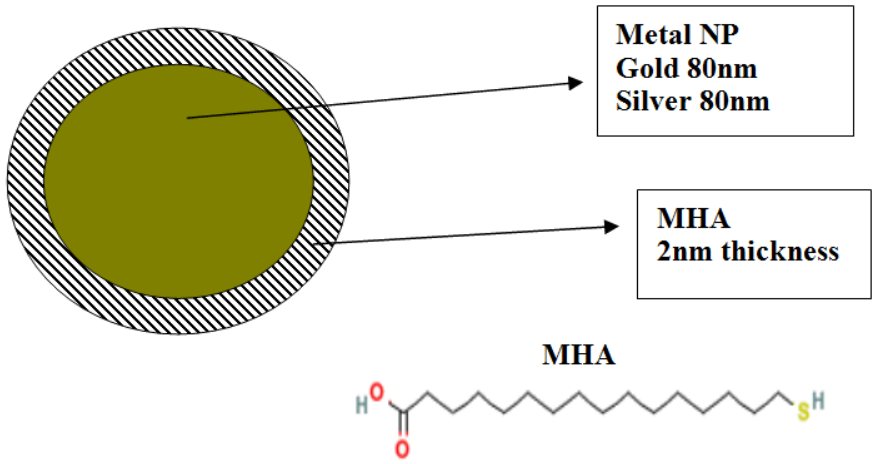

Figure 5.4: Metal NP surrounded with MHA layer.

sample was sonicated briefly, covered in tinfoil and placed on a shaker @ 250rpm for 15-36 hours to allow the MHA to form a self assembled monolayer on the NPs [7]. Next the solution was centrifuged at 17,000rpm for 5 minutes, to separate the NPs from the MHA solution. The supernatant was removed and the residue was re-suspended in 1ml 75:25 DMF in water. In order to remove all unbound MHA repeated wash steps were performed, slowly increasing the ratio of water to DMF. The solution was centrifuged and re-suspended in 0.5ml 50:50 DMF in water, then repeated and re-suspended in 0.5ml of deionised water, and finally, after washing once more, left suspended in 0.5ml water. This resulted in a 2nm densely packed layer of MHA around the metal NPs (MHA-NPs), with carboxyl (COOH) surface groups.

Secondary Spacer Layer

A poly(ethylene glycol) (PEG) linker was used to compete with the oligonucleotides for surface groups on the MHA layer, as shown in Fig. 5.5. The MHA-NPs were centrifuged at 17,000 rpm for 5mins to remove the water. The MHA-NP residue was then re-suspended in 25μl of 200mM EDC (1-(3-Dimethylaminopropyl)-3-ethylcarbodiimide hydrochloride - MW=191.5g), 25μl of 4x10^{-6}M PEG_4 (MW=265.3g) linker and 50μl 2x10^{-7}M donor oligonucleotide. The sample was then covered in tinfoil and placed on a shaker at 250rpm for 1 hour. Next the sample was centrifuged and the EDC/PEG_4 suspension removed. The residue was washed with

water twice using the sonicate - centrifuge - remove - re-suspend method as before. This resulted in a 1.81nm layer around the MHA-NPs (PEG_4-MHA-NPs), with carboxyl (COOH) surface groups.

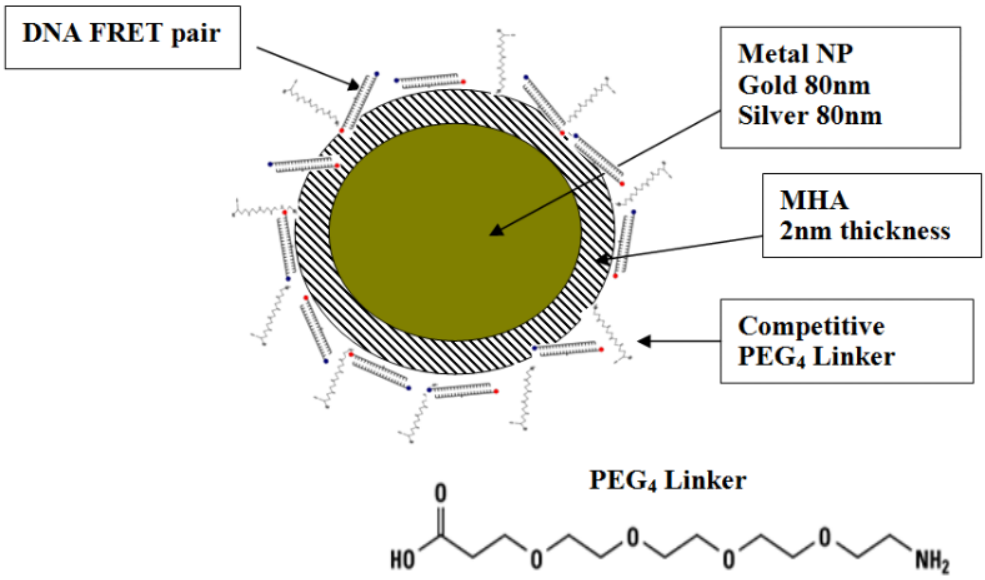

Figure 5.5: Metal NP surrounded with MHA and PEG layer.

Polyelectrolyte Spacer Layer

In order to increase the spacer layer between the NP and the D and A to the optimum thickness of 6nm (see Chapter 3), another type of spacer layer was also used which incorporated polyelectrolytes, as described by Gittins et al [8–11], and shown in Fig. 5.6. The negatively charged MHA-NPs were centrifuged to remove the water. They were re-suspended in a solution of positively charged PEL (PAH) as described in Chapter 3.4. The sample was then covered in tinfoil and placed on a shaker for 20 minutes. The sample was centrifuged and the residue washed three times with deionised water. The PAH-MHA-NPs were then re-suspended in a solution of negatively charged PEL (PSS), left for 20 minutes and washed. This layer-by-layer approach continued with another layer of PAH, PSS, PAH and then a layer of negatively charged PAC (poly acrylic acid) was deposited. The PAC layer resulted in a carboxyl surface with which the oligonucleotides could react. The composition of all polyelectrolyte solutions was 1mg/ml polyelectrolyte with

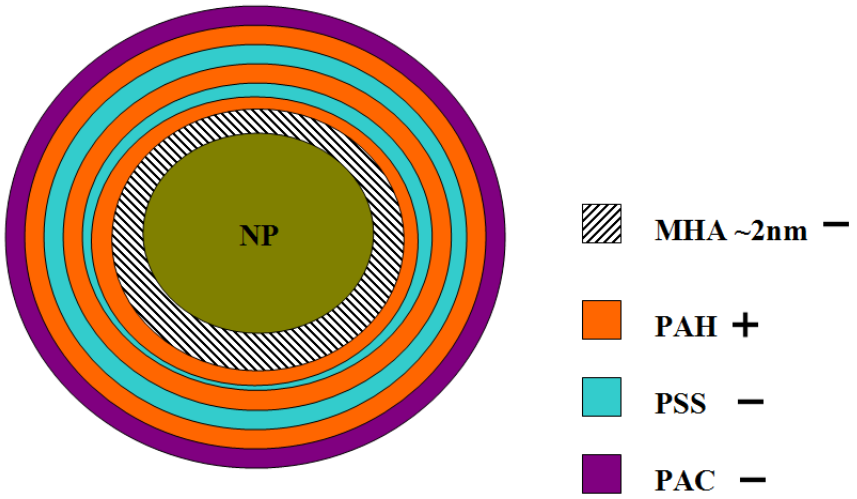

Figure 5.6: Metal NP surrounded by MHA and PEL layers.

1mM NaCl in water.

DNA Attachment

The donor dye (Cy5) labeled oligonucleotides contained an amino moiety in the centre of their sequences, as shown in Fig. 5.7. This amino moiety bound with the carboxyl moiety on the surface of the NPs. 50μl of 100mM EDC and 50μl of 2 x 10^{-6}M donor labeled oligonucleotide was added to the residue of the MHA-NPs. The sample was sonicated, covered in tinfoil and placed on a shaker at 250 rpm for 1 hour. Next the sample was centrifuged and the EDC-oligonucleotide suspension removed. The residue was washed with water three times using the sonicate - centrifuge - remove - re-suspend method as before. The sample was then re-suspended in 0.5ml of water and 150μl was pipetted into three wells of a microtitre plate. The fluorescence intensity of the samples was measured using a Tecan Safire II Spectrophotometer exciting at 610nm. The samples were returned to the original container and centrifuged to remove the unbound oligonucleotides. Next the complementary acceptor dye (Cy5.5) labeled oligonucleotide was hybridised to the first (100μl of 1 x 10^{-7}M acceptor labeled oligonucleotide, diluted using hybridisation buffer (obtained from Roche Diagnostics GmbH)). The sample was placed in an oven at 37°C for 1 hour and then centrifuged to remove the unbound

oligonucleotides. The residue was then washed with water three times using the sonicate - centrifuge - remove - re-suspend method as before and the fluorescence intensity was recorded again.

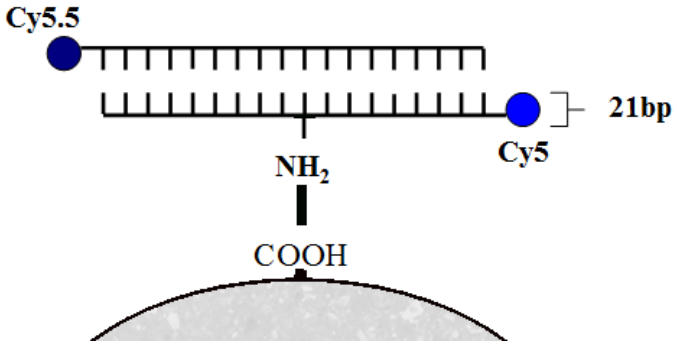

Figure 5.7: DNA attachment to the NPs.

5.3 Results and Discussion

This section reports the results of the solution-based FRET model system. First the energy transfer between the complementary oligonucleotides in solution was investigated. Next, the oligonucleotides were attached to the metal NPs and the model investigated the possible homo-FRET interactions between the donors and acceptors at high concentrations. The optimum distance for MEF enhancement of fluorescence was shown in Chapter 3 to be 6nm. Therefore, the metal NPs were coated in polyelectrolyte spacer layers, which increased the distance between the FRET pair and the metal NP. FRET was achieved and the energy transfer was compared to that of the FRET dye pair on silica nanoparticles.

5.3.1 DNA-FRET without NPs

In order to measure the energy transfer between the donor and acceptor in solution, 1 x 10^{-8}M of the donor labeled oligonucleotide was placed in 0.5ml of hybridisation buffer and the fluorescence intensity measured on the spectrophotometer. 1 x 10^{-8}M of the complementary acceptor dye labeled oligonucleotide was then added to the solution and the donor fluorescence intensity measured again. Fig. 5.8 shows a schematic of the experiment.

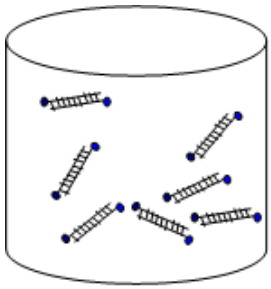

Figure 5.8: Schematic of the complementary oligonucleotides in solution without NPs.

DNA-FRET was successfully demonstrated using fluorescence intensity measurements from spectral analysis, as shown in Fig. 5.9. The transfer efficiency was calculated using the values for the donor fluorescence intensity in the absence and presence of the acceptor and Eqn.(4.1). It was expected that, if the 21bp oligonucleotides remained uncurled, they would have the higher transfer efficiency. However, Fig. 5.10 shows that the 43bp oligonucleotides had a greater energy transfer. Therefore it was concluded that the oligonucleotides did not act as rigid rods but that the longer ones curled up upon themselves [12]. This would place the dyes closer together and hence give a higher transfer efficiency. To avoid the issue of folding, shorter oligonucleotides were used in subsequent experiments.

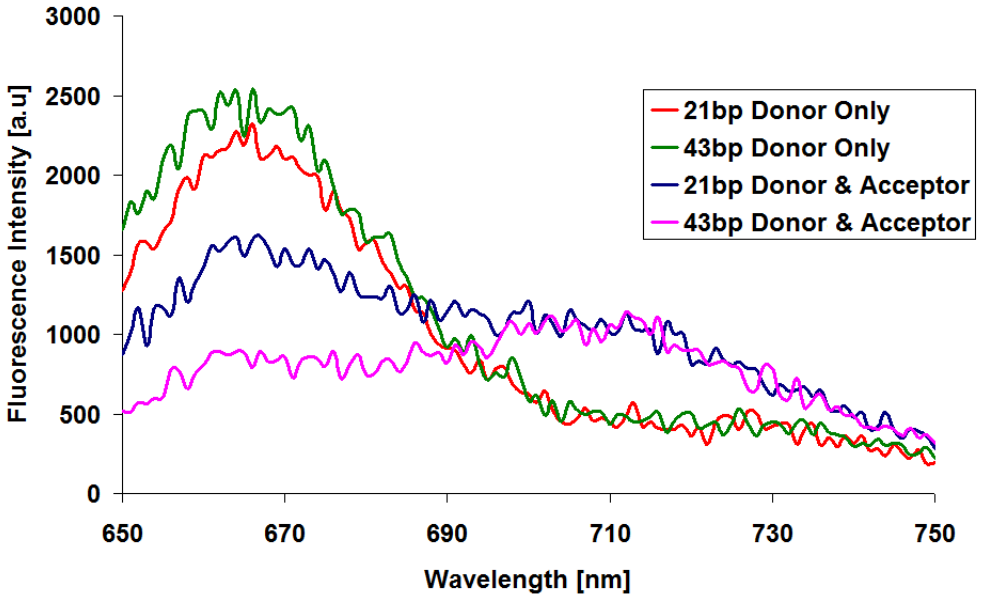

Figure 5.9: FRET spectral response for 21bp and 43bp complementary oligonucleotides in water.

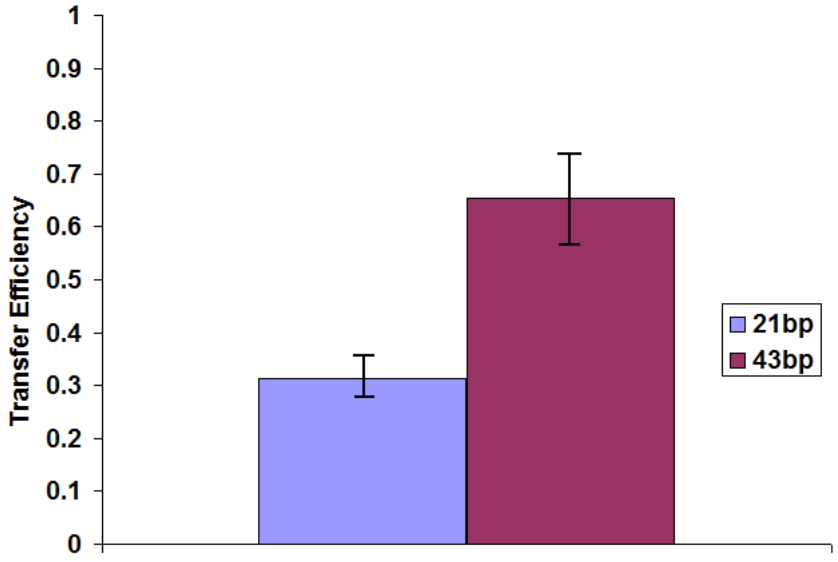

Figure 5.10: Transfer efficiency of 21bp and 43bp complementary oligonucleotides in water.

5.3.2 DNA-FRET with NPs

DNA-FRET was successfully demonstrated in solution using two complementary dye-labeled oligonucleotides. Next, the interaction between DNA-FRET and the plasmonic enhancement of fluorescence was investigated. The concentration of dye molecules on a surface is important, and too high a concentration can lead to homo-FRET (donor-donor or acceptor-acceptor energy transfer), which reduces the transfer efficiency of the donor-acceptor pair. The first experiment involves using PEG spacers on metal NPs to determine if homo-FRET is occurring. The second experiment uses PELs as spacer layers to increase the distance between the metal NP and the FRET pair to 6nm, the optimum distance for MEF, as discussed in Section 3.5.3. Silica NPs are used in this experiment as a control to compare non-plasmonic versus plasmonic enhancement.

Homo-FRET Investigation

In order to test for homo-FRET and self quenching effects, which would happen if the dyes were too densely packed on the surface, in this experiment the donor oligonucleotide was made to compete for surface groups with PEG_4 in one of the samples. This meant that less donor oligonucleotides were bound to the surface. Higher donor emissions in this sample compared to the non-competitive sample would imply that homo-FRET was occurring and the concentration of oligonucleotides would need to be reduced. The complementary oligonucleotides were attached to the gold and silver metal NPs as described in Section 5.1.3. The unbound oligonucleotides were removed from the solutions via centrifugation and re-suspension in deionised water. Fig. 5.11 shows a schematic of the layering system around the NP.

FRET was successfully demonstrated and Fig. 5.12 shows the spectral response of the non-competitive sample for silver NPs and Fig. 5.13 shows the spectral response of the non-competitive sample for gold NPs. The fluorescence intensity of the donor on the silver NP is much greater than on the gold NP. This is due to the greater overlap of the donor absorption and emission bands with the plasmon resonance band of the silver, compared to that of the gold, and the greater plasmon effect of silver as discussed in Chapter 2. This con-

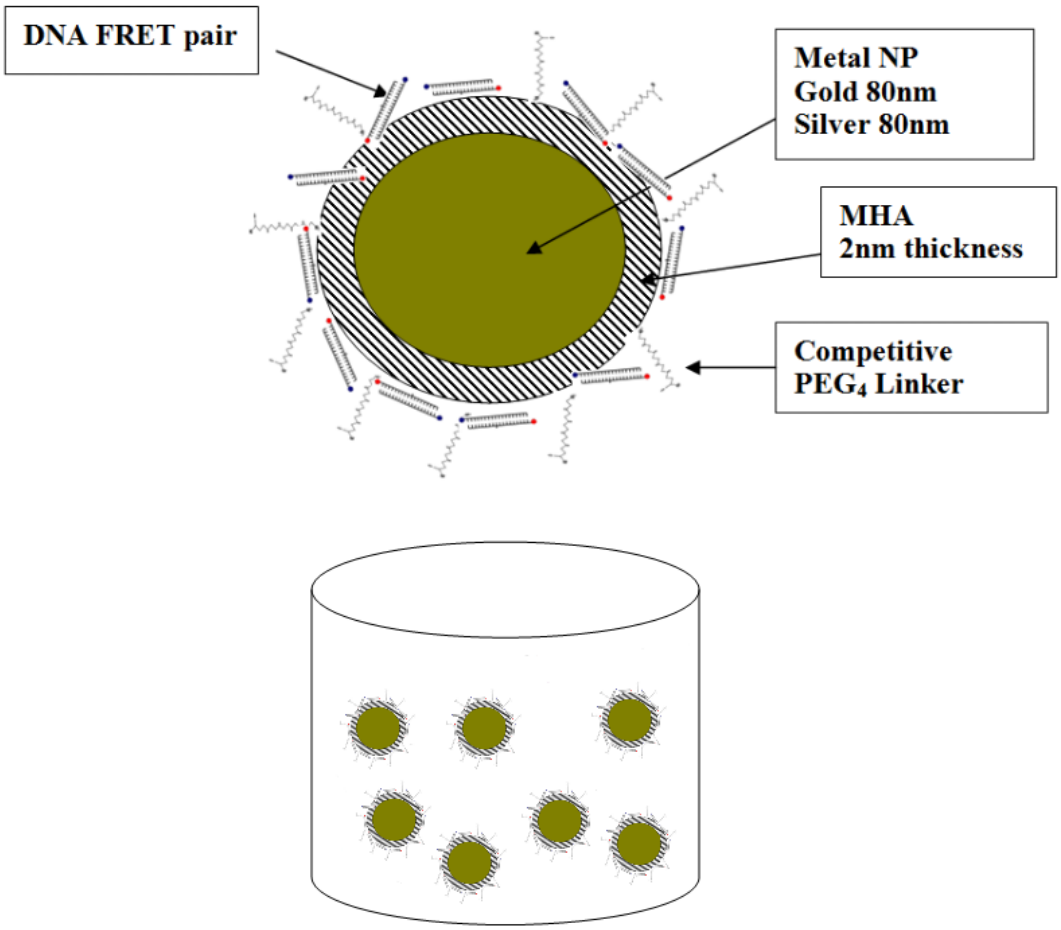

Figure 5.11: Spacer layering around the metal NP with oligonucleotides attached. Inset shows schematic of the NPs in solution.

firms plasmonic enhancement of the donor labeled oligonucleotide. When the acceptor labeled oligonucleotide is hybridised to the donor, energy transfer occurs. The transfer efficiency is higher on the gold NPs than on the silver NPs. It appears that the transfer efficiency decreases when there is greater plasmonic enhancement. This is consistent with the observations made in Chapter 4 with the spherical and triangular NPs.

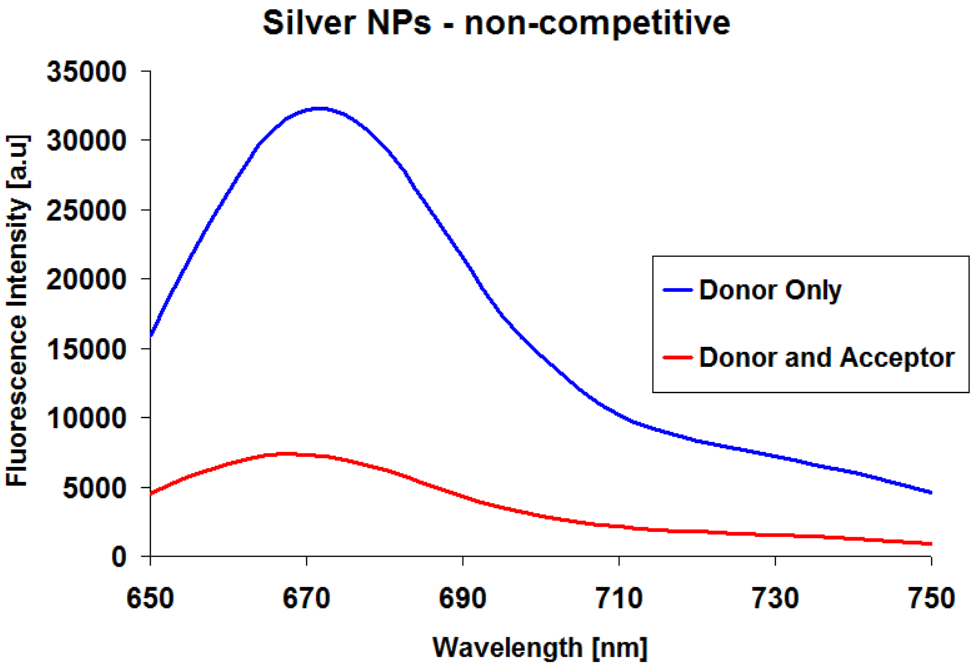

Figure 5.12: Non-competitive sample: Fluorescence intensity measurements of oligonucleotides on silver NPs, donor only emission and donor plus acceptor emission (excitation λ610nm).

The competitive sample shown in Fig. 5.14 shows that the intensity of the donor emission for both gold and silver NPs is less than for the non-competitive sample. This confirms that the donor is not self-quenching for the given concentration of oligonucleotides. The results show the same trend as the non-competitive sample, the silver NPs show a greater plasmonic enhancement, but the transfer efficiency is lower than the gold NPs.

Fig. 5.15 shows the transfer efficiencies of all samples. It can be seen that the values for the transfer efficiency are similar for the competitive and non-competitive samples. This confirms that the donor and acceptor are interacting one to one and not between neighbouring oligonucleotides. If this was occurring there would be a greater transfer efficiency in the non-competitive sample. The

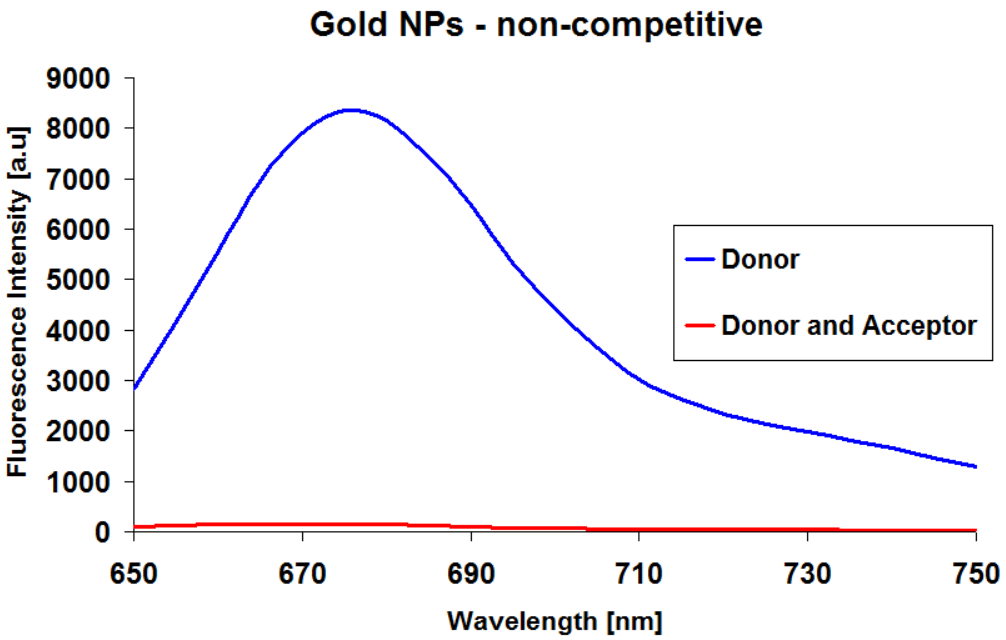

Figure 5.13: Non-competitive sample: Fluorescence intensity measurements of oligonucleotides on gold NPs, donor only emission and donor plus acceptor emission (excitation λ610nm).

other main conclusion from this experiment is that there is less energy transfer occurring on the silver NPs even though they give the greatest plasmonic enhancement compared to the gold NPs.

The energy transfer between the donor and acceptor oligonucleotides on a metal NP has been demonstrated. However, when calculating this using donor intensities one cannot be sure if the reduction in intensity when the acceptor is attached is due to energy transfer or due to some of the NPs being removed during the wash step. The ideal would be to have no wash steps. It would also be beneficial to compare this data to the same concentrations of oligonucleotides on NPs without metal present. The subsequent experiments tackled both of these issues by removing the wash step between the donor and acceptor hybridisation and by employing silica NPs as a control to compare DNA-FRET with and without plasmonic enhancement.

Enhanced FRET Investigation

In order to ensure adequate spacing of the metal NP and the FRET pair, polyelectrolyte layers were attached to the MHA coated metal NPs as described in

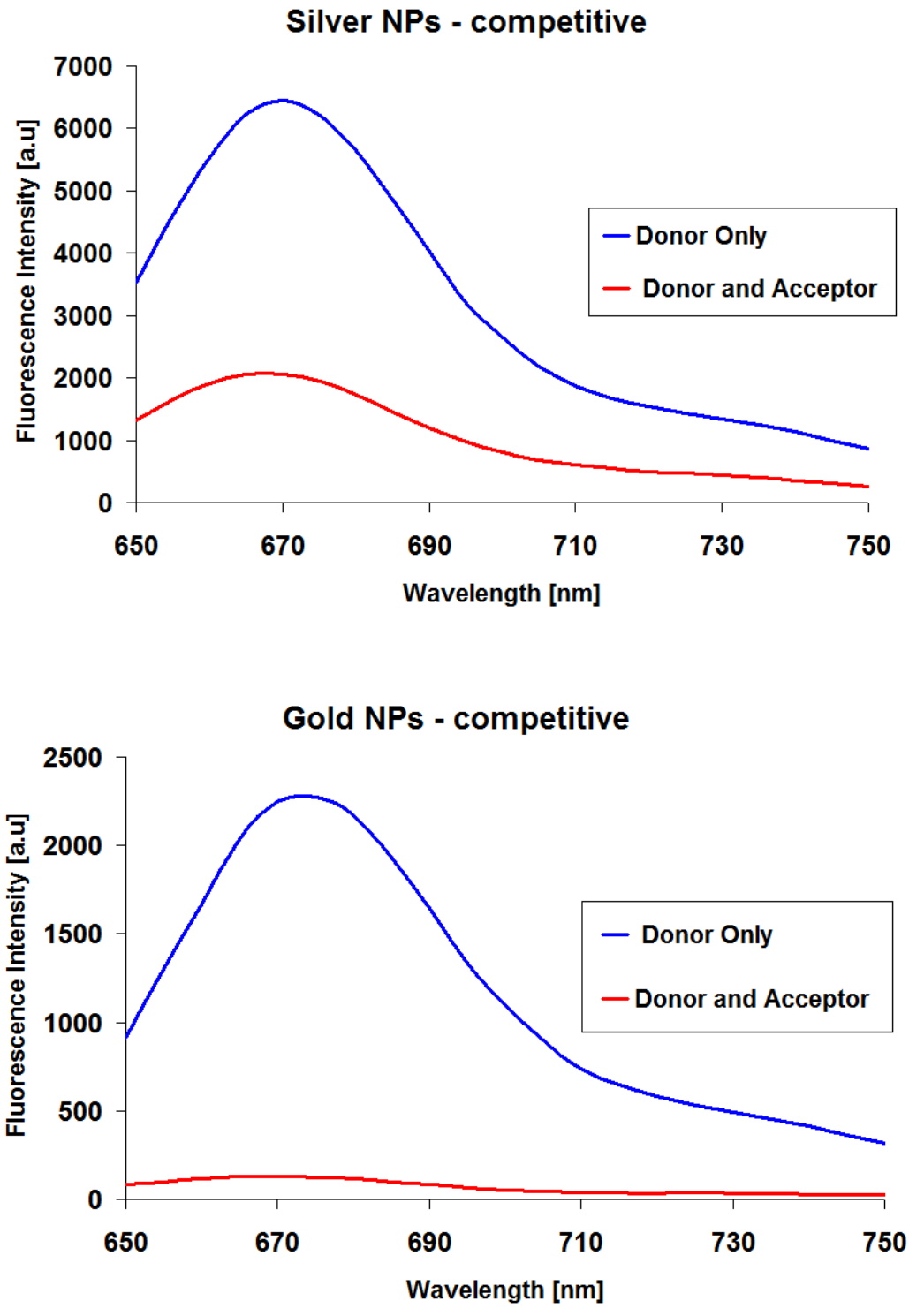

Figure 5.14: Competitive sample: Fluorescence intensity measurements of oligonucleotides on silver and gold NPs, donor only emission and donor plus acceptor emission (excitation λ610nm).

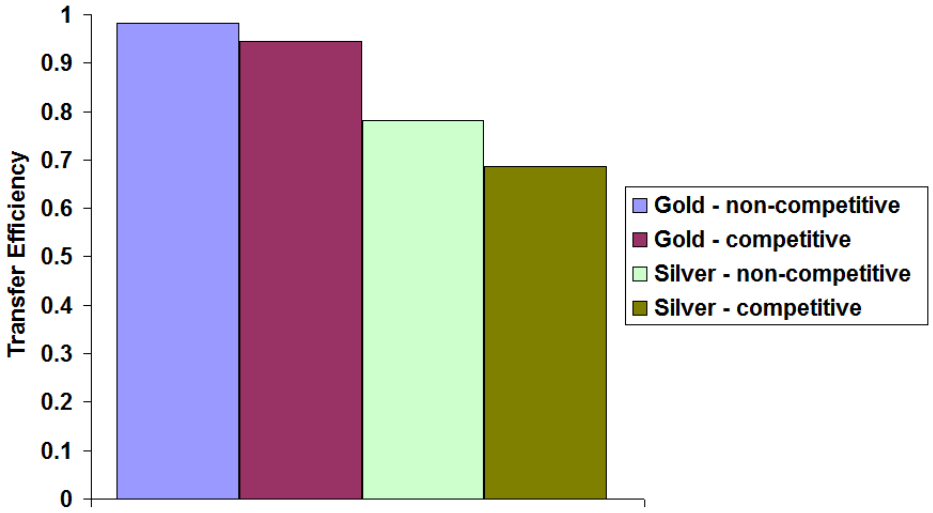

Figure 5.15: Transfer efficiencies for all samples.

Section 5.1.3. The complementary oligonucleotides (10^{-9}M) were attached to the gold and silver metal NPs through the carboxyl groups on the outermost PAC layer using the method described in Section 5.1.3. In this experiment the unbound oligonucleotides were not removed from the solution to prevent discrepancies due to possible removal of the NPs during wash steps. Fig. 5.16 shows a schematic of the layering system around the NP. Silica NPs (10^9particles/ml) were also used in this experiment as a control to compare the MEF effect on the energy transfer. The fluorescence intensities were measured on the Tecan Safire II Spectrophotometer and are shown in Fig. 5.17.

Fig. 5.17 shows the plasmonic enhancement of the donor labeled oligonucleotide for both the gold and silver NPs compared to the silica NPs. The enhancement is greater for the gold NPs than for the silver. This could be attributed to possible etching of the silver in the buffers as discussed in Chapter 2, or the loss of some NPs during the layering wash steps.

Next the acceptor-labeled oligonucleotide was hybridised to the donor as in Section 5.3.1. The fluorescence intensities were measured again using the spectophotometer and are presented in Fig. 5.18.

The peak values of the donor emission are very similar to that of the donor only oligonucleotide (Fig. 5.17). This is due to the overlap between the emission bands of the donor and acceptor, as mentioned previously. This can be overcome

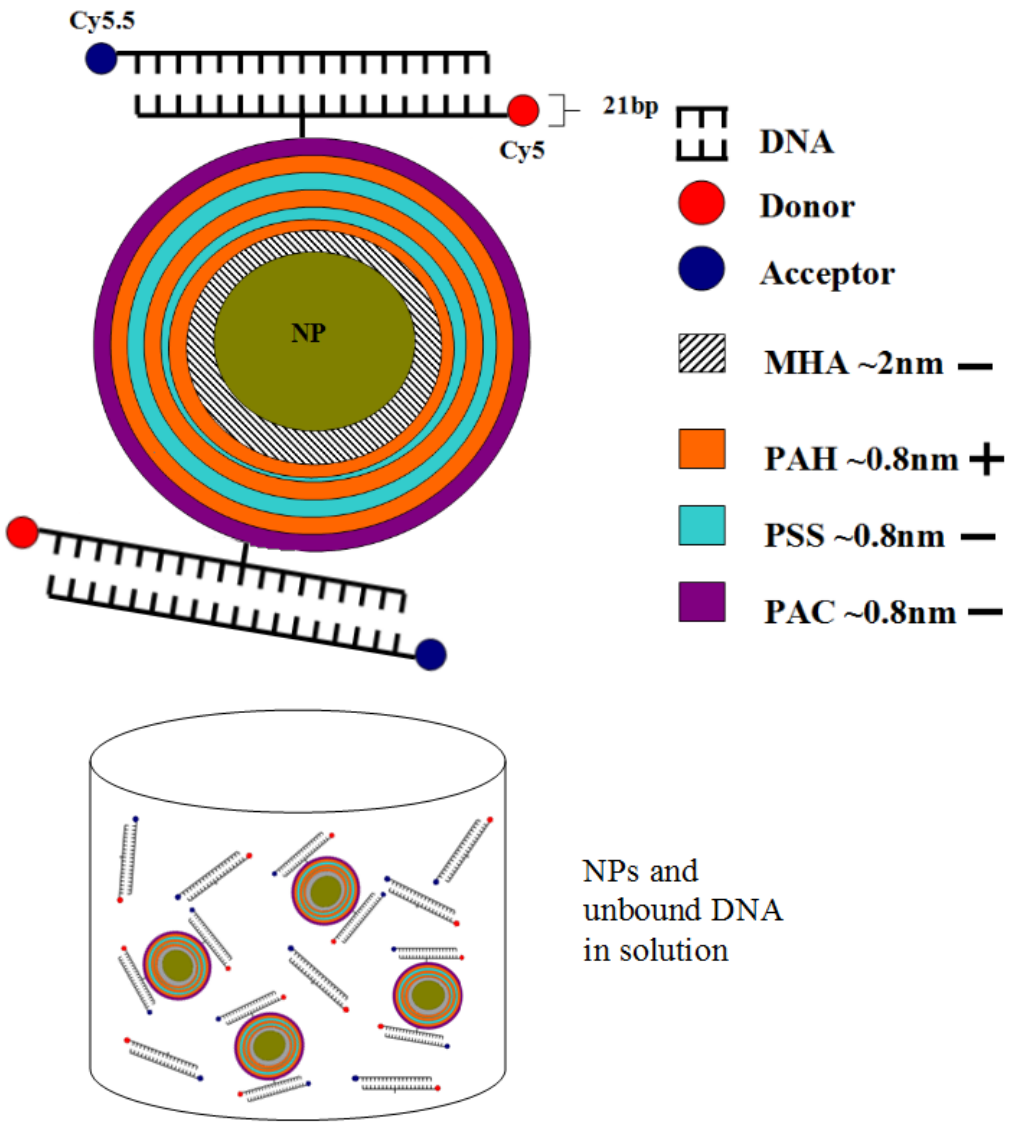

Figure 5.16: PEL spacer layering around the metal NP with oligonucleotides attached. Inset shows schematic of the NPs in solution with unbound oligonucleotides.

by measuring the emission of an acceptor only sample. As the acceptor does not have an amino moiety in the centre of its sequence it cannot be attached to the NPs alone, to allow removal of its contribution to the signal. Peak fitting in Origin can help to overcome this problem. Fig. 5.19 shows how this was done and the values for the donor only intensity, I_D and donor in the presence of the acceptor intensity, I_{DA}. It was these value that were then used to calculated the transfer efficiency for each of the NPs, both metal and silica.

The transfer efficiency for each of the NPs is shown in Fig. 5.20. While the overall fluorescence intensity for the silica NPs is less than for the metal NPs due to a lack of plasmonic enhancement, the transfer efficiency is higher. However as

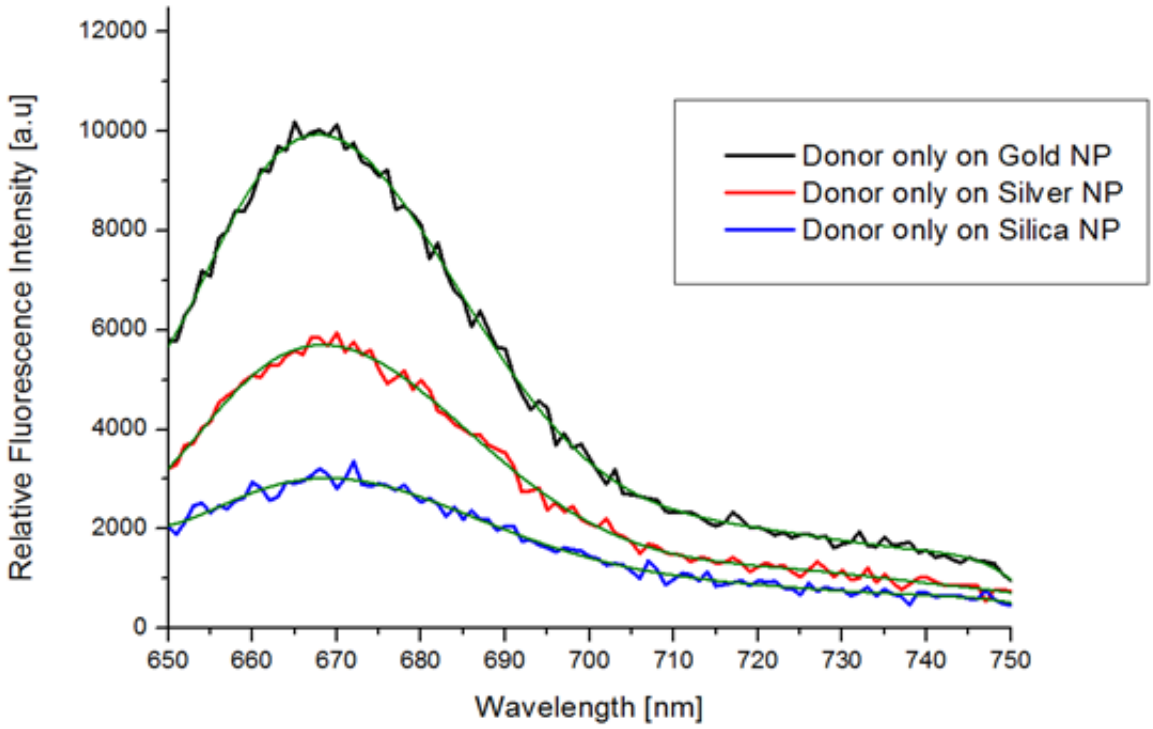

Figure 5.17: Fluorescence emission of donor only on gold, silver and silica NPs (excitation λ610nm).

observed in Section 4.3, there is a decrease in the transfer efficiency of the FRET pair for the gold or silver NPs compared to that of the silica NPs.

While the results of this experiment are in disagreement with the findings by Zhang et al and Lessard-Viger et al, they are in agreement with the results found in the planar configuration in Chapter 4, and by Reil et al [13]. No increase in the FRET efficiency is observed. This negative result was consistent with modeling results, reported in the next section, carried out in light of these results, by Dr. Ondrej Stranik, who did some early work in the BDI on plasmonic enhancement.

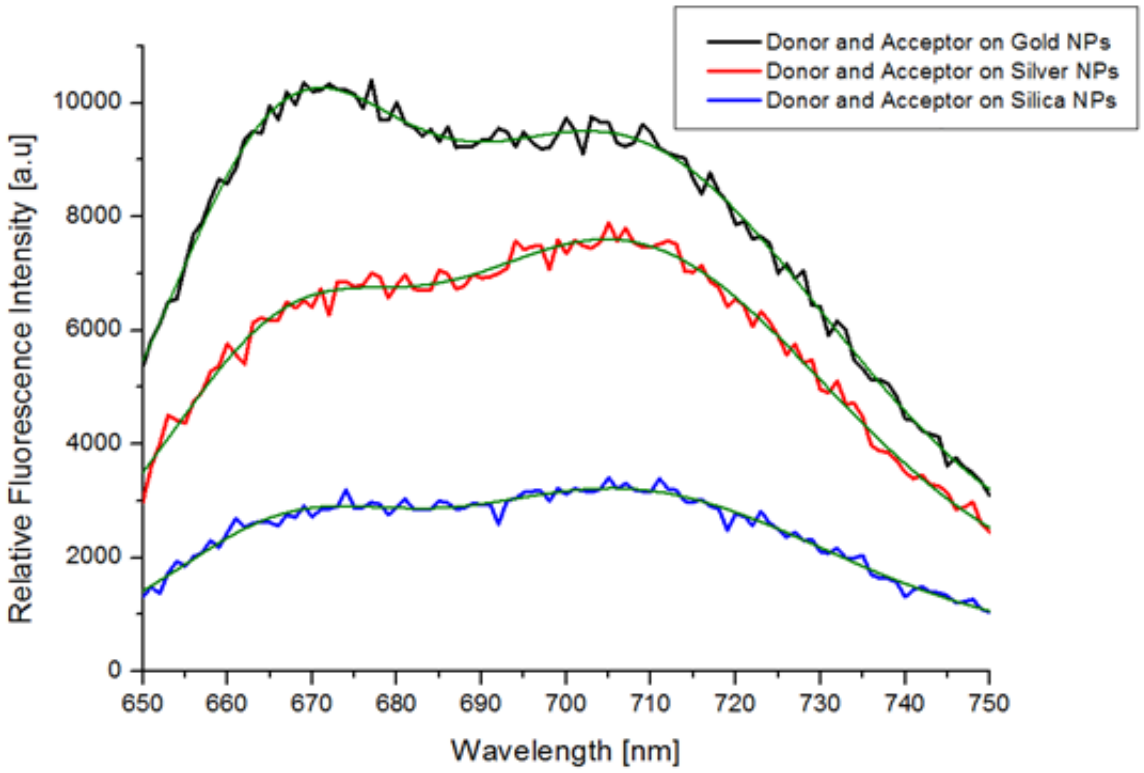

Figure 5.18: Fluorescence emission of donor and acceptor on gold,silver and silica NPs (excitation λ610nm).

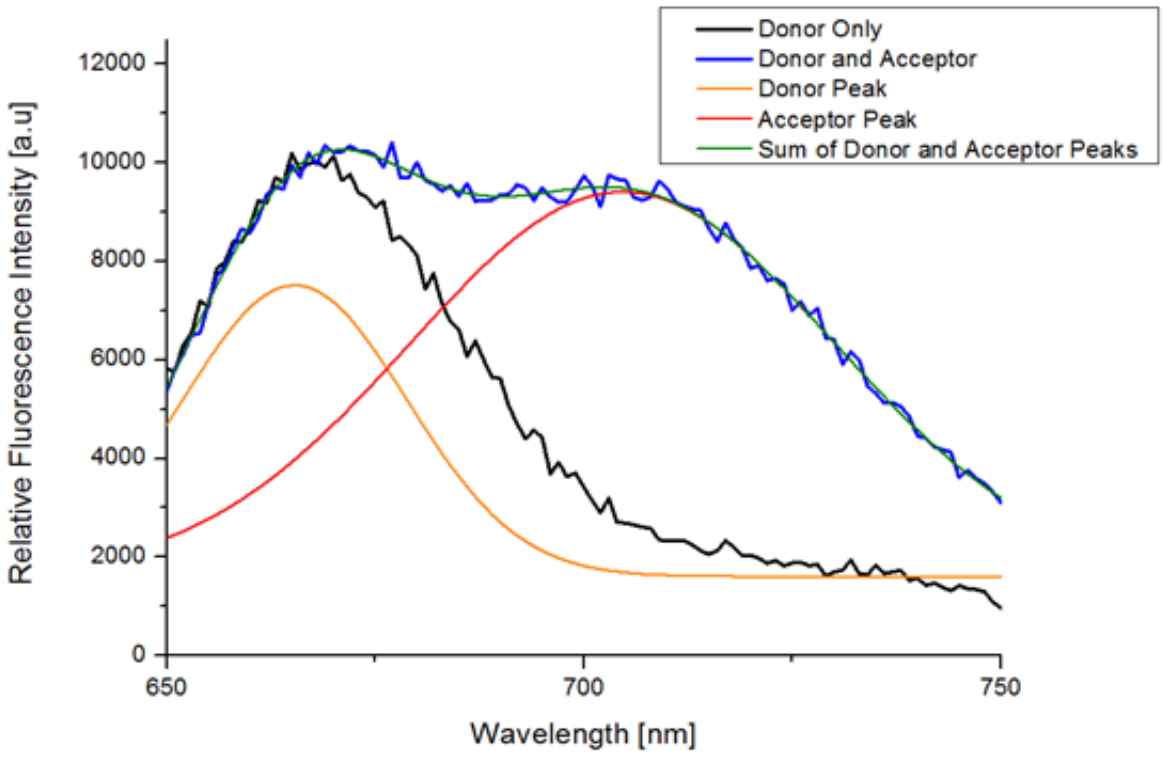

Figure 5.19: Peak fitting of donor and acceptor spectra

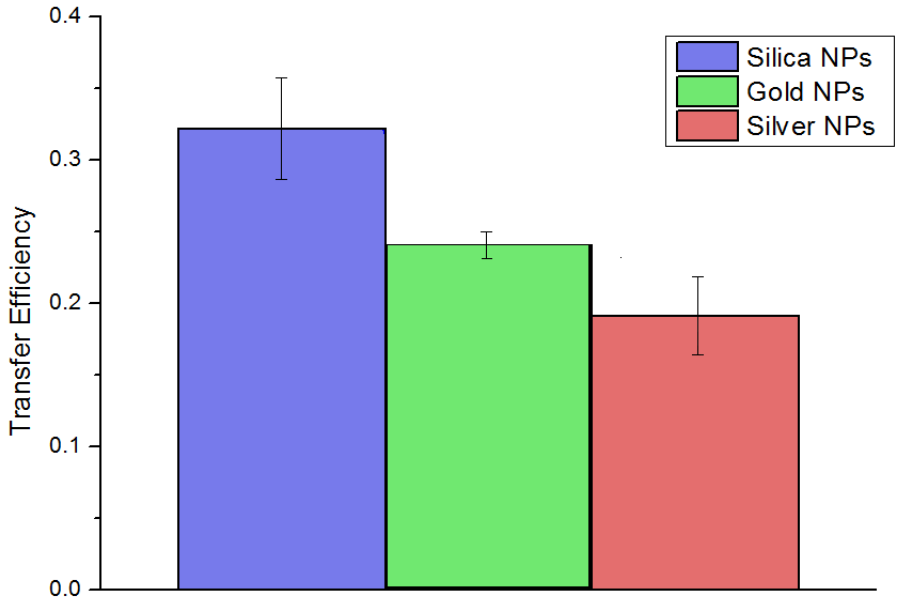

Figure 5.20: Transfer efficiency of silica, gold and silver NPs.

5.4 Theoretical Modeling

In tandem with this experimental work, Dr. Ondrej Stranik modeled the theoretical interactions between metal NPs and a FRET dye pair using MaX-1, a visual electromagnetics platform described in Chapter 3. A summary of these models is included in this section. The models consist of a donor molecule, an acceptor molecule and a metal NP with different geometries and are theoretically analysed in terms of semi-classical approach, where the donor and acceptor are treated as oscillating dipoles. Model One determines the change in transfer efficiency between a FRET pair positioned along the x-axis of a metal NP. This configuration is most similar to the experimental design in this chapter. Model Two determines the change in transfer efficiency between a FRET pair positioned linearly along the y-axis of the NP, which is most similar to the experimental design in Chapter 4. All of the examples are calculated for the case that the donor emission is at one specific wavelength and the absorption of the acceptor is at the same, and all relevant equations governing the system are described in Appendix 4.

5.4.1 Model One - Single FRET pair positioned along the x-axis of the metal NP

This model shows the theoretical calculations for the interaction of a single FRET pair positioned along the x-axis of the metal NP. First a single FRET pair was modeled and the E field distribution around the pair is shown in Fig. 5.21(A). Next the donor was positioned 5nm from the metal NP and the acceptor was moved perpendicularly along the x-axis (through the rotational symmetry axes of the NP). The modified electric field around the FRET pair due to the presence of a metal NP is shown in Fig. 5.21(B).

The change in the radiative (kr) and non-radiative (knr) de-excitation rates of the donor can be seen in Fig. 5.22(A), while Fig. 5.22(B) shows the change in the quantum efficiency of the donor due to the presence of the metal NP.

The Förster Radius (R_0) is the distance at which E_T is 50%. Therefore, in the presence of a NP the modified Förster Radius (R_0^{NP}) is the distance at which E_T^{NP} is 50%. Fig. 5.23 shows R_0 and R_0^{NP} and it can clearly be seen that $R_0^{NP} < R_0$ showing a decrease in the transfer efficiency due to the NP.

The distance between the FRET pair and the NP was also varied in order to ascertain the impact on the FRET efficiency, but no increase was observed at any distance. The shortened Förster Radius is mostly caused by the decrease of the lifetime, due to energy flow through the kr^{NP} and knr^{NP} channels.

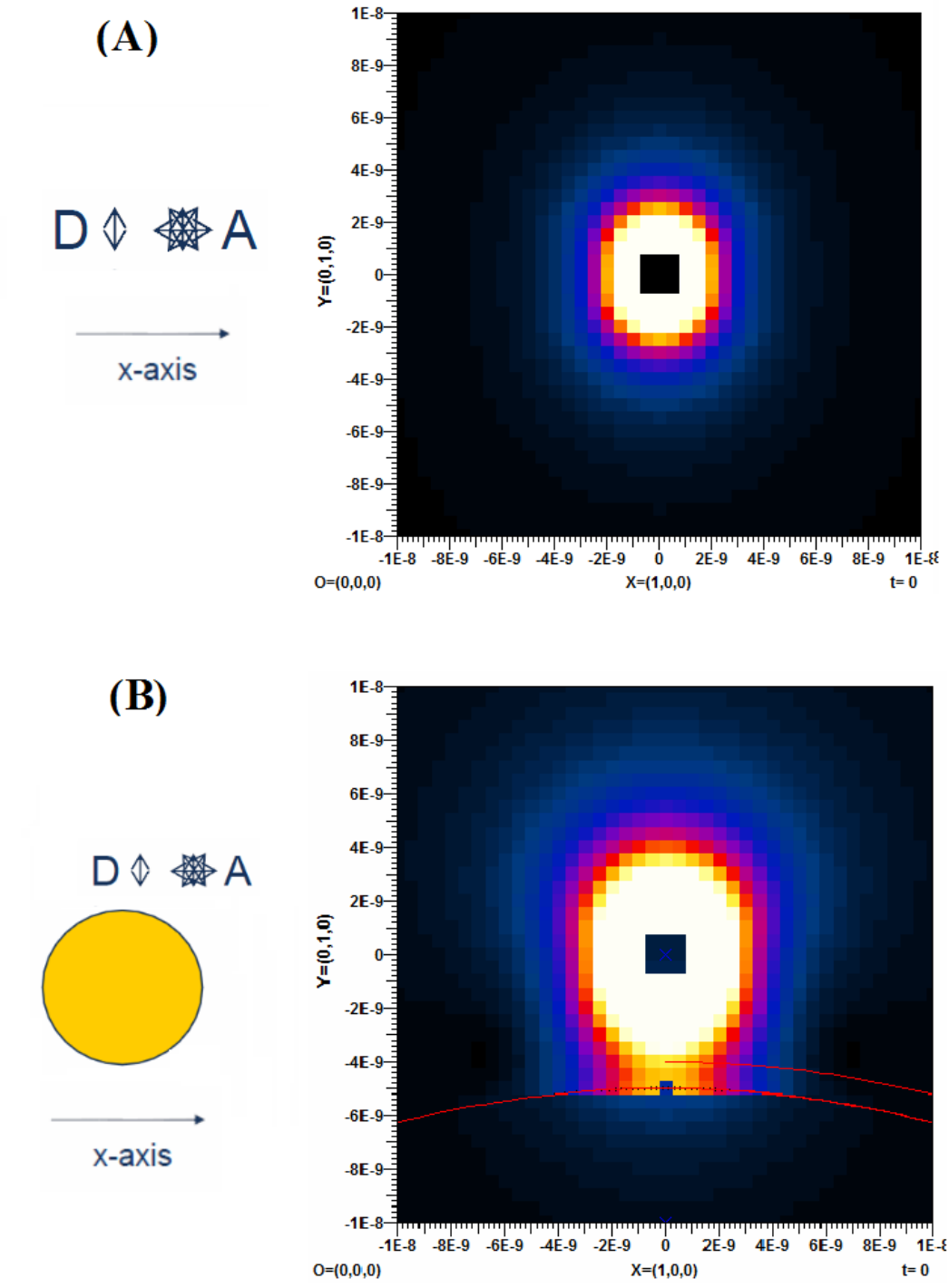

Figure 5.21: E field distribution around (A) the FRET pair and (B) the FRET pair 5nm from a 80nm Au NP (excitation λ600nm).

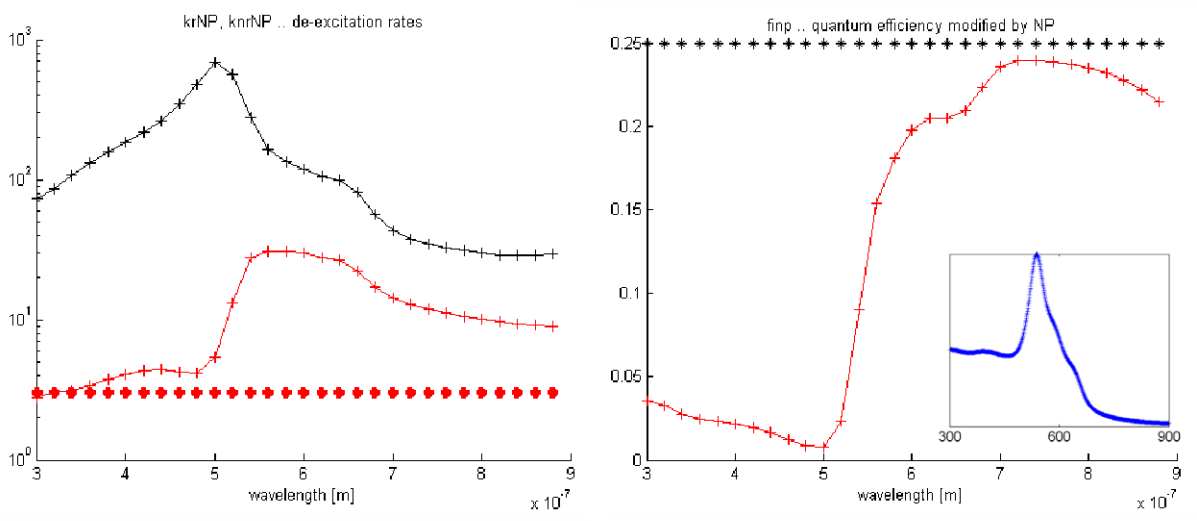

Figure 5.22: (A)The change in de-excitation rates due to the presence of the NP. Black line - kr^{NP}/kr Red line - knr^{NP}/kr Red dots - knr/kr. (B) The change in quantum efficiency due to the presence of the NP. Black line - ϕ Red line - ϕ^{NP}. Insert shows the extinction cross section of the gold NP.

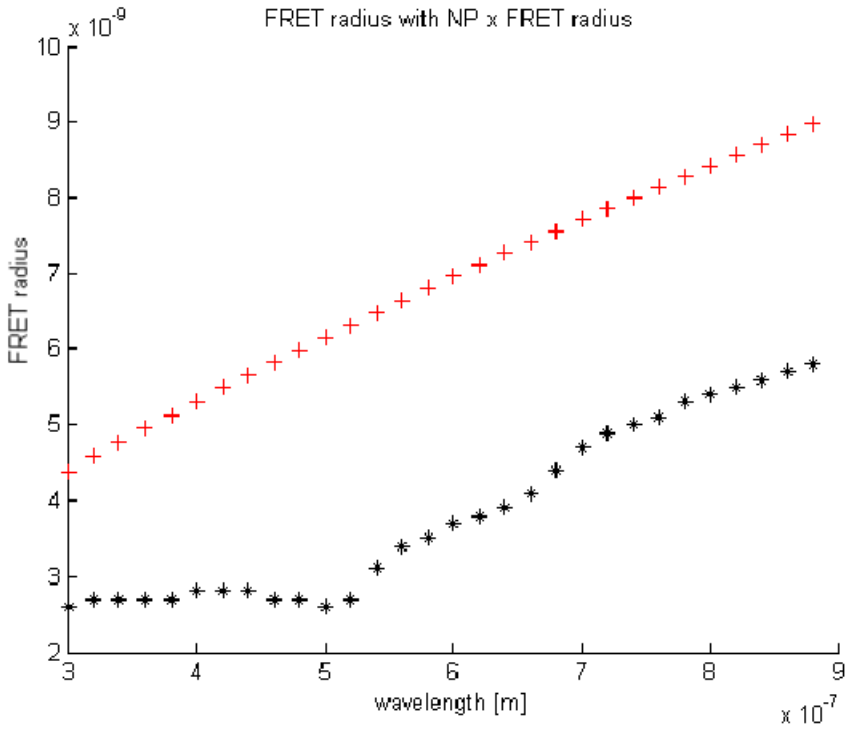

Figure 5.23: Förster Radius: Red line - FRET pair without the NP present (R_0). Black line - FRET pair in the presence of the NP R_0^{NP}

5.4.2 Model Two - Donor and Acceptor positioned along the y-axis of the metal NP

The previous model was adapted to describe a donor and acceptor in linear configuration along the y-axis of a silver NP. This configuration is similar to that used in Chapter 4, where layers of dye are placed consecutively above or below a silver NP. In order to simplify the model the interaction between a single donor and acceptor directly above a NP is evaluated. This single donor and acceptor should experience the most influence of the NP and all other D and A would be influenced less. In this model the acceptor is considered to be closer to the NP than the donor, as depicted in Fig. 5.24. Two different orientations of the donor dipole were evaluated. First the dipole is orientated along the y-axis and the change in de-excitation rates and quantum efficiency is shown in Fig. 5.25. The change in de-excitation rates kr^{NP} and knr^{NP} due to the presence of the NP translates to a decrease in E_T, and in turn a decrease in R_0, as is shown in Fig. 5.26.

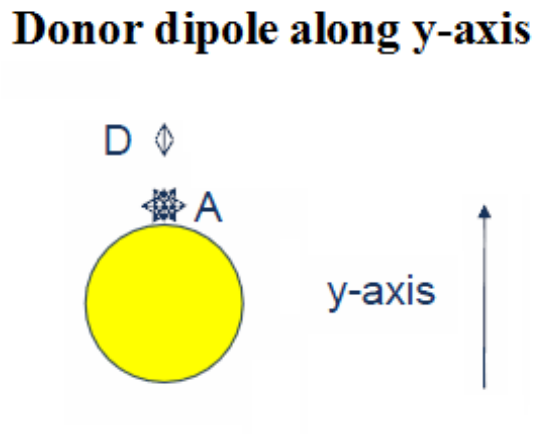

Figure 5.24: Location of donor and acceptor in relation to the metal NP. Dipole oriented along y-axis.

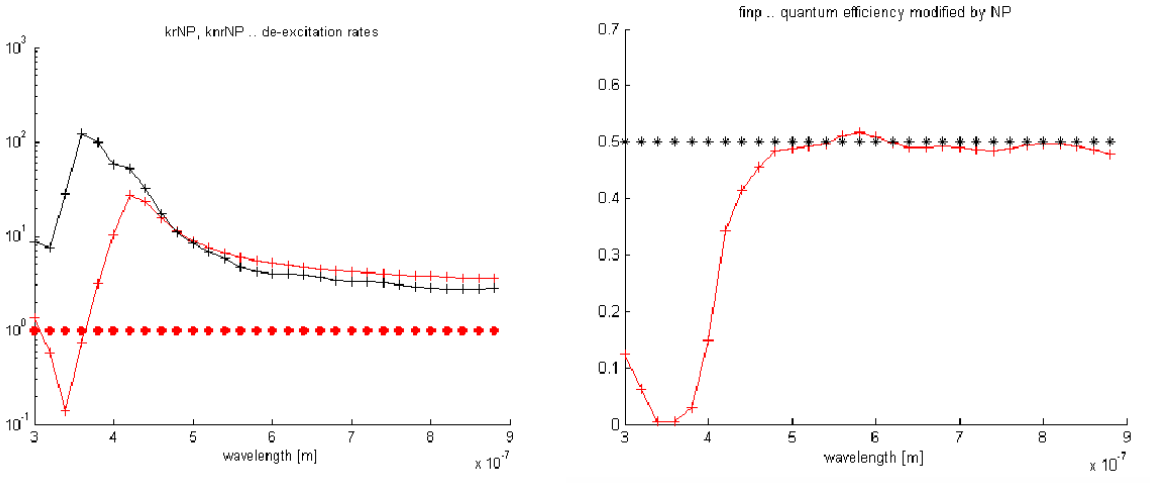

Figure 5.25: (A)The change in de-excitation rates due to the presence of the NP. Black line - kr^{NP}/kr Red line - knr^{NP}/kr Red dots - knr/kr. (B) The change in quantum efficiency due to the presence of the NP. Black line - ϕ Red line - ϕ^{NP}.

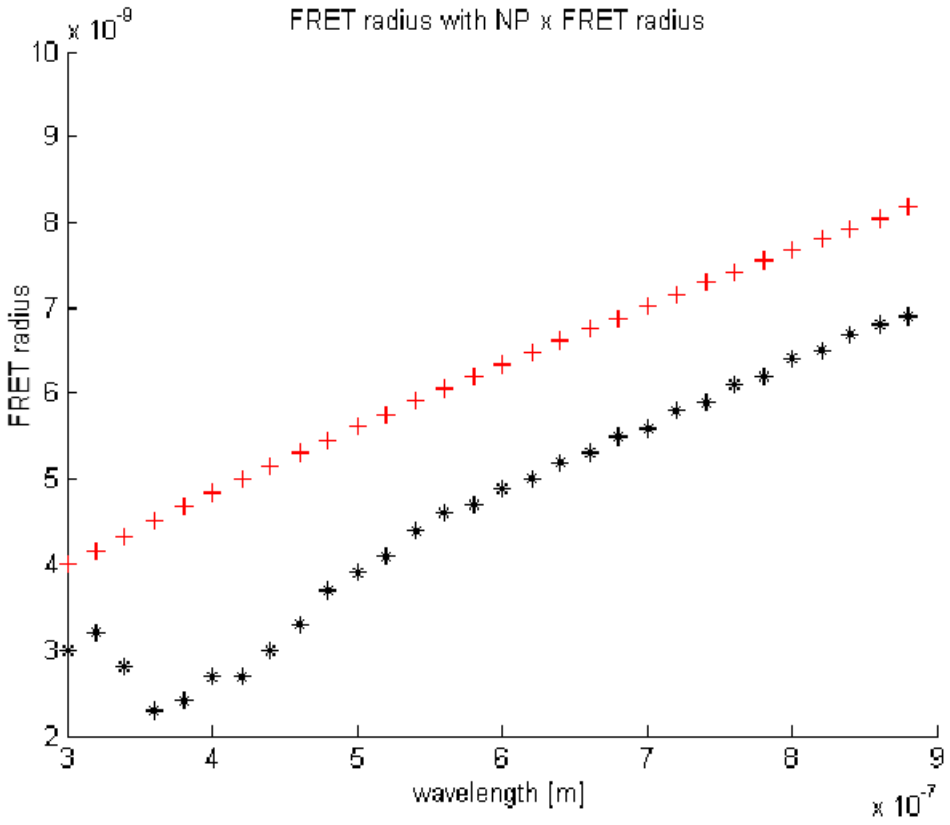

Figure 5.26: Förster Radius: Red line - FRET pair without the NP present (R_0). Black line - FRET pair in the presence of the NP R_0^{NP}

The donor dipole was then orientated along the x-axis to give a comprehensive account of the possible interactions between the different orientations of donor and acceptor. Fig. 5.27 shows the configuration of this model and Fig. 5.28 reports the change in de-excitation rates of the system when compared to the FRET pair without the metal NP present. The change in the de-excitation rates and the quantum efficiency again translates to a decrease in R_0, which is shown in Fig. 5.29. In all configurations for a FRET dye pair in proximity to a metal NP, there is a decrease in the transfer efficiency and the Förster Radius. This system can be compared to the work reported in Chapter 4.3.3 where the dye layers were placed over immobilised NPs, and matches the reduction in E_T seen there also. Theoretical modeling of both systems has shown a decrease in the energy transfer between the FRET pair for all orientations of the dipoles. This supports the findings of the experiments reported in both Chapter 4 and 5.

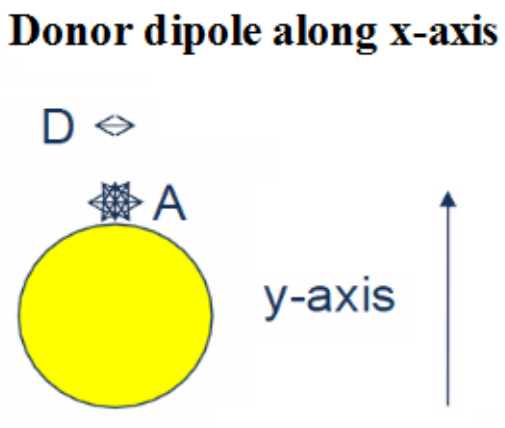

Figure 5.27: Location of donor and acceptor in relation to NP. Dipole oriented along x-axis.

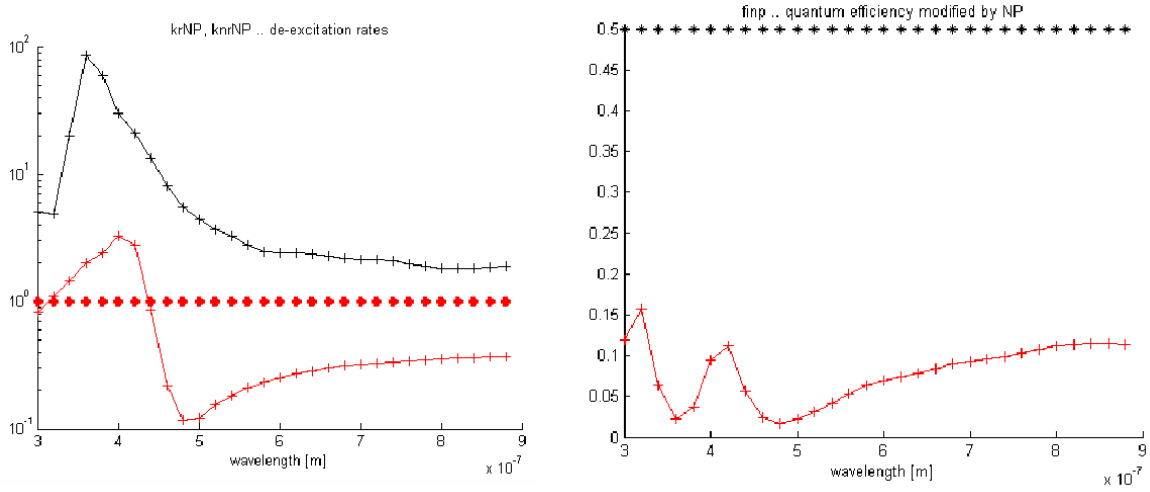

Figure 5.28: (A)The change in de-excitation rates due to the presence of the NP. Black line - kr^{NP}/kr Red line - knr^{NP}/kr Red dots - knr/kr. (B) The change in quantum efficiency due to the presence of the NP. Black line - ϕ Red line - ϕ^{NP}.

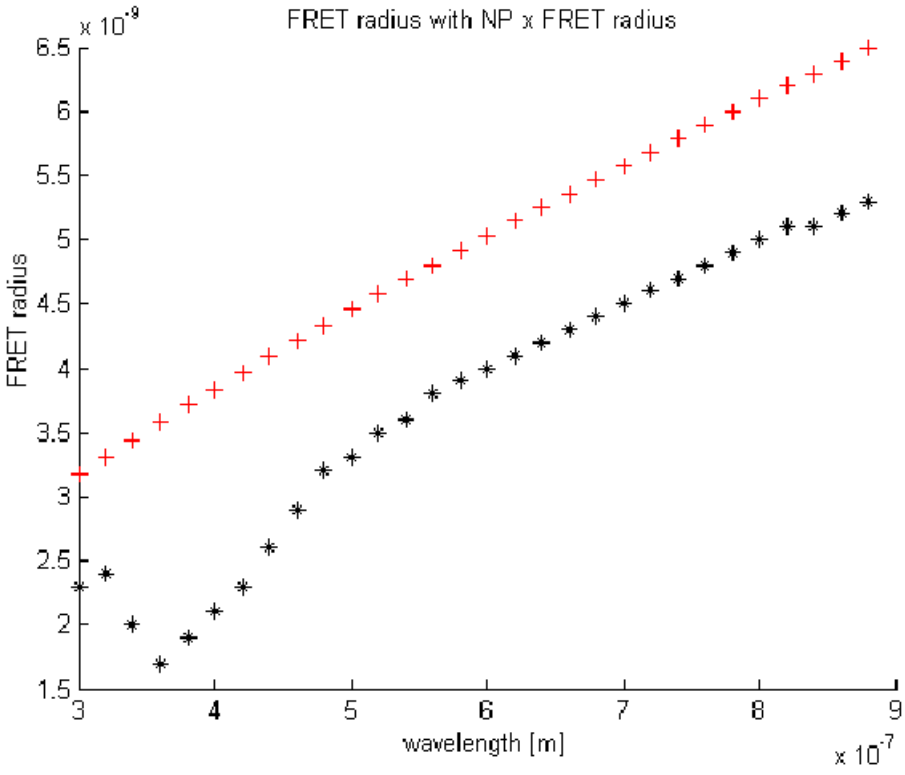

Figure 5.29: Förster Radius: Red line - FRET pair without the NP present (R_0). Black line - FRET pair in the presence of the NP R_0^{NP}.

5.5 Summary

A solution-based FRET model system was designed to investigate plasmonic FRET, which complements the planar configuration reported in Chapter 4. DNA-FRET was shown using donor and acceptor-labeled oligonucleotides. These oligonucleotides were subsequently attached to metal NPs and the plasmonic enhancement of the individual donor and acceptor dye fluorescence was successfully demonstrated. Comparing the transfer efficiency of D-A on metal NPs to D-A on silica NPs, showed no FRET enhancement. Although this effect has been reported in a small number of recent publications, theoretical modeling carried out in our group indicates that for our particular experimental configurations, enhanced FRET is not predicted to occur due to the increase in de-excitation rates through the NP channels and the implications this has on the quantum efficiency and lifetime of the donor. The interaction between the enhanced electric field of the NP, the individual dye fluorescence pathways and the FRET pathway is complex. Therefore, although the experimental configuration reported in this chapter is quite similar to that reported by Zhang et al [1], it is likely that the effect is highly sensitive to the details of the experimental configuration.

References

[1] J. Zhang, Y. Fu, M.H. Chowdhury, and J.R. Lakowicz. Enhanced forster resonance energy transfer on single metal particle. 2. dependence on donor-acceptor separation distance, particle size, and distance from metal surface. *J. Phys. Chem. C*, 111(32):11784–11792, 2007.

[2] M. Lessard-Viger, M. Rioux, L. Rainville, and D. Boudreau. FRET enhancement in multilayer core-shell nanoparticles. *Nano Letters*, 2009.

[3] G. W. Gordon, G. Berry, X. H. Liang, B. Levine, and B. Herman. Quantitative fluorescence resonance energy transfer measurements using fluorescence microscopy. *Biophysical Journal*, 74(5):2702–2713, 1998.

[4] C. L. Takanishi, E. A. Bykova, W. Cheng, and J. Zheng. Gfp-based FRET analysis in live cells. *Brain Research*, 1091(1):132–139, 2006.

[5] A. S. Kumbhar, M. K. Kinnan, and G. Chumanov. Multipole plasmon resonances of submicron silver particles. *Journal of the American Chemical Society*, 127(36):12444–12445, 2005.

[6] K. L. Kelly, E. Coronado, L. L. Zhao, and G. C. Schatz. The optical properties of metal nanoparticles: The influence of size, shape, and dielectric environment. *Journal of Physical Chemistry B*, 107(3):668–677, 2003.

[7] X. Z. Zhou, X. Huang, X. Y. Qi, S. X. Wu, C. Xue, F. Y. C. Boey, Q. Y. Yan, P. Chen, and H. Zhang. In situ synthesis of metal nanoparticles on single-layer graphene oxide and reduced graphene oxide surfaces. *Journal of Physical Chemistry C*, 113(25):10842–10846, 2009.

[8] D. I. Gittins and F. Caruso. Tailoring the polyelectrolyte coating of metal nanoparticles. *The Journal of Physical Chemistry B*, 105(29):6846–6852, 2001.

[9] F. Caruso, E. Donath, and H. Mohwald. Influence of polyelectrolyte multilayer coatings on forster resonance energy transfer between 6-carboxyfluorescein and rhodamine b-labeled particles in aqueous solution. *The Journal of Physical Chemistry B*, 102(11):2011–2016, 1998.

[10] G. Schneider and G. Decher. From functional core/shell nanoparticles prepared via layer-by-layer deposition to empty nanospheres. *Nano Letters*, 4(10):1833–1839, 2004.

[11] G. Schneider, G. Decher, N. Nerambourg, R. Praho, M. H. V. Werts, and M. Blanchard-Desce. Distance-dependent fluorescence quenching on gold nanoparticles ensheathed with layer-by-layer assembled polyelectrolytes. *Nano Letters*, 6(3):530–536, 2006.

[12] A.B. Steel, R.L. Levicky, T.M. Herne, and M.J. Tarlov. Immobilization of nucleic acids at solid surfaces: effect of oligonucleotide length on layer assembly. *Biophysical Journal*, 79(2):975–981, 2000.

[13] F. Reil, U. Hohenester, J. R. Krenn, and A. Leitner. Forster-type resonant energy transfer influenced by metal nanoparticles. *Nano Letters*, 8(12):4128–4133, 2008.

Chapter 6

Conclusions and Future Perspectives

6.1 Summary of Results

Two different investigation platforms were designed and successfully employed to demonstrate FRET. The 2-D planar platform described in Chapter 4 was shown to demonstrate FRET using a Ruthenium complex as donor and Cy5 dye as acceptor. Conventional FRET equations were not adequate to describe the complexity of the FRET interaction in the 2-D layer structure. Therefore, a model was developed based on donor to multiple acceptor transfer in the layers. The experimental results were shown to match well to this model. An investigation of the plasmonic interaction with the FRET process was undertaken and it was postulated that the presence of adjacent metal NPs could enhance the FRET efficiency and subsequently enable longer Förster distances and hence FRET over longer distances. This was explored initially using the 2-D platform, which allowed a range of combinations of NPs and experimental configurations to be investigated. It was determined that, for this system, while there was substantial plasmonic enhancement of the individual donor and acceptor fluorescence, there was no overall enhancement of FRET. On the contrary, in the presence of NPs, the FRET efficiency was found to decrease. In Chapter 5, a separate model was designed to investigate plasmonic-FRET in solution. This experimental platform investigated a FRET dye pair attached to a metal NP using a linker complex.

The FRET dyes employed were Cy5 as donor and Cy5.5 as acceptor and were separated by controlled lengths of DNA. As above, FRET was observed but the presence of the metal NP invariably reduced, rather than increased, the transfer efficiency. In this approach, a pure silica NP was used as a control in order to quantify the effect of the metal. A theoretical model of the experimental system, carried out by a colleague using the MaX-1 package, predicted that enhancement of FRET would not be expected from this system due to the decrease in quantum efficiency and lifetime of the FRET pair. The results of the theoretical model validated the experimental results presented in both Chapter 4 and Chapter 5.

6.2 Objectives Revisited

Referring back to section 1.7, all five objectives have been successfully achieved. A model was designed to demonstrate planar FRET (a) and a strategy was developed to enable accurate control of the donor-acceptor separation (b). The transfer efficiency of the planar FRET model was also measured and compared with theory for both distance and concentration dependence (c). The plasmonic effect of metal NPs on the transfer efficiency of 2-D FRET was investigated in different configurations, by adjusting the model to include NP layers at different positions around the FRET pair (d). The plasmonic effect of metal NPs on the transfer efficiency of solution-FRET was also investigated (e). Both of these investigations showed plasmonic enhancement of the donor and acceptor, while the overall effect was a decrease in the transfer efficiency. Theoretical modeling of the system verified this decrease.

6.3 Future Perspectives

As emphasised in this thesis, FRET is becoming increasingly useful in biomedical applications such as monitoring DNA hybridisation and cleavage, study of protein dynamics, cell membrane studies and intracellular processes [1–4]. In particular, with the advent of more advanced optical detection instrumentation, single molecule FRET is fast becoming a very sensitive tool in the study of biomolecules [5–8]. Plasmonically enhanced FRET, a major focus of this thesis work, has sig-

nificant potential for extending the range of the FRET interaction and hence opening up a broader range of applications. The application of this effect is still at an early stage. While the possibility of enhanced FRET in the presence of metal films was discussed in very early theoretical publications [9–11] experimental work on this topic has emerged only in the last few years. In chapter 4, the work of two groups who observed this effect for single dye FRET systems similar to those presented here was discussed. There have also been a number of publications reporting evidence of FRET enhancement using quantum dot FRET pairs [12–14]. These authors relate the enhancement to the interaction between the more complex field distribution of the quantum dots and the multipole resonances of the NPs. The interaction between the enhanced electric field of the NP, the individual dye fluorescence pathways and the FRET pathway is complex. Much work still needs to be carried out to elucidate (i) the theory of the plasmon-FRET interaction and (ii) to establish and characterise in detail the optimum experimental conditions for enhanced FRET in terms of NP size, shape and composition, FRET dyes, NP-dye separation and experimental configuration. Both experimental and theoretical investigations will be continued in our laboratory in order to establish the optimum design rules for an efficient and versatile plasmon-enhanced FRET platform, which can be used to extend the application fields for optical biosensors.

References

[1] S. Jiang and Y. Zhang. Upconversion nanoparticle-based FRET system for study of siRNA in live cells. *Langmuir*, 26(9):6689–6694, 2010.

[2] G. Crivat, S. M. Da Silva, D. R. Reyes, L. E. Locascio, M. Gaitan, N. Rosenzweig, and Z. Rosenzweig. Quantum dot FRET-based probes in thin films grown in microfluidic channels. *Journal of the American Chemical Society*, 132(5):1460–1461, 2010.

[3] P. M. Bendix, M. S. Pedersen, and D. Stamou. Quantification of nanoscale intermembrane contact areas by using fluorescence resonance energy transfer. *Proceedings of the National Academy of Sciences*, 106(30):12341–12346, 2009.

[4] M. Lundin, E. Blomberg, and R. D. Tilton. Polymer dynamics in layer-by-layer assemblies of chitosan and heparin. *Langmuir*, 26(5):3242–3251, 2010.

[5] B. Schuler and W. A. Eaton. Protein folding studied by single-molecule FRET. *Current Opinion in Structural Biology*, 18(1):16–26, 2008.

[6] N. Di Fiori and A. Meller. The effect of dye-dye interactions on the spatial resolution of single-molecule FRET measurements in nucleic acids. *Biophysical Journal*, 98(10):2265–2272, 2010.

[7] H. S. Chung, J. M. Louis, and W. A. Eaton. Distinguishing between protein dynamics and dye photophysics in single-molecule FRET experiments. *Biophysical Journal*, 98(4):696–706, 2010.

[8] P. Ray, G. Darbha, A. Ray, J. Walker, and W. Hardy. Gold nanoparticle based FRET for DNA detection. *Plasmonics*, 2(4):173–183, 2007.

[9] J. I. Gersten and A. Nitzan. Accelerated energy-transfer between molecules near a solid particle. *Chemical Physics Letters*, 104(1):31–37, 1984.

[10] X. M. Hua, J. I. Gersten, and A. Nitzan. Theory of energy transfer between molecules near solid state particles. *Journal of Chemical Physics*, 83(7):3650–3659, 1985.

[11] P. Andrew and W. L. Barnes. Energy transfer across a metal film mediated by surface plasmon polaritons. *Science*, 306(5698):1002–1005, 2004.

[12] V. K. Komarala, A. L. Bradley, Y. P. Rakovich, S. J. Byrne, Y. K. Gun'ko, and A. L. Rogach. Surface plasmon enhanced forster resonance energy transfer between the cdte quantum dots. *Applied Physics Letters*, 93(12):123102–3, 2008.

[13] X-R. Su, W. Zhang, L. Zhou, X-N. Peng, D-W. Pang, S-D. Liu, Z-K. Zhou, and Q-Q. Wang. Multipole-plasmon-enhanced forster energy transfer between semiconductor quantum dots via dual-resonance nanoantenna effects. *Applied Physics Letters*, 96(4):043106–3, 2010.

[14] X-R. Su, W. Zhang, L. Zhou, X-N. Peng, and Q-Q. Wang. Plasmon-enhanced forster energy transfer between semiconductor quantum dots: multipole effects. *Opt. Express*, 18(7):6516–6521, 2010.

List of Publications and Conference Presentations

Peer-Reviewed Publications

1. Bird A., Stranik O., MacCraith B. D., McDonagh C., "FRET in 2-D: Experiment and Model", in draft

2. Bird A., Stranik O., Gubala, V., MacCraith B. D., McDonagh C., "Plasmonic interaction of FRET: Experiment and Model", in preparation

Poster presentations

1. "FRET for Biomedical Sensor Applications: Distance Dependence and Plasmonic Interaction", NCSR Poster Day, November 2009, Dublin, Ireland

2. "FRET for Biomedical Sensor Applications: Distance Dependence and Plasmonic Interaction", International Conference on Trends in Bioanalytical Sciences and Biosensors, January 2009, Dublin, Ireland (awarded Best Poster Prize)

3. "FRET for Biomedical Sensor Applications: Distance Dependence and Plasmonic Interaction", Europtrode IX, March 2008, Dublin, Ireland

4. "FRET for Biomedical Sensor Applications: Distance Dependence and Plasmonic Interaction", SFI site visit postgraduate meeting, February 2008, Dublin City University, Ireland

5. "FRET for Biomedical Sensor Applications: Distance Dependence and Plasmonic Interaction", Photonics West, January 2008, San Jose, USA

6. "FRET for Biomedical Sensor Applications: A distance dependence study", BOC Gases Poster Competition, , November 2007, Dublin City University, Ireland (awarded 2nd Prize)

7. "FRET for Biomedical Sensor Applications: A distance dependence study", Photonics Ireland, September 2007, Galway, Ireland

8. "FRET for Biomedical Sensor Applications: A distance dependence study", 36th Spring Weekend Meeting of the IOP, March 2007, Birr, Ireland

Appendix